

***Republic of Iraq  
Ministry of Higher Education and  
Scientific Research  
University of Baghdad  
College of Education for Pure Science  
(Ibn-AL-Haitham)***



# **Correction of the Line Profiles for X- Ray Diffraction Peaks by Using Three Analysis Methods**

***A Thesis***

***Submitted to Council of College of Education for Pure Science  
(Ibn-AL-Haitham)/ University of Baghdad in partial Fulfillment of  
the Requirements for the Degree of Master of Science in Physics***

***By***

***Rasha Munir Chellab***

***Supervisor***

***Prof. Dr. Khalid Helal Harbbi***

**2019 A.D**

**1441 A.H**

بِسْمِ اللَّهِ الرَّحْمَنِ الرَّحِيمِ

اللَّهُ نُورُ السَّمَاوَاتِ وَالْأَرْضِ ۚ مَثَلُ نُورِهِ كَمِشْكَاةٍ فِيهَا مِصْبَاحٌ ۚ  
الْمِصْبَاحُ فِي زُجَاجَةٍ ۚ الزُّجَاجَةُ كَأَنَّهَا كَوْكَبٌ دُرِّيٌّ يُوقَدُ مِنْ شَجَرَةٍ  
مُبَارَكَةٍ زَيْتُونَةٍ لَا شَرْقِيَّةٍ وَلَا غَرْبِيَّةٍ يَكَادُ زَيْتُهَا يُضِيءُ وَلَوْ لَمْ  
تَمْسَسْهُ نَارٌ ۚ نُورٌ عَلَى نُورٍ ۗ يَهْدِي اللَّهُ لِنُورِهِ مَن يَشَاءُ ۚ وَيَضْرِبُ اللَّهُ  
الْأَمْثَالَ لِلنَّاسِ ۚ وَاللَّهُ بِكُلِّ شَيْءٍ عَلِيمٌ

صدق الله العلي العظيم

سورة النور – اية رقم 35

## Supervisore Certification

I certify that this thesis titled “**Correction of the Line Profiles for X- Ray Diffraction Peaks by Using Three Analysis Methods**” was prepared by (**Rasha Munir Chellab**), under my supervision at the University of Baghdad / Education College for Pure Science (Ibn-AL-Haitham) / Department of Physics in partial fulfillment of the requirements for the degree of Master of Science in Physics.

Signature:



Name: Dr. Khalid Helal Harbbi

Title: Professor.

University of Baghdad / College of Education for Pure Science (Ibn-AL-Haitham) / Department of Physics

Date: 30/6/2019

The Council of the Department of Physics has approved the examining committee.

Signature: S. A. MAKI

Name: Dr. Samir Ata Maki

Title: Professor.

# Certification of Examiners

We certify that we have read the thesis, titled “**Correction of the Line Profiles for X- Ray Diffraction Peaks by Using Three Analysis Methods**” presented by (**Rasha Munir Chellab**) and as an examination committee, we examined the student on its contents, and in what is related to it, and that in our opinion it is meets the standard of a thesis for the degree of Master of science in physics.

(Chairman)

Signature:

Name: **Dr. Kareem Ali Jasim**

Title: **Professor**

Address: University of Baghdad

Date: 24/11/2019

(Member)

Signature:

Name: **Dr. Anwar H. Ali Al-Fouadi**

Title: **Assist. Professor**

Address: Al-mustansiriyah University

Date: 26/11/2019

(Member)

Signature:

Name: **Dr. Muthafar F. Al-Hilli**

Title: **Assist. Professor**

Address: University of Baghdad

Date: 26/11/2019

(Supervisor)

Signature:

Name: **Dr. Khalid Helal Harbbi**

Title: **Professor**

Address: University of Baghdad

Date: 26/11/2019

*Firas A. Abdlateef*

**Assist. Prof. Dr. Firas A. Abdlateef**  
The Dean of College of Education for  
Pure Science / Ibn Al-Haitham

17/12/2019

# *Dedications*

*To my brother martyr who sacrificed his blood for the homeland. My brother Ahmed you will always be in my heart and my mind.*

*My colleagues who encouraged me along the way who supported me and gave me everything that is necessary to finish what I started.*

*My parents, brothers and sisters who have affected in every way possible by this endeavor.*

*Thank you so much. You can never measure my love for you all. God bless you*

*Rasha*

## *Acknowledgments*

*I would like gratefully acknowledge to God who gave me this opportunity and gave me patience to complete my studies and inspired me wisdom, knowledge and understanding. He was the source of my strength all my way and thanks to him only rose.*

*To the support of the department of Physics – College of Education for Pure Sciences (Ibn Al-Haitham) – University of Baghdad represented by professor Dr. Samir Ata Maki, and Dr. Karim Ali, for their efforts and noble contributions, which have made this volume a valuable addition. I wish to express my special gratitude to Supervisor Professor Dr. Khalid Helal Harbbi ,who originally continuing support, cooperation, and encouragement this would not have become a reality.*

## Abstract

In this thesis, Williamson Hall method, Size-Strain Plot method, and Halder Wagner method were used to analyze the X-ray diffraction patterns and calculate the crystallite size and lattice strain of nickel oxide (NiO) nano particles. The results obtained from these methods were then compared with those obtained from both classical Scherrer and modified Scherrer methods. The crystallite size were: (0.3087) nm, (0.8626) nm, and (0.2228) nm. Whereas, the lattice strain were: (0.1441), (0.8216), and (0.5207) for Williamson Hall, Size-Strain Plot, and Halder Wagner methods respectively. On the other hand, the crystallite size and lattice strain calculated from classical Scherrer were ( $D = 0.31511$ ) nm, ( $\epsilon = 0.32471$ ), and modified Scherrer methods were ( $D = 0.1350$ ) nm. From that the results detected for all of the methods in this thesis, we notice that the Halder – Wagner method is the best analysis method to calculate the crystallite size and lattice strain by given accurate result and nearly to this found by the Scherrer and modified Scherrer methods. The Specific Surface Area was calculate using the crystallite size of the Halder –Wagner method, it was found ( $s = 4.0375 * 10^9 m^2/g$ ). The dislocation density depends on the crystallite size for Halder-Wagner, it was found ( $\delta = 2.1186 * 10^{18}$ ).Morphology Index was calculated from full width at half maximum and the highest value was (2.63530922) for the reflection (220), while the lowest value was (1.304537008) for the reflection (222). The texture coefficient for all line profile was (0.429331599). By Modified Halder-Wagner method calculate the stress and the energy density, were ( $\sigma = 36449*10^6 N/m^2$ ), and ( $u = 9489*10^6 N/m^2$ ) respectively. The Halder-Wagner plot used to calculate the density of energy from the y-intercept and gives same value to this was found by the modified Halder-Wagner. The crystallite size for the reflections (111, 200) is calculated at different temperatures (200, 300, 400)°C. The crystallite sizes for (111) were decreased with increasing

temperature from (200-400)° C, and they were (0.34174 nm), (0.32985nm), and (0.32160 nm) respectively. The (D) values for the line (200) were (0.49210 nm), (0.45336 nm), and (0.83588 nm), for (200, 300, 400) o C respectively.

## List of Contents

<b>Abstract</b> .....	
<b>List of Contents</b> .....	I-II
<b>List of Figures</b> .....	III
<b>List of Tables</b> .....	VI
<b>List of Abbreviations</b> .....	VIII
<b>List of Symbols</b> .....	VIII
<b>Chapter One -Introduction and Literature Review</b> .....	1-15
<b>1.1 Introduction</b> .....	1
<b>1.2 Literature Review</b> .....	4
<b>1.3 The Aim of the Work</b> .....	15
<b>Chapter Two -Theoretical Part</b> .....	16-28
<b>2.1 Introduction</b> .....	16
<b>2.2 X-Ray Diffraction</b> .....	16
<b>2.3 The Full Width at Half Maximum (FWHM)</b> .....	19
<b>2.4 Analysis Methods of X- ray Diffraction</b> .....	20
<b>2.4.1 Scherrer Method</b> .....	20
<b>2.4.2 The Modified Scherrer Method</b> .....	21
<b>2.4.3 The Williamson- Hall Method</b> .....	21
<b>2.4.4 The Size-Strain Plot Method</b> .....	22
<b>2.4.5 The Halder-Wagner Method</b> .....	23
<b>2.5 Some of Lattice Parameters</b> .....	24
<b>2.5.1 Specific Surface Area (SSA)</b> .....	24
<b>2.5.2 Dislocation Density</b> .....	25
<b>2.5.3 Morphology Index (MI)</b> .....	26
<b>2.5.4 Texture Coefficient</b> .....	26
<b>2.6 Calculation of Crystallite Size with Change Temperatures</b> .....	27

<b>2.7 Modified Halder-Wagner Method</b> .....	27
<b>Chapter Three- Results and Discussions</b> .....	29-70
<b>3.1 Introduction</b> .....	29
<b>3.2 Calculation of The Full Width at Half Maximum (FWHM) and The Integral Breadth (<math>\beta_{hkl}</math>)</b> .....	29
<b>3.3 Calculation of Crystallite Size and The Lattice Strain</b> .....	49
<b>3.3.1 The Scherrer Method</b> .....	49
<b>3.3.2 The Modified Scherrer Method</b> .....	51
<b>3.3.3 The Williamson- Hall Method</b> .....	52
<b>3.3.4 The Size-Strain Plot Method</b> .....	53
<b>3.3.5 The Halder -Wagner Method</b> .....	55
<b>3.4 Determination of The Lattice Parameters</b> .....	56
<b>3.4.1 Specific Surface Area (SSA)</b> .....	56
<b>3.4.2 Dislocation Density</b> .....	56
<b>3.4.3 Morphology Index (MI)</b> .....	57
<b>3.4.4 Texture Coefficient</b> .....	57
<b>3.5 Modified Halder-Wagner Method</b> .....	58
<b>3.6 The Crystallite Size at Different Temperatures</b> .....	59
<b>Chapter Four -Conclusions and Suggestions for Future Work</b> .....	71-72
<b>4.1 Conclusions</b> .....	71
<b>4.2 Future Works</b> .....	72
<b>References</b> .....	73-80

## List of figures

<b>Figure (2.1):</b> X-ray diffraction pattern of NiO powder [37].....	17
<b>Figure (2.2):</b> Geometrical condition for diffraction from lattice planes [39]...	18
<b>Figure (2.3):</b> Diffraction peak and information content that extracted [39].....	19
<b>Figure (2.4):</b> The X-ray diffraction pattern of NiO nanomaterial with varies temperature [51].....	27
<b>Figure (3.1):</b> The profile line (111) and the fitted curve .....	30
<b>Figure (3.2):</b> The profile line (200) and the fitted curve .....	30
<b>Figure (3.3):</b> The profile line (220) and the fitted curve .....	31
<b>Figure (3.4):</b> The profile line (221) and the fitted curve .....	31
<b>Figure (3.5):</b> The profile line (222) and the fitted curve .....	32
<b>Figure (3.6):</b> The profile line (311) and the fitted curve .....	32
<b>Figure (3.7):</b> The fitted curve of the profile line (111).....	33
<b>Figure (3.8):</b> The fitted curve of the profile line (200).....	33
<b>Figure (3.9):</b> The fitted curve of the profile line (220).....	34
<b>Figure (3.10):</b> The fitted curve of the profile line (221).....	34
<b>Figure (3.11):</b> The fitted curve of the profile line (222).....	35
<b>Figure (3.12):</b> The fitted curve of the profile line (311) .....	35
<b>Figure (3.13):</b> Fitted profile steps of the line (111) with 20 steps to the right and 20 steps to the left. ....	36
<b>Figure (3.14):</b> Fitted profile line (200) with 20 steps to the right and 20 steps to the left.....	36

<b>Figure (3.15):</b> Fitted profile line (220) with 20 steps to the right and 20 steps to the left.....	37
<b>Figure (3.16):</b> Fitted profile line (221) with 20 steps to the right and 20 steps to the left.....	37
<b>Figure (3.17):</b> Fitted profile line (222) with 20 steps to the right and 20 steps to the left.....	38
<b>Figure (3.18):</b> Fitted profile line (311) with 20 steps to the right and 20 steps to the left.....	38
<b>Figure (3.19):</b> Determined (FWHM) for line (111).....	45
<b>Figure (3.20):</b> Determined (FWHM) for line (200).....	45
<b>Figure (3.21):</b> Determined (FWHM) for line (220).....	46
<b>Figure (3.22):</b> Determined (FWHM) for line (221).....	46
<b>Figure (3.23):</b> Determined (FWHM) for line (222).....	47
<b>Figure (3.24):</b> Determined (FWHM) for line (311).....	47
<b>Figure (3.25):</b> Plot of modified Scherrer method.....	52
<b>Figure (3.26):</b> Plot of Williamson-Hall method.....	53
<b>Figure (3.27):</b> Plot of Size-Strain plot method.....	54
<b>Figure (3.28):</b> Plot of Halder-Wagner method.....	55
<b>Figure (3.29):</b> Analysis steps of (111) line at (200°C).....	59
<b>Figure (3.30):</b> Analysis steps of (200) line at (200°C).....	60
<b>Figure (3.31):</b> Analysis steps of (111) line at (300°C).....	61
<b>Figure (3.32):</b> Analysis steps of (200) line at (300°C).....	62
<b>Figure (3.33):</b> Analysis steps of (111) line at (400°C).....	63

**Figure (3.34):** Analysis steps of (200) line at (400°C).....64

**Figure (3.35):** Relation between crystallite size and temperature .....70

## List of Tables

<b>Table (3.1):</b> The area under the curve for line (111).....	39
<b>Table (3.2):</b> The area under the curve for line (200).....	40
<b>Table (3.3):</b> The area under the curve for line (220).....	41
<b>Table (3.4):</b> The area under the curve for line (221).....	42
<b>Table (3.5):</b> The area under the curve for line (222).....	43
<b>Table (3.6):</b> The area under the curve for line (311).....	44
<b>Table (3.7):</b> The FWHM and integral breadth ( $\beta$ ) of the lines (111), (200), (220), (221), (222), and (311) for NiO powder.....	48
<b>Table (3-8):</b> The values of $\beta$ for the profile lines (111), (200), (220), (221), (222), and (311).....	49
<b>Table (3.9):</b> The values of crystallite size and lattice strain determined by the Scherrer method .....	50
<b>Table (3.10):</b> The values of $\ln\beta_{hkl}$ and $\ln\frac{1}{\cos\theta}$ for all the profile line.....	51
<b>Table (3-11):</b> The values of the $\beta\cos\theta$ and $4\sin\theta$ for all profile lines .....	52
<b>Table (3.12):</b> The results of $(d_{hkl}^2\beta_{hkl}\cos\theta)$ and $(d_{hkl}\beta_{hkl}\cos\theta)^2$ for all the profile lines .....	54
<b>Table (3-13):</b> The results of $(\beta*/d*)^2$ and $(\beta*/d^{*2})$ for all profile lines.....	55
<b>Table (3.14):</b> The values of crystallite size and lattice strain for all applied methods .....	59
<b>Table (3.15):</b> The results of MI for all profile lines.....	57
<b>Table (3.16):</b> The results of $(T_c)$ for (111), (200), (220), (221), (222), and (311) profile lines.....	58

<b>Table (3.17):</b> The area under the curve for the line (111) at 200°C.....	65
<b>Table (3.18):</b> The area under the curve for the line (200) at 200°C.....	65
<b>Table (3.19):</b> The area under the curve for the line (111) at 300°C.....	66
<b>Table (3.20):</b> The area under the curve for the line (200) at 300°C.....	66
<b>Table (3.21):</b> The area under the curve for the line (111) at 400°C.....	67
<b>Table (3.22):</b> The area under the curve for the line (200) at 400°C.....	67
<b>Table (3.23):</b> The FWHM and integral breadth ( $\beta$ ) of the lines (111), and (200) at three different temperatures .....	68
<b>Table (3-24):</b> The values of $\beta$ for profile lines (111), and (200) at three different temperatures .....	68
<b>Table (3.25):</b> The results of crystallite size for two lines profile of the NiO at three different temperatures .....	69

### List of Abbreviations

XRD	X-Ray Diffraction
FCC	Face-Centered Cubic
TC	Texture Coefficient
MI	Morphology Index
SSA	Specific Surface Area
FWHM	Full-Width at Half-Maximum intensity
W-H	Williamson-Hall
SSP	Size-Strain Plot
H-W	Halder-Wagner
JCPDS	The Joint Committee on Powder Diffraction Standards
NiO	Nickel Oxide

### List of Symbols

$\lambda$	Wavelength
n	Integer number
$d_{hkl}$	Inter planer spacing
hkl	Miller indices
$\beta$	Integral breadth
A	The peak area
I	Intensity
$\theta$	Reflection angle
$2\theta$	Diffraction angle
D	The crystallite size
$\varepsilon$	Lattice strain
K	Scherrer constant
$\delta$	The dislocation density
SSA	The specific surface area
$\rho$	The density
V	part Particle volume
SA	part Surface area
T	Temperature

# *Chapter One*

*Introduction and literature*

*Review*

## 1.1 INTRODUCTION

Nickel oxide NiO is an important transition metal oxide with cubic lattice structure. It has attracted increasing attention owing to its potential use in a variety of applications; NiO as a semiconductor is a motivating topic in the new area of research, because of its properties distinguished it from others [1].

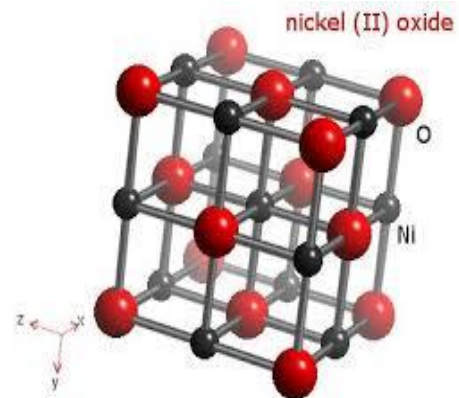
Nickel(II) oxide is the chemical compound with the formula NiO. It is notable as being the only well-characterized oxide of nickel (although nickel(III) oxide, Ni<sub>2</sub>O<sub>3</sub> and NiO<sub>2</sub> have been claimed) [2]. The mineralogical form of NiO, bunsenite, is very rare. It is classified as a basic metal oxide. Several million kilograms are produced in varying quality annually, mainly as an intermediate in the production of nickel alloys [3].

Chemical formula	NiO
Molar mass	74.6928 g/mol
Appearance	green crystalline solid
Density	6.67 g/cm <sup>3</sup>
Melting point	1,955 °C (3,551 °F; 2,228 K)
Solubility in water	negligible
Solubility	soluble in KCN
Magnetic susceptibility ( $\chi$ )	+660.0·10 <sup>-6</sup> cm <sup>3</sup> /mol
Refractive index ( $n_D$ )	2.1818

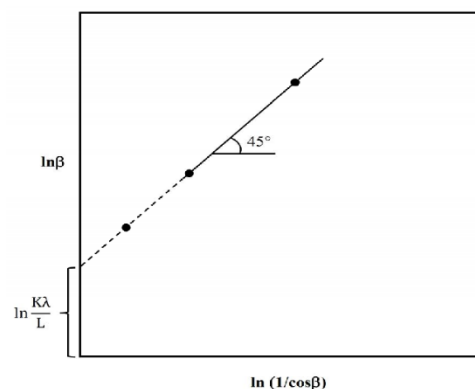
NiO can be prepared by multiple methods. Upon heating above 400 °C, nickel powder reacts with oxygen to give NiO. In some commercial processes, green nickel oxide is made by heating a mixture of nickel powder and water at 1000 °C, the rate for this reaction can be increased by the addition of NiO [4]. The simplest and most successful method of preparation is through pyrolysis of a nickel(II) compounds such as the hydroxide, nitrate, and carbonate, which yield a light green powder[2]. Synthesis from the elements by heating the metal in oxygen can yield grey to black powders which indicates nonstoichiometry[2].



NiO adopts the NaCl structure, with octahedral Ni<sup>+2</sup> and O<sup>-2</sup> sites. The conceptually simple structure is commonly known as the rock salt structure. Like many other binary metal oxides, NiO is often non-stoichiometric, meaning that the Ni:O ratio deviates from 1:1. In nickel oxide this non-stoichiometry is accompanied by a color change, with the stoichiometrically correct NiO being green and the non-stoichiometric NiO being black.



X-ray diffraction is the most appropriate way to understand the crystallite structure and to determine the average size of the nano particles in nano materials. Paul Scherrer was published in 1918 what known as the Scherrer formula. Scherrer Equation was developed in (1918) to calculate the crystallite size (D) for Nano materials using the full width at half maximum value of the peaks in the X-ray diffraction pattern. Scherrer equation is defined as ( $D = \frac{k\lambda}{\beta \cos\theta}$ ). Shape factor (k) can be (0.62 to 2.08) depending at the crystal shape and it is usually take as (0.89) for the spherical crystal. For a crystallite size of 5 nm and a Cu-K $\alpha$  source of 0.1540 nm wavelength the peak width at  $2\theta = 170^\circ$  should be 10 times wider that that at  $2\theta = 10^\circ$ . The aim of modifying the Scherrer equation is to provide a new approach for calculating (D) with less error. In modified Scherrer method, by plotting  $\ln\beta$  versus  $\ln(\cos\theta)^{-1}$ , the intercept found. The (D) value obtained from the available peaks. While the errors related with experimental data, a smallest squares manner gives the better slope with most exact ( $\ln K/D$ ). The exponential of the intercept found after getting the intercept [5].



Scherrer-equation depends on  $1/\cos\theta$ , unlike W-H method that depends on  $\tan\theta$ . This basic difference due to both microstructures results in a small crystallite size and micro strain together from the reflection broadening. Regarding different  $\theta$  positions, the separation of crystallite size and strain broadening analysis was made using Williamson – Hall method. The results below are the addition of Scherrer equation and  $\varepsilon \approx \beta_{hkl} / \tan\theta$  [6].

Williamson–Hall plotting is a simple technique to link the contributions of crystallite size and lattice strain to the peak broadening in the X-ray diffraction patterns. Williamson–Hall plotting is a simple way to separate the contributions of both micro strain and particle size to the line broadening in the X-ray diffraction patterns with Lorentzian profiles. A practical application of this method includes plotting  $(\beta\cos\theta)$  versus  $4\sin\theta$ . As the sample reveals a homogeneous distribution of both micro-strain and crystallite size, the Williamson–Hall plot appears as a straight line. Linear function used to fit the chart and offers determine the lattice strain value from the slope and the crystallite size from the intercept with the axis. A positive slope refers to lattice expansion, while the negative slope refers to lattice compression. A horizontal slope shows refer to the crystals which means (particles free of lattice strain) [7].

The Size-Strain plot method has an important advantage over other methods. Therefore, less importance is assumed to the great angle peaks which supposed that (strain profile) is controlled by the Gaussian function [8].

Halder-Wagner method is used to determine the particle size from x-ray diffraction data. In this method, the slopes yield the (H-W) particle size, and the intercept gives the (H-W) lattice strain. However, the (H-W) method is known to be limited compared to the (W-H) method [9].

By using these methods, we can notice the differences between obtained values of the crystallite size (D) and the lattice strain, then determine the best analysis way .

## 1.2 Literature Review

**In (2008) Mikrajuddin Abdullah and Khairurrijal, [10]** Derived the Scherrer relation using a “multi slits interference” approach studied in basic physics course. They found that the dependence of the size of the crystals on the height of the XRD peak is consistent with the original Scherrer formula. Simple procedure for using Scherrer formula to predict crystal sizes from  $Y_2O_3$  material is also discussed.

**In (2008) V. Biju Neena, et al, [11]** Used Williamson-Hall method analysis with uniform distortion, uniform distortion stress and uniform distortion energy density models to estimate that the micro strain in nano crystalline Silver samples with an average particle size of about (50 nm) related to the XRD line broadening. While separating the contributions of both the particle size and strain to the line broadening, the anisotropy of the crystallite size considered. The lattice strain properly modeled using a uniform deformation energy density model. The results of the lattice strain that obtained from the inter-planar spacing data compared with those of a uniform energy density model. The lattice strain in a nano crystalline silver showed contributions from dislocations over the contribution from additional volume of grain boundaries related to both vacancies and vacancy clusters.

**In (2009) B .G .Jeyaprakash, et al, [12]** Studied the X-ray diffraction (XRD) of the polycrystalline CdO phase along (111) plane. X-ray line expansion technique used to study the effect of substrate temperature on the particle size and micro strain, using Williamson–Hall method .

**In (2012) Gh.H. Khorrami, et al, [13]** Produced Pure and X doped zirconate Titanate Nano particles (PZT-NPs) (X = Mg, Mn, and Zn) chief by using sol-combustion method. Xerogel calcined at (700 ° C) for (2 hours). The resulted powder structure characterized by X-Ray Diffraction (XRD) and Fourier analysis

of infrared (FTIR). X-Ray diffraction results display that the (PZT-NPs) of a perovskite structure and rhombohedral phase. Furthermore, a small shift noticed in (XRD) patterns of doped (PZT-NPs). X-ray diffraction results examined by Size Strain Plot (SSP) to estimate the micro strain for gastric specimens, which exposed that the micro strain depends on the ionic radius of the dopants.

**In (2014) Fujio Izumi, et al, [14]** Stated that the microstructural determination is very important aspect in understanding the physical and chemical properties of polycrystalline materials, especially in the field of nanotechnology. RIETAN-FP which is the latest version of a multi-purpose pattern-fitting system provide new features of Williamson–Hall and Halder–Wagner approaches to estimate crystallite sizes and micro strains from the integral breadths that evaluated using the Rietveld and/or Le Bail analysis of the X-ray and neutron powder diffraction data. In this method, the contributions of instrumental broadening deducted with experimental results of instrumental standards displaying insignificant sample broadening. The graphical representation of linear relationships: ( $\beta\cos\theta$  vs.  $\sin\theta$ ) in the Williamson–Hall plot and ( $(\beta/\tan\theta)^2$  vs.  $\beta/(\tan\theta \sin\theta)$ ) in the Halder–Wagner plot is represented by Gnu plot. The resultant figure shows the deviations from the linear relationships. By using these two approaches, the mean crystallite size (D) of a microcrystalline  $\text{CeO}_2$  sample was determined at 29.96 nm for Williamson–Hall and 28.92 nm for Halder–Wagner, which are consistent with the results reported for the round-robin sample.

**In (2014) A. Gaber, et al, [15]** Synthesize crystalline tin dioxide nano particles by adding ammonia solution ( $\text{NH}_4\text{OH}$ ) to a solution containing tin chloride pentahydrate ( $\text{SnCl}_{4.5}\text{H}_2\text{O}$ ). The products characterized by X-ray diffraction (XRD), Scanning Electron Microscopy (SEM) and High Resolution Transmission Electron Microscopy (HRTEM). The results indicate that the size of the crystals increases from (3.45 to 23.5 nm) as the temperature of the calcination increases from (300 ° C to 1050 ° C). The (XRD) analysis shows a

rutile tetragonal phase of the SnO<sub>2</sub>. Developed the crystallinity because of decrease of (lattice distortion ratio and dislocation density) as the calcination temperature is increases. Calculate surface area and porosity of SnO<sub>2</sub> nano particles. The specific surface area decreases from (140 m<sup>2</sup>/g at 100 °C) to (8.3 m<sup>2</sup>/g at 1050 °C) related to pore volume.

**In (2014) Hiten Sarma and K.C. Sarma, [16]** Prepared ZnO nano particles in a precipitation process of ammonia and zinc chloride in aqueous solutions of pH (8.0). The nano particles then manufactured by heating the precursors in an overcast oven at (623 K) for (3 hours) then allowed for cool until (room temperature). The achieved (ZnO) nano particles were characterization using scanning electron microscopy (SEM), X-ray diffraction (XRD), and X-ray dispersion analysis (EDAX). Results of (XRD) reveal that the samples are of a hexagonal structure with a wurtzite crystalline phase. The X-ray expansion method used to calculate the particle size with micro strain in the Williamson-Hall analysis method (W-H). The physical parameters like a pressure, stress and energy density determine by using (W-H) analysis method with different models, such as the model of uniform distortion, model of uniform distortion stress and model of uniform distortion energy density.

**In (2014) Mohammad Ramzan Parra and Fozia Z. Haque, [17]** Synthesized ZnO nano particles by simple aqueous chemical route without the involvement of any capping agent to control the particle size. The effect of different calcification temperatures on the size of ZnO nanoparticles was studied. The results of x-ray diffraction indicated that all samples had a wurtzite crystalline phase, and peak expansion analysis used to evaluate the average particle size and micro strain using the Scherrer equation and the (W-H) method. Investigated Morphology and elemental compositions using Atomic Force Microscopy (AFM), Scanning Electron Microscopy (SEM), and Energy-Dispersive X-ray (EDX) spectroscopy. Estimated the average particle size of ZnO nanoparticles,

by the Scherrer's method and (W-H) analysis found that the particle size increase with the increase in calcination temperature. These results agree with (AFM) results. The optical properties that examined using (UV) spectroscopy in diffraction reflection (DR) mode, with a sharp increase in reflection at (375 nm). The material has a strong reflective property after (420 nm) at (500 ° C). This study suggests that ZnO nano particles prepared with band gap control used as a window layer in optical electronic devices.

**In (2014) L Motevalizadeh, et al, [18]** Manufactured ZnO nano rods at low temperature by water heating (0.1 M) of ZnCl<sub>2</sub> for (5, 10 and 15 h) at pH of (10). No template, grains substrate, catalyst and autoclave used to synthesize ZnO nano rods. The result of heating periods on the structure crystal orientation with crystallization studied by using the X-ray and scanning electron microscope, respectively. Images of (SEM) showed the formation of flower-like structures in a (5-hour) thermally heated sample, while hexagonal zinc oxide nano rods optimized to optimize time of growth. (XRD) results have shown that the chosen orientation of nano rods controlled by hydrothermal processing time. The crystal size and micro strain analyzed by (W-H) method and (H-W) method. The results exposed the presence of some errors at (ZnO) nano rods. However, these errors in crystal size and lattice were reduced by increasing the time of hydrothermal process.

**In (2014) P. Bindu and Sabu Thomas, [19]** Synthesized (ZnO) nano particles from zinc chloride with chitosan by precipitation technique. The composite nano particles of (ZnO) characterized in Fourier analysis of ultraviolet spectroscopy, (XRD) analysis, Scanning Electron Microscopes (SEM), Transmission Electron Microscopy (TEM), and optical fluorescence. The samples have crystallized and a hexagonal phase revealed by (XRD) results. They have studied the evolution of crystals at (ZnO) nano particles by analysis of X-ray peak. (W-H) and (SSP) analysis used to study different contributions of particle size with micro strain on

the peak expansion of (ZnO) nano particles. the value of stress, pressure and energy density were determined for all peaks of the (XRD) peak corresponding to the hexadecimal phase of the Z-O of ZnO located in the range (20-80) using a uniform form of (W-H) plots and the (SSP) method. Results revealed that the estimated particle size of the Scherrer method, the (W-H), the (SSP), and the estimated particle size of the (TEM) are highly correlated. (XRD) and (SEM) provide a smaller deviation between the size of crystals and particle size at current state.

**In (2015) Tamil Many K. Thandavan, et al, [20]** Presented the synthesis of ZnO nanowires (NWs) via a vapor phase transport method (VPT) aided with a thermal evaporation of brass (CuZn). Field emission scanning electron microscope (FESEM) and X-ray diffraction (XRD) were used to investigate the effects of aliphatic alcohols such as ethanol and methanol as sources of oxygen on the morphological and structural properties of synthesized ZnO NWs. Two types of ZnO/NWs were synthesized based on ethanol and methanol alcohols such as ZnO / ENWs . ZnO / MNWs, respectively. Debye Scherer (DS) , Williamson–Hall (W-H) and size–strain plot (SSP) investigation on the XRD peak broadening showed that ZnO / MNWs exhibited lower strain and stress value compared to ZnO / ENWs . ZnO / MNWs with a (002) crystallographic orientation found to be a hexagonal isotropic crystalline structure, whereas ZnO / ENWs with a (101) crystallographic orientation is anisotropic crystalline structure.

**In (2015) L. B. Patle, et al, [21]** Prepare pure and doped  $Ti_{1-x}Cu_xO_2$  nanoparticles with a nominal compound of (0.0, 0.01, 0.02, and 0.03) at room temperature via coagulation technique. The precursors calcined from in the range (500 - 600) °C for 6 hours in the furnace resulting in the formation of different combinations of  $TiO_2$  phase. Structural analysis conducted by X-ray diffraction (Bruker D8 Cu- $K\alpha_1$ ). X-ray peak expansion analysis used to evaluate the crystal volume, lattice parameters, number of unit cell per particle, (C / A) ratio and unit cell volume.

Williamson-Hall analysis used to find the grain size and strain of TiO<sub>2</sub> nanoparticles. The X-ray diffraction analysis confirmed the crystalline structure of TiO<sub>2</sub> with a tetragonal anatase phase. The grain size of pure and doped copper samples found within (10 nm to 18 nm). All the physical parameters of TiO<sub>2</sub> tetragonal nano particles were calculated more accurately using the modified (W-H) model of uniform deformation model (UDM). The calculated results were almost identical with the standard values.

**In (2016) Hossein Mahmoudi Chenaria, et al, [22]** Synthesized ZnO nano particles and La-Zr nano tubes using a sol-gel technique, and the zinc acetate remover (Zn (Ac)<sub>2</sub>H<sub>2</sub>O), hexahydrate nitrate lanthanum (La<sup>+3</sup>) and (6 H<sub>2</sub>O) and zirconium chloride (ZrCl<sub>4</sub>) as precursors. The structure and morphology of the prepared nanoparticles were studied using X-ray diffraction and transmission electron microscope. X-ray diffraction results indicated that all samples had the crystalline wurtzite phase. The microscopic effects of crystalline materials in terms of crystal sizes and lattice strain studied on peak expansion using the Williamson-Hall analysis (W-H) and the Size-Strain Plot method (SSP). The average crystalline size of the Zn<sub>(1-x)</sub>La<sub>x</sub>Zr<sub>x</sub>O Nano particles differed from Williamson-Hall and Size-Strain Plot analysis with increased doping concentration. The combination of Zr<sup>4+</sup> ion in place of Zn<sup>2+</sup> caused an increase in the size of the nanoparticles compared to the non-dependent ZnO.

**In (2016) Francisco Tiago L. Muniz, et al, [23]** Calculated the particle sizes of (Si, LaB<sub>6</sub> and CeO<sub>2</sub>) using the dynamic theory of (XRD). The full width at half the maximum then extracted and the crystallite size is calculated using the Scherrer equation. The Scherrer equation appears to be valid for crystallites of sizes up to (600 nm) for crystals with a linear absorption rate of less than (2117.3 cm). It is also clear that the larger the volume, the higher the peaks of the data give good results, If one uses peaks with ( $2\theta > 60^\circ$ ), the maximum use of Scherrer equation will rise to (1  $\mu$ m).

**In (2017) R. G. Solanki, et al, [24]** Characterized and estimated the micro strain and particle size CdS nano particles by X-ray peak analysis. CdS nano particles manufactured in a non-aqueous thermal process and characterized by (TEM), (XRD), Raman and ultraviolet visible spectra. (XRD) asserts that the (CdS) Nano particles have a hexagonal structure. (W-H) method was used to study the X-ray peak analysis of the profile. (SSP) method used to study separate contributions of the crystalline size and micro strain of X-ray peaks. Stress, strain, and energy intensity values were determined using different models, such as (an isotropic strain model, isotropic strain model, and a uniform distortion intensity model). The results confirm that the calculated crystalline size of (W-H), Scherrer, and (SSP) are consistent with those determined by (TEM) images.

**In (2017) Toshiro Sakae, et al, [25]** Illustrated a laboratory that uses (XRD) technology to analyze human bone metals and the variation in the size of the crystals in a small bone mass. The bone trephine rod pulled small dorsal cortex blocks. The micro-XRD patterns showed broaden peaks, but the (FWHM) was obtained from the diffraction peak of (200). The values showed a wide aberration, indicating crystal length of (12.4 nm) to (18.5 nm). The value of FWHM in adjacent areas was observed closely within a single small bone mass separated by only (1 mm). These findings indicate that the crystals in the bone may vary in size from to the parts due to bone remodeling and tissue texture.

**In (2017) Tetiana Tatarchuk, et al, [26]** Prepared (Zn-doped  $\text{CoFe}_2\text{O}_4$ ) Nano particles (NPs) by the chemical co-precipitation route. The structural magnetic and optical properties of  $\text{CoFe}_2\text{O}_4$  nanoparticles were examined with respect to Zn content. Both (XRD) and (FTIR) analysis confirm the formation of a cube spinel phase, where the crystal size varies from (46 -77 nm) with (Zn) content. The crystals size was studied by means Scherrer method, (W-H) method, and (SSP) method. The results of (TEM) are in a good agreement with (SSP) method. (SEM) images reveals that the surface is of spherical particles. Zn doping

concentration remarkably enhances the magnetic properties of the sample where the saturation magnetization ( $M_s$ ) increases then decreases along with continuously decrease of both coercivity ( $H_c$ ) and remnant magnetization ( $M_r$ ). This related to the change in the particle size and preferential site occupancy.

**In (2017) B. Rajesh Kumar and B. Hymavathi, [27]** Used a conventional solid-state reaction method to fabricate (ZnO) doped with different concentrations of Al (2wt%, 4wt%, 6wt%, 8wt% and 10wt%). The (XRD) results showed that the samples crystallized with a hexagonal wurtzite phase. With increasing concentration in (ZnO), the (XRD) peaks shift to a higher angle. This shift in the peak position and decreases in its intensity were due to the successful replacement of Zn in the (ZnO) matrix. X-ray peak expansion analysis used to evaluate the particle size and the micro strain by both (W-H) and (SSP) methods. Stress, strain, and energy density values were determine using (W-H) method with different models, such as a standard uniform distortion model, a uniform stress distortion model, and a uniform energy distortion intensity model.

**In (2018) Shashidhargouda H. R. and Shridhar N. Mathad, [28]** Described the synthesis and the structural properties of ( $Ni_{0.45}Cu_{0.55}Mn_2O_4$ ) nano powder, obtained by co-precipitation. The X-ray diffraction pattern reveals a cubic structure with a lattice parameter of (8.305 Å). They also reported the size of the crystals ( $D$ ), the lattice strain ( $\epsilon$ ), the dissociation density ( $\rho_D$ ), the lengths of mobility ( $L_A$  and  $L_B$ ), and the preferential trend in tissue treatments  $T_c$  (h k l). The Williamson Hall plot and the stress plot used to understand the mechanical properties of materials.

**In (2018) Francisco Marcone Lima, et al, [29]** Reported on using of modified Scherrer formula to estimate the size of nanomaterials more accurately. Titanium dioxide powder with a Nano size structure of about (21 nm) used as a reference standard for determining the accuracy of the modified equation. From X-ray diffraction data, the average crystalline size achieved at about (20.63 nm) for the

non-heated sample. To establish a relation between the obtained result with the modified Scherrer equation and the mean nominal crystal size, a statistical treatment and comparative evaluation performed. The average absolute spacing does not exceed (0.70 nm). The value of the crystallized volume of x-ray data was in good agreement with those reported by the supplier. In addition, the sample behavior studied as a function of temperature.

**In (2018) Rashi Gupta, et al, [30]** Used an electrode position technique coupled with a template synthesis method to fabricate copper nanowires with a 200 nm diameter into the pores of a polycarbonate track-etched (PCTE) membrane. The synthesized Cu nanowires were irradiated with 150-MeV  $\text{Ti}^{+9}$  swift heavy ions at Inter University Accelerator Centre (IUAC), New Delhi, India. (XDR), scanning electron microscopy (SEM), EDS, and Keithley (2400) series source meter were used to study the structural, morphological, and electrical properties, respectively. X-ray diffraction analysis confirmed a cube-centered crystal structure for as prepared irradiated samples. The lattice strain and crystalline size were estimated using line expansion analysis methods and the modified Scherrer equation. Young's modulus and the stress generated in the nanowires were theoretically calculated. A change in the electrical conductivity of nanowires observed with an increase in flounce attributable to the change in the direction of grain boundaries and the formation of defects.

**In (2018) Mosayeb Geravand and Farid Jamali-Sheini, [31]** Grew the nanomaterials of the unsaturated Silver Sulphide and Aluminum (Al) by using a sonochemical method. Samples studied using different identification methods including (XRD), (FESEM), (PL), Raman spectroscopy and (UV-vis). The results showed that the addition of Al dopant converts the diffraction peaks to higher angles and reduces their intensity. In addition, the size of Nano crystalline crystal has been reduced compared to the undamaged sample. Stress in drug samples found to be greater than the non-narcotic sample using the Hall-Williamson (W-

H) method. The effect of parameters that affect the crystalline and optical properties of the material on the growth process investigated using Raman analysis.

**In (2018) B. Rajesh Kumar and B. Hymavathi, [32]** Synthesized ZnO with  $\text{Sb}_2\text{O}_3$  (2, 4, 6, 8 and 10% weight) with conventional solid state reaction. The intensity of the (XRD) intensity is sharp and narrow, confirming that the sample is of high quality with good crystallization. The full supply intensity decreases at peak X-ray reflection at the maximum (100) and (101) with increasing  $\text{Sb}_2\text{O}_3$  dopant in ZnO. A personal X-ray peak analysis used to evaluate the size of the crystalline and lattice strain through the Williamson-Hall (W-H) method. Using models such as the Uniform Deformation Model (UDM), the Uniform Stress Deformation Model (USDm) and the Uniform Deformation Energy Density Model (UDEDm) for the (W-H) method, physical parameters such as stress, pressure and energy density values were calculated.

**In (2018) H. Irfan, et al, [33]** Prepared  $\text{CoAl}_2\text{O}_4$  Nano particles by a Pechini method Using Citric Acid Claw Agent.  $\text{CoAl}_2\text{O}_4$  nanoparticles manufactured at different calcification temperatures ranging from (600-900 °C). The cubic phase of crystalline spinel confirmed by (XRD) results. The Williamson-Hall (WH) method and the Size-Strain Plot (SSP) method were used to assess the size of the crystals and the strain in the expansion of  $\text{CoAl}_2\text{O}_4$  nanoparticles. Physical parameters such as pressure and stress values for all XRD reversal peaks corresponding to the  $\text{CoAl}_2\text{O}_4$  spinel phase were calculated in the range of (20 to 70 )degrees from the shape of a piece modified by the (WH) scheme, assuming a uniform distortion model, the uniform distortion model (USDm) UDEDm), the (SSP) method. The size of the  $\text{CoAl}_2\text{O}_4$  NPS crystals calculated on the (WH) and (SSP) patterns corresponds to the good compatibility with (HRSEM) and Scherrer.

**In (2018) Hosein Kafashan** [34] Prepare undoped and Se-doped (SnS) thin film by used an electromechanical method. Six specimens including undoped and Se-doped SnS thin films deposited on the activated oxide glass oxide substrate. A water solution containing (2mM SnCl<sub>2</sub>) and (16mM Na<sub>2</sub>S<sub>2</sub>O<sub>3</sub>) used in electrolyte. Prepared changed (SnS) Se-doped samples by adding different depths of (4 Mm SeO<sub>2</sub>) solution to the electrolyte. The practical properties (E), sedimentation time (t), temperature of bath (T), and pH, were maintained in (-1) V, (30) minutes, (333 K), and (2.1) respectively. Next the sedimentation process was completed, x-ray diffraction (XRD) and TEM were used to describe the deposited in the deposited fins. (XRD) patterns showed clearly that the synthetization of thin and (SnS) synthesized non-anesthetic and anesthetized se at the orthopedic structure. Calculated the crystallite size of the deposited by using the Scherrer method. The size of the crystal and the micro strain determine by using a uniform form of (WH) method inclosing a uniform distortion pattern, a uniform distortion stress model, a uniform distortion density pattern, and by (SSP) method. The (Sns) crystals shaped spherically in images of (TEM). The results revealed good agreement on particle size gotten from the (W-H) method, (SSP) method, and images of (TEM).

**In (2019) Ahmed A. Al-Tabbakh, et al**, [35] manufactured using the sol-gel method of rechargeable lithium battery, ball of high-energy grinding is performed on (Li<sub>1.1</sub>Mn<sub>1.95</sub>Fe<sub>0.05</sub>O<sub>4</sub>) Spinel, at various times to obtain micro powders of limited size distributions. The powders examined by scanning electron microscope, particle size distribution, and X-ray diffraction measurements (XRD). Performed powders structural analysis to study the milling effect on crystallite size, and micro strain. The image of scanning electron microscopy with volume supply measurements show that crystallite size reductions with increased grinding time. Results of (XRD) show that the width of the diffraction peaks increases with reduced crystallite size (increasing the duration of the milling).

This expansion examined by to Scherrer method, (W-H) method, and (H-W) methods. The peak expansion accredited to contributions of particle size with micro strain. However, reducing crystallite sizes is required to reach a greater specific capacity with density of energy for the dynamic material of the battery, lattice strain results in material squalor and reduced retention of capacity. Therefore, while mechanical grinding performed, a poetic strain taken extremely in order to improve grinding standards with improve the electrochemical feat of the material.

### **1.3 The Aim of the Work**

- 1- Camper between three analysis X-ray diffraction methods.
- 2- Modified a better method among these methods to calculate the crystallite size and lattice strain.
- 3- Calculated the physical and lattice parameter by using a better method.
- 4- Studying the effect of calcination temperature on the crystallite size and the lattice strain.

# *Chapter Two*

## *Theoretical Part*

## 2.1 Introduction

This Chapter includes the method that used for calculate the full width at half maximum (FWHM) and integral breadth ( $\beta$ ) with distinguish between (FWHM) and ( $\beta$ ) (which is dependent on the X - ray diffraction method with the Bragg's law). Also, includes the methods of analysis X-ray line profile to calculate crystallite size and lattice strain such as Scherrer method, modified Scherrer method, and Williamson –Hall method, Size-Strain plot method, and Halder-Wagner method. Furthermore, calculation method some of lattice parameters and physical factors. Studying the effect of calcination temperatures on the (D) and ( $\epsilon$ ). Developed Halder-Wagner method to calculate a new parameters for example the stress and lattice energy.

## 2.2 X-Ray diffraction

X-ray diffraction analysis (XRD) is an effective way for examining ultrafine-grained materials (UFG) structure properties, and provides information about the crystal lattice system, lattice parameter, texture, etc. Furthermore, quantitative estimates of crystallite size and lattice strain can be obtained from peak broadening. In fact, diffraction lines for ultrafine-grained materials (UFG) are broader than that found in coarse granules (CG). The presentation of the experimental line is the result of three contributions, which are the coherence length (or crystallite size), internal poetic abnormalities and beneficial effects. A reduction in crystallite size or improved strains leads to widely broader diffraction lines [36].

X-ray diffraction lines analyzed by using analytical program such as (Origin). In this method. obtained of the area under the curve for all the curves to the x-ray diffraction pattern of NiO powder , as shown in figure (2.1).

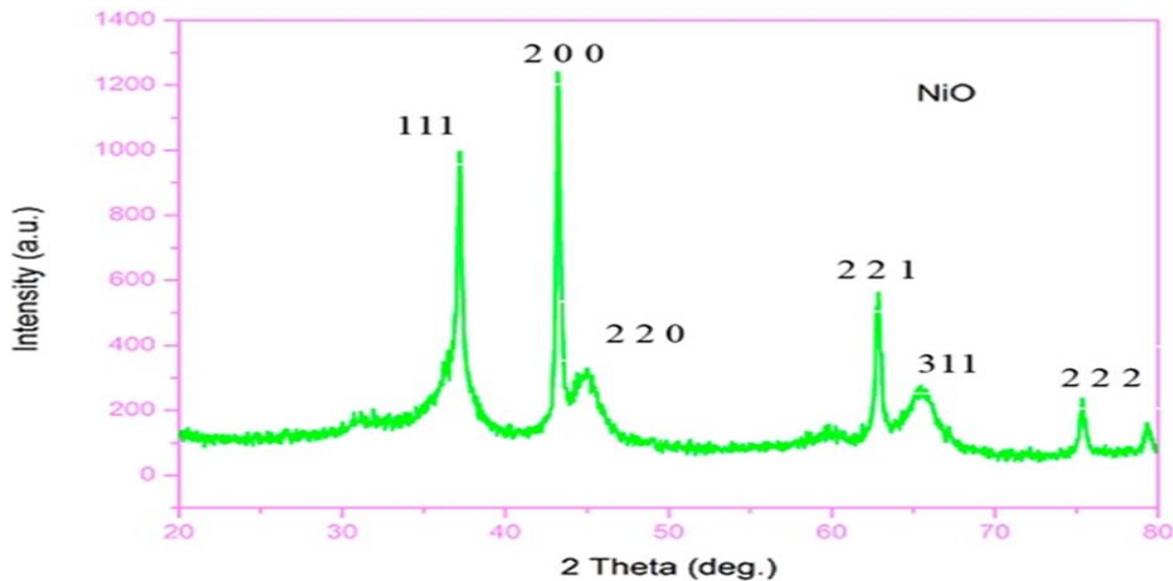


**Figure (2.1):** X-ray diffraction pattern of NiO powder [37].

Three methods used for (XRD) analysis including :- (powder diffraction, single crystal (XRD), and grazing incidence diffraction). In these techniques, the monochromatic x-ray beam is used. X-ray diffraction analysis is a suitable technique to analyze the structural properties and phase of individual crystals and crystalline materials. It is very important to study the mechanical actions of micro-scale / nanoscale structures of the electronic devices. The mechanical properties of metals depend on the feature size. For instance, the yield strength of Au increases by 80 times, when its dimensions decrease to smaller than  $1\mu\text{m}$  due to the dislocation starvation effect. According to this effect, dislocation defects may be eliminated without any interferences with other defects and gliding along their planes to the surfaces. In addition, the crystallite size of the particles differed from the particle size owing to the existence of the grain boundaries and/or polycrystalline aggregates. [38].

Methods principle based on (XRD) by serial atomic planes with angle or detect the power solution of the diffraction signal. The Engineering Interpretation of X-ray diffraction (constructive interferences) given by W .L. Bragg. Figure (2.2)

gives the details about the determination of Bragg's law with the diffraction geometrical condition. Bragg's law given in:

$$n \lambda = 2d \sin \theta \quad (2.1)$$

where,

- $n$  is the diffraction order
- $\lambda$  the incident beam wavelength in nm
- $d$  the inter planer distance in nm
- $\theta$  the reflection beam angle in degree

In polycrystalline, an impermeable material with very small grains, the diffraction happens for each lattice flat surface with direction that meets the Bragg's law in the constructive interferences case.

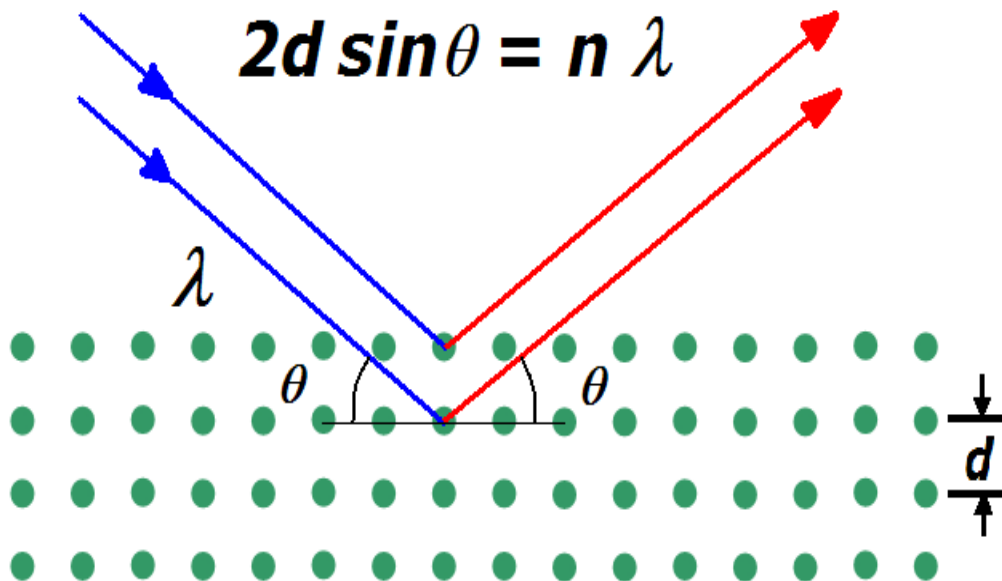


**Figure (2.2):** Geometrical condition for diffraction from lattice planes [39].

### 2.3 The Full Width at Half Maximum (FWHM)

Generally, the diffraction data is represented as a distribution function of angle ( $2\theta$ ), as in Figure (2.3).

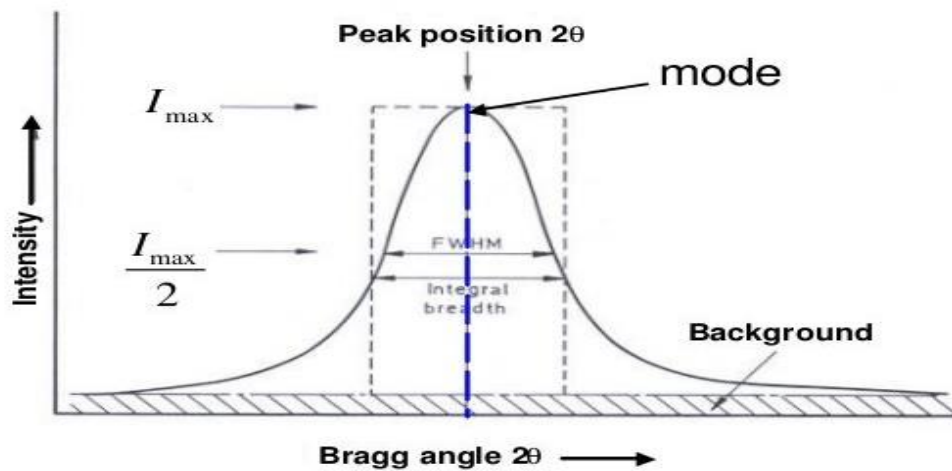


**Figure (2.3):** Diffraction peak and information content that extracted [39].

The maximum peak intensity ( $I_{\max}$ ) and the integrated intensity  $I$  (i.e., area under the peak) were defined after the background subtraction. The peak position calculate by numerous ways (fit of changed mathematical function, center of gravity, etc). The width of peak can generally be marked either by the Full Width at Half Maximum (FWHM) relating with the largest width peak at half the greatest intensity, or by the Integral Breadth (IB) which relates with a rectangular display of the similar highest density and integral as the measured peak. Different peak parameters used depending on the measurements purpose [39].

## 2.4 Analysis methods of X ray diffraction

### 2.4.1 Scherrer method

Scherrer's equation derived for a perfect case of parallel, extremely narrow and monochromatic (X-ray) beams that incident on the monodisperse powder of the crystals in the form of a cube, the equation is [40]:

$$\beta_{hkl} = \frac{k\lambda}{D\cos\theta} \quad (2.2)$$

$$D = \frac{k\lambda}{\beta_{hkl}\cos\theta}$$

Where,

$D$  is the mean size of the ordered (crystalline) domains, which may be smaller or equal to the crystallite size.

$K$  is a dimensionless shape factor, with a value close to unity. The shape factor has a typical value of about 0.9, but varies with the actual shape of the crystallite.

$\lambda$  is X-ray wavelength .

$\beta_{hkl}$  is the line broadening at half the maximum intensity (FWHM), after subtracting the instrumental line broadening, in radians . This quantity also sometimes denoted as  $\Delta (2\theta)$ .

$\theta$  is Bragg's angle.

It is important to note that Scherrer equation can only be applied to medium sizes of about (100-200) nm (depending on the instrument, sample ratio and noise signal), because the diffraction-peak expansion decreases with increasing crystal size. Equation (2.2) used to determine the ( $D$ ) while, Equation (2.3) used to determine the ( $\varepsilon$ ) [41].

$$\varepsilon = \frac{\beta_{hkl}}{4\tan\theta} \quad (2.3)$$

### 2.4.2 Modified Scherrer method

Modified Scherrer equation can support the advantage of reducing the amount of errors absolute values,  $\sum(\pm\Delta \ln\beta)^2$  with creating one line through the points to give one value for the  $(\ln k \lambda / D)$  intersection. Taking the logarithm of both sides in equation (2.2), we get equation (2.4). By drawing the results of  $\ln\beta$  versus  $\ln$  (inverse  $\cos \theta$ ), the slope of the straight line y-axis represents  $\ln (k\lambda / D)$ . Equation (2.4) used to determine the (D) [42].

$$\ln\beta_{hkl} = \ln \frac{k\lambda}{D} + \ln \frac{1}{\cos\theta} \quad (2.4)$$

$$\ln \frac{k\lambda}{D} = \ln\beta_{hkl} - \ln \frac{1}{\cos\theta}$$

$$\text{slope} = \ln \frac{k\lambda}{D}$$

$$\frac{\lambda k}{D} = e^{\text{slope}}$$

### 2.4.3 The Williamson- Hall method

A simple way to separate the crystallite size and lattice strain contributions in the peak broadening in (XRD) patterns is Williamson-Hall method (WH). This analysis assumes that the crystallite size (D) and lattice strain ( $\epsilon$ ) contribute to the line broadening with Lorentzian profiles described by equation (2.5):

$$\beta_{hkl} \cos\theta = \left(\frac{k\lambda}{D}\right) + (4\epsilon \sin\theta) \quad (2.5)$$

The practical application of the W-H plotting involves the construction of plotting  $\beta/\lambda\cos\theta$  against  $\sin\theta$ . (WH) plot has a straight line when the sample reveals a homogeneous distribution for the crystallite size and lattice strain. The diagram can be fitted by a linear function that requires from the slope of the lattice strain value and the crystallite size towards y-axis. The positive slope shows increased lattice, the negative slope shows decreased lattice, while the horizontal slope

shows (particles free of lattice strain) perfect crystals. From equation (2.5) extracted (D) and ( $\varepsilon$ ) [43]:

If ( $\varepsilon$ ) = 0

Therefore,

$$\frac{k\lambda}{D} = \beta_{hkl} \cos\theta$$

$$\beta_{hkl} \cos\theta = y\_intercept$$

$$D = \frac{k\lambda}{\beta_{hkl} \cos\theta} = \frac{k\lambda}{y\_intercept}$$

If (D) =  $\infty$

Therefore,

$$(4\varepsilon \sin\theta) = \beta_{hkl} \cos\theta$$

$$\varepsilon = \frac{\beta_{hkl} \cos\theta}{4 \sin\theta} = slope$$

#### 2.4.4 The Size-Strain plot method

The conforming of (W–H) plots explained that line expansion was isotropic. This focuses on the fact that the bending areas were specific due to contribution of lattice strain. In the case of expansion of the characteristics line, the best calculation of the size-strain parameters found by considering the mean Size-Strain Plot. This method has a less important feature of data than reflections at high angles, where accuracy is usually much lower. In this way, assumed that the crystallite size profile expressed by a Lorentzian role and the strain profile by a Gaussian role. Therefore, we have:

$$(d_{hkl} \beta_{hkl} \cos\theta)^2 = \left(\frac{k}{D}\right)^2 (d_{hkl}^2 \beta_{hkl} \cos\theta) + \left(\frac{\varepsilon}{2}\right)^2 \quad (2.6)$$

The crystallite size is calculated from the linearly fixed data slope and the strain maybe calculate from the root of y-intercept [44].

If ( $\varepsilon = 0$ )

$$D = \frac{k(d_{hkl}^2 \beta_{hkl} \cos\theta)}{(d_{hkl} \beta_{hkl} \cos\theta)^2}$$

$$\text{Slope} = (d_{hkl} \beta_{hkl} \cos\theta)^2 / (d_{hkl}^2 \beta_{hkl} \cos\theta)$$

$$D = \frac{k}{\text{slope}}$$

If ( $D = \infty$ )

$$\left(\frac{\varepsilon}{2}\right)^2 = (d_{hkl} \beta_{hkl} \cos\theta)^2 = y\_intercept$$

$$\frac{\varepsilon}{2} = \sqrt{y\_intercept}$$

$$\varepsilon = 2\sqrt{y\_intercept}$$

### 2.4.5 The Halder-Wagner method

For the determination of ( $D$ ) and ( $\varepsilon$ ), Halder-Wagner proposed a different formula containing the integral breadth ( $\beta^*$ ) of the mutual lattice point and the lattice plane spacing ( $d^*$ ) [45]:

where  $\beta^*_{hkl} = \beta_{hkl} \cos\theta / \lambda$  and  $d^*_{hkl} = 2 \sin\theta / \lambda$

$$\left(\frac{\beta^*_{hkl}}{d^*_{hkl}}\right)^2 = \left(\frac{1}{D}\right) \left(\frac{\beta^*_{hkl}}{d^*_{hkl}^2}\right) + \left(\frac{\varepsilon}{2}\right)^2 \quad (2.7)$$

The plot of  $\left(\frac{\beta^*_{hkl}}{d^*_{hkl}}\right)^2$  against  $\left(\frac{\beta^*_{hkl}}{d^*_{hkl}^2}\right)$  is a straight line. The intercept gives the mean value of ( $\varepsilon$ ) and the slope gives the average proper size ( $D$ ). Although rounding and additions, this plot have the advantage is that data re-bending at low intermediate angles gives greater weight than those in higher angles, it is often less reliable [46].

If ( $\varepsilon = 0$ )

$$D = \left(\frac{\beta^*_{hkl}}{d^*_{hkl}^2}\right) / \left(\frac{\beta^*_{hkl}}{d^*_{hkl}}\right)^2$$

$$\frac{1}{\text{slope}} = \left( \frac{\beta^*_{hkl}}{d^*_{hkl}{}^2} \right) / \left( \frac{\beta^*_{hkl}}{d^*_{hkl}} \right)^2$$

$$D = 1/\text{slope}$$

If ( $D = \infty$ )

$$\left( \frac{\beta^*_{hkl}}{d^*_{hkl}} \right)^2 = \left( \frac{\varepsilon}{2} \right)^2$$

$$\left( \frac{\beta^*_{hkl}}{d^*_{hkl}} \right)^2 = y\_intercept$$

$$\varepsilon = 2\sqrt{y\_intercept}$$

The size parameter ( $\varepsilon\beta$ ) determine from ( $\beta f$ ) in the same way as point out in the Langford method. The Williamson–Hall method plot ( $\beta^* f$  against  $d^*$ ) is the base on the analysis, it is useful as a preliminary estimate of the nature of structural defects in the sample. It is possible to see if there are contributions based on both the ( $d^*$ -independent) and ( $d^*$ -dependent) contributions to the line width. If all values of ( $\beta f^*$ ) lie on a horizontal line, then, the strain broadening is small and the crystallites are spherical on average. If the values of ( $\beta^* f$ ), corresponding to unlike reflection groups, lie on many horizontal lines, the breadth of stress again is negligible and the crystal shape is not spherical [47].

## 2.5 Some of lattice parameters

### 2.5.1 Specific Surface Area (SSA)

Surface states will play an important role in nanoparticles, due to their large surface to volume ratio and low particle size. The (SSA) with (SA) ratio increases significantly with the decrease in material size. Mathematically, (SSA) can be determine by using equation (2.8) [48]:

$$s = 6 * 10^3 / D\rho \quad (2.8)$$

where,

- $S$  are the specific surface area
- $D$  is the size (spherical shaped)
- $\rho$  is the density of NiO ( $6.67 \text{ g/cm}^3$ ).

The surface area defined (SSA) is a physical property. Derived scientific value used to determine the type of material and its properties. Are particularly important in the case of adsorption, heterogeneous catalysis and reactions on surfaces. (SSA) is the surface area (SA) of each mass [49].

### ***2.5.2 Dislocation Density***

The length of disruption lines for each unit volume in the crystal known as the dislocation density. A disruption is a crystallographic fault, or anomaly inside the structure of crystal. Exfoliation strongly affects many properties of substances. It is a kind of topological faults, mathematically, increases with plastic distortion. The dislocation prevents other disorders in the sample. Therefore, greater dislocation intensity means greater rigidity. Hendrickson and Chen calculated with fixed disruption density and numerous silver crystals hardness, and then found that the crystals and the greatest density of dislocation were harder. It revealed that the density of the disintegration rises as the grains size reduces with raising pressure and these factors reach the values of saturation. It is known that the strength of the material exceeds the allowable size of the grain (about 20 nm) while reducing the grain size. The X-ray line profile analysis used to determine internal stress and deformation intensity. For the sample the dislocation density ( $\delta$ ) calculate by using equation (2.9) [48].

$$\delta = 1/D^2 \quad (2.9)$$

where,

- $\delta$  dislocation density
- D crystallite size (nm)

### 2.5.3 Morphology Index (MI)

Morphology Index is calculated from (FWHM) of X-ray diffraction peak based on a previous report. (MI) is found by using equation (2.10) [48].

$$MI = \frac{FWHM_h}{FWHM_h - FWHM_p} \quad (2.10)$$

where,

- M.I. is morphology index
- $FWHM_h$  is highest (FWHM) value obtained from peaks.
- $FWHM_p$  is particular peak's (FWHM) for which (M.I) is to be calculated

### 2.5.4 Texture Coefficient

Texture coefficient is calculated as a measure of the predominance of crystalline orientations using equation (2.11) [50].

$$T_c = \frac{I(hkl)/I_0(hkl)}{\frac{1}{n} \sum_n I(hkl)/I_0(hkl)} \quad (2.11)$$

where,

- $I(hkl)$  and  $I_0(hkl)$  are the obtained and standard intensity of the  $(hkl)$  plane respectively.
- N is the number of diffraction peaks.

The difference in the texture coefficient values helps the discussion on the prevalence of different angles.

## 2.6 Calculation of crystallite size with change temperatures

To find the relation between the calcination temperatures of NiO and the crystallite size, must be choose three calcination temperature (200, 300, and 400)°C from the figure (2.4) then calculate the crystallite size of NiO nanomaterial by using equation (2.2).

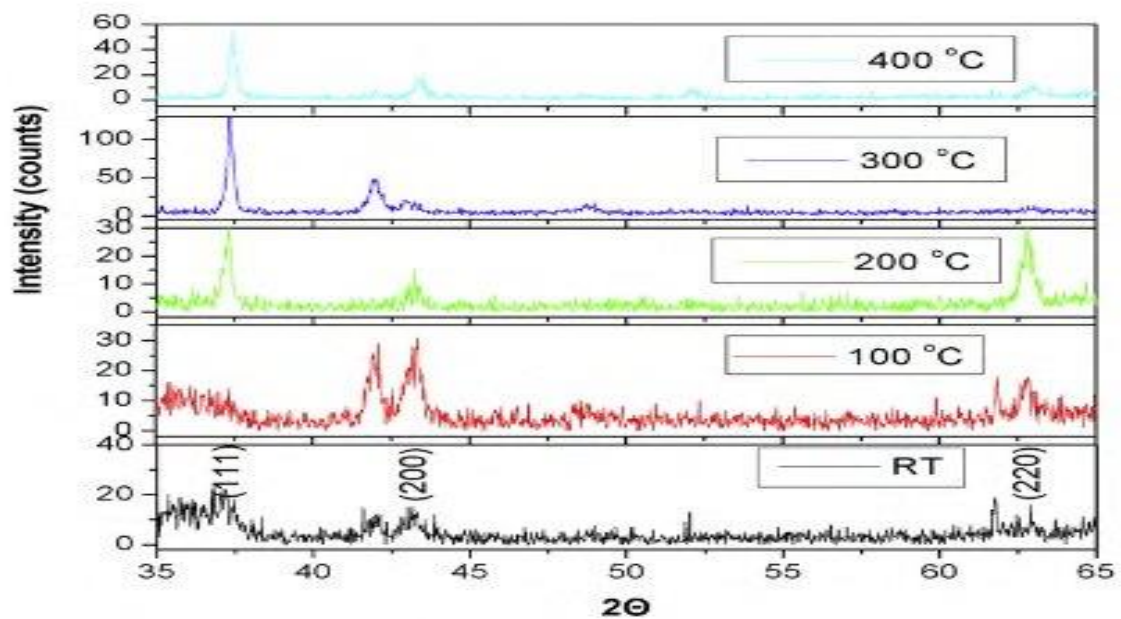


**Figure (2.4):** The X-ray diffraction pattern of NiO nanomaterial with varies temperature [51]

## 2.7 Modified Halder-Wagner method

Strain calculated from Uniform Stress Deformation Model (USDM) using Hook's Law by maintaining linear consistency between stresses with strain follow the relation:

$$\sigma = Y \varepsilon \quad (2.12)$$

where,

- $\sigma$  is the stress
- $Y$  is the Young's modulus.

This Hooke's law is valid for a significantly small strain. Assuming a small strain to be existing in the NiO with different fuels, here Hooke's law can be used. Applying the Hooke's law approximation to equation (2.13) yields:

$$\left(\frac{\beta^*_{hkl}}{d^*_{hkl}}\right)^2 = \left(\frac{1}{D}\right)\left(\frac{\beta^*_{hkl}}{d^*_{hkl}{}^2}\right) + \left(\frac{\sigma}{2Y}\right)^2 \quad (2.13)$$

Determine the energy density of a crystal from a model called Uniform Deformation Energy Density Model (UDEDM). We need to underlie the crystals to be homogeneous and isotropic nature from Equation (2.13). The energy density ( $u$ ) calculated by the equation (2.14):

$$u = \frac{\varepsilon^2 Y}{2} \quad (2.14)$$

$$\frac{u}{2Y} = \left(\frac{\beta^*_{hkl}}{d^*_{hkl}}\right)^2$$

$$\left(\frac{\beta^*_{hkl}}{d^*_{hkl}}\right)^2 = y\_intercept$$

$$\frac{u}{2Y} = y\_intercept$$

$$u = 2 * Y * y\_intercept$$

Using Hooke's law, the energy and strain relation can be modified as in the Equation (2.15) [52].

$$\left(\frac{\beta^*_{hkl}}{d^*_{hkl}}\right)^2 = \left(\frac{1}{D}\right)\left(\frac{\beta^*_{hkl}}{d^*_{hkl}{}^2}\right) + \frac{u}{2Y} \quad (2.15)$$

# *Chapter Three*

## *Results and Discussions*

### 3.1 Introduction

In this chapter, the full width at half maximum (FWHM) and the integral breadth ( $\beta_{hkl}$ ) of NiO were calculated. Williamson-Hall, Size-Strain Plot, and Halder-Wagner methods were used to calculate the crystallite size and the lattice strain of NiO. The results were compared with the results Debye Scherrer and modified Scherrer methods. Also, the physical and lattice parameters such as specific surface area (SSA), dislocation density ( $\delta$ ), morphology index (MI), and Texture coefficient for NiO have been calculated. Modified Halder-Wagner method was used to calculate the strain and the energy density of NiO. Finally, crystallite size of NiO at three different calcination temperature have been calculated.

### 3.2 Calculation of the full- width at half-maximum (FWHM) and the integral Breadth ( $\beta_{hkl}$ )

By using (Get Data Graph Digitalizer 2.24) program, we can get the data for the intensity and  $2\theta$  of NiO nanoparticles to all profile lines (111), (200), (220), (221), (222), and (311) as shown in figure (2.1). The data is used to plot the figure by the analytical program (Origin 9.1). We can take each line separately and fit it. Began the analyzing process by zooming each peak, then click on the (gadget) tool tab on the top of the (Origin 9.1) window and will pop up another window, go to the find peak tab, set the height to the maximum, set the baseline to the straight line. After that, make sure the line under the curve is a straight line to complete the fitting by chose fit peak and tab on the Gaussian to apply the fitting as shown in the figures (3.1), (3.2), (3.3), (3.4), (3.5), and (3.6).

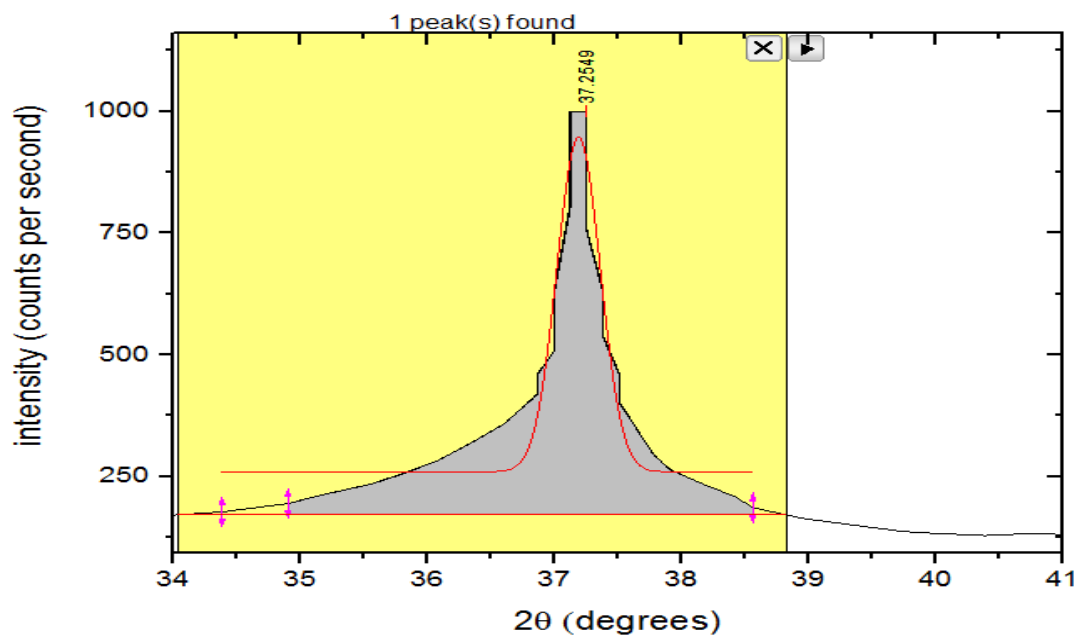


**Figure (3.1):** The profile line (111) and the fitted curve

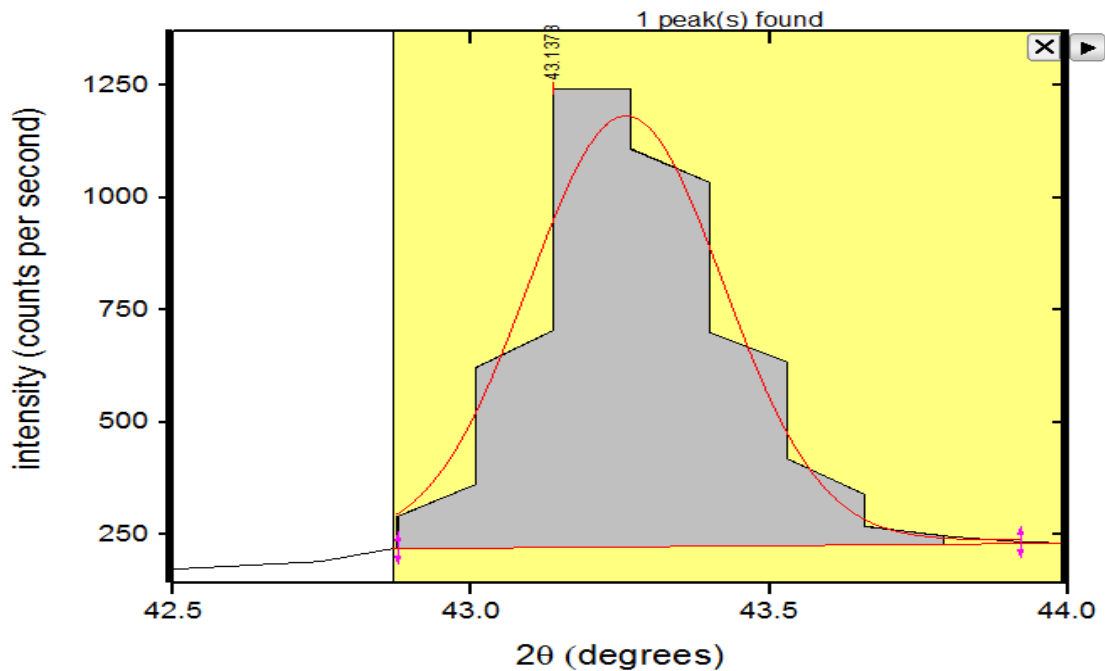


**Figure (3.2):** The profile line (200) and the fitted curve

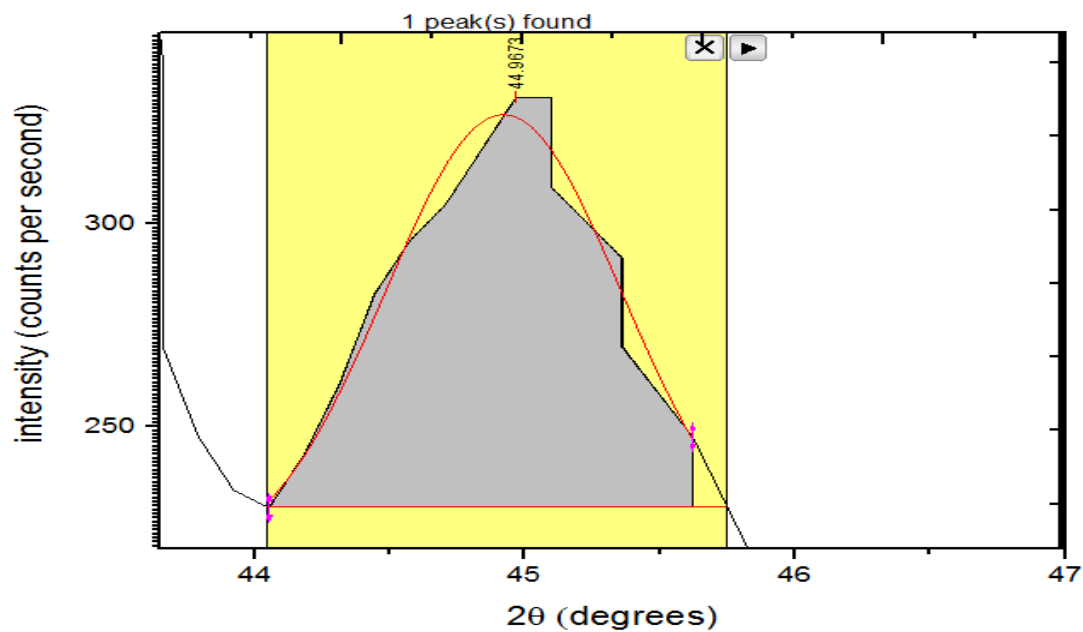


**Figure (3.3):** The profile line (220) and the fitted curve

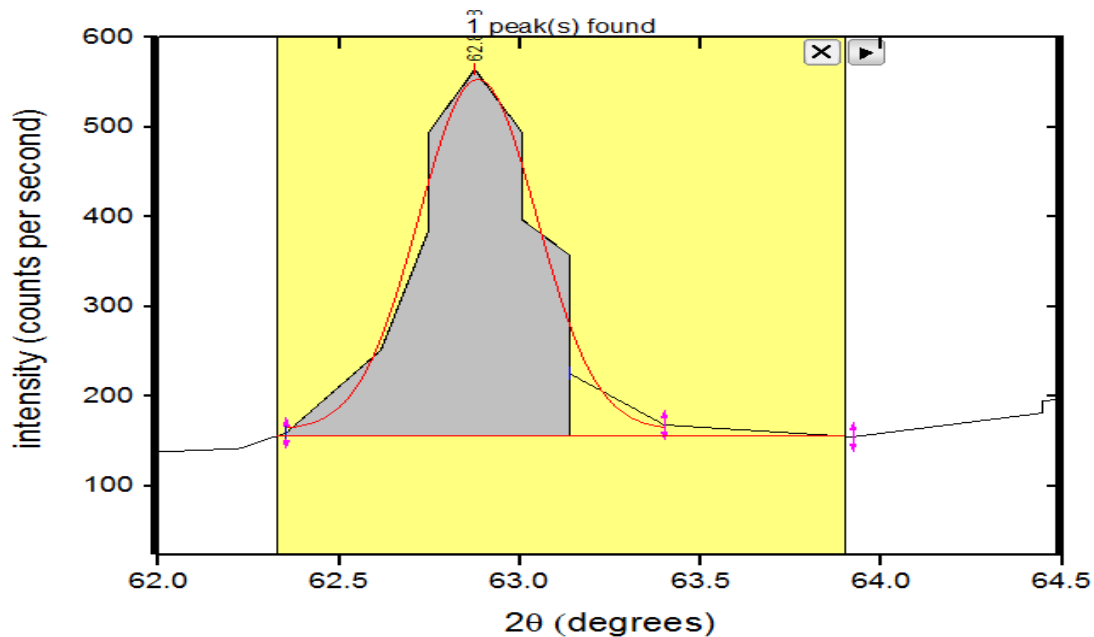


**Figure (3.4):** The profile line (221) and the fitted curve

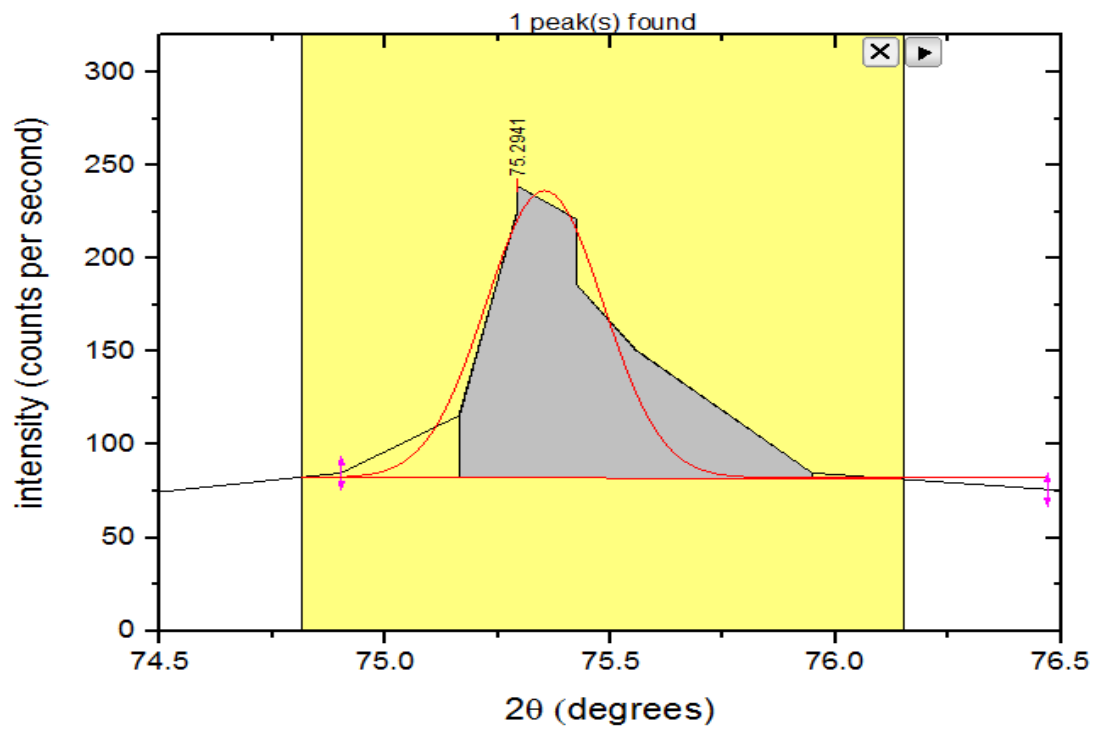


**Figure (3.5):** The profile line (222) and the fitted curve

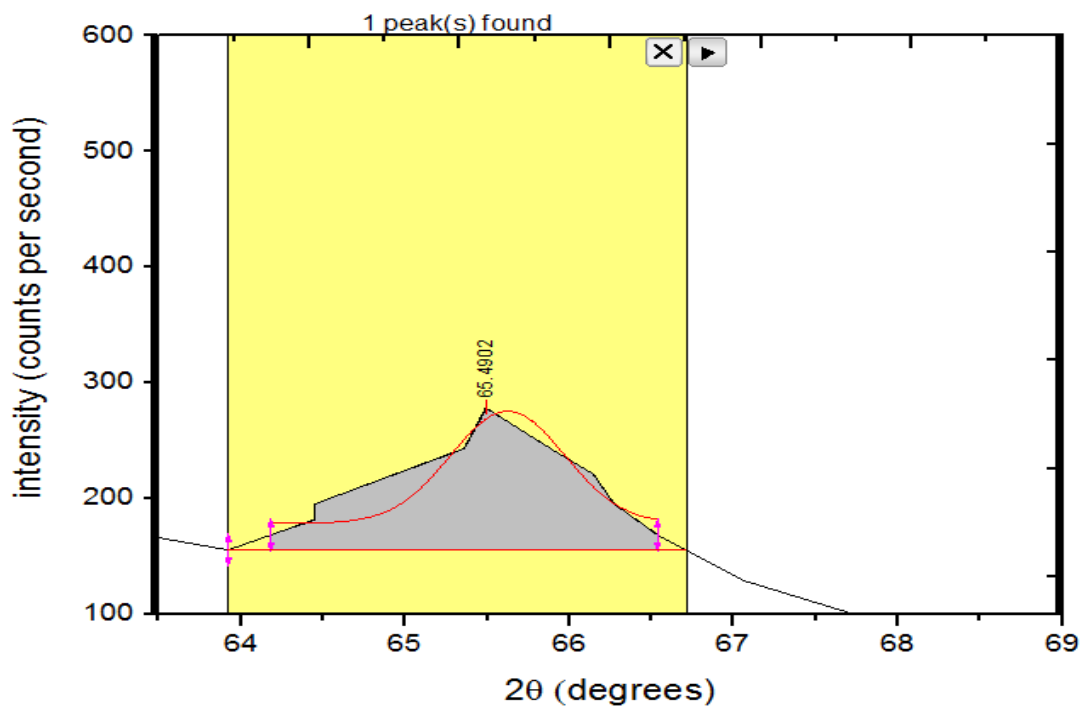


**Figure (3.6):** The profile line (311) and the fitted curve

The fitted curves shown in figures (3.7),(3.8),(3.9),(3.10),(3.11),and (3.12) were used to calculate the FWHM and integral breadth.

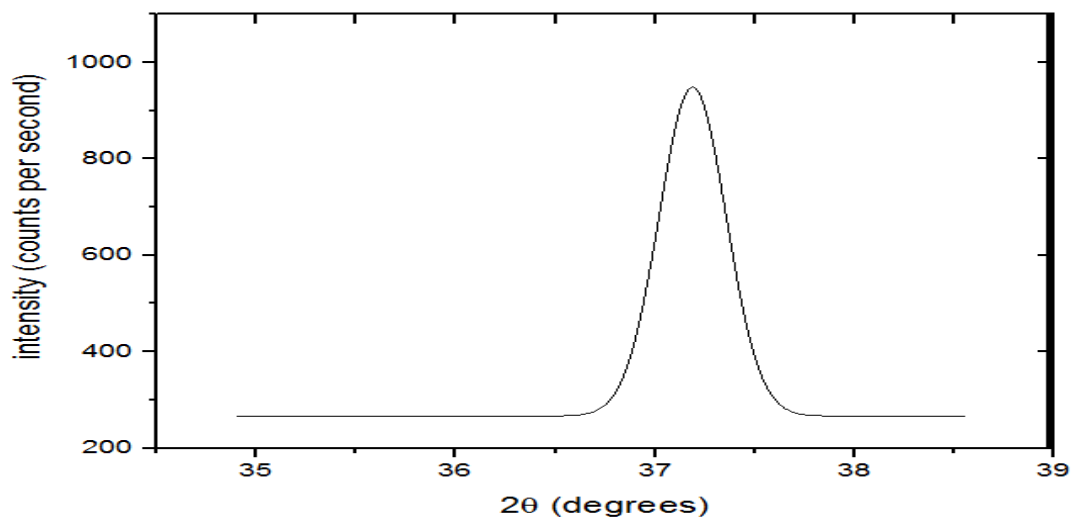


**Figure (3.7):** The fitted curve of the profile line (111)

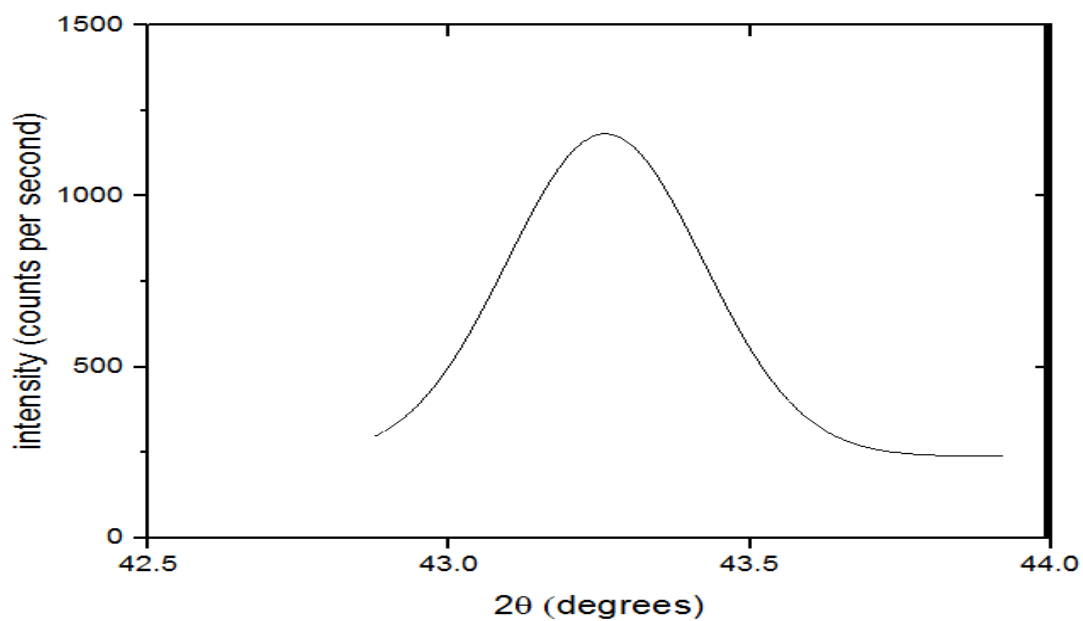


**Figure (3.8):** The fitted curve of the profile line (200)

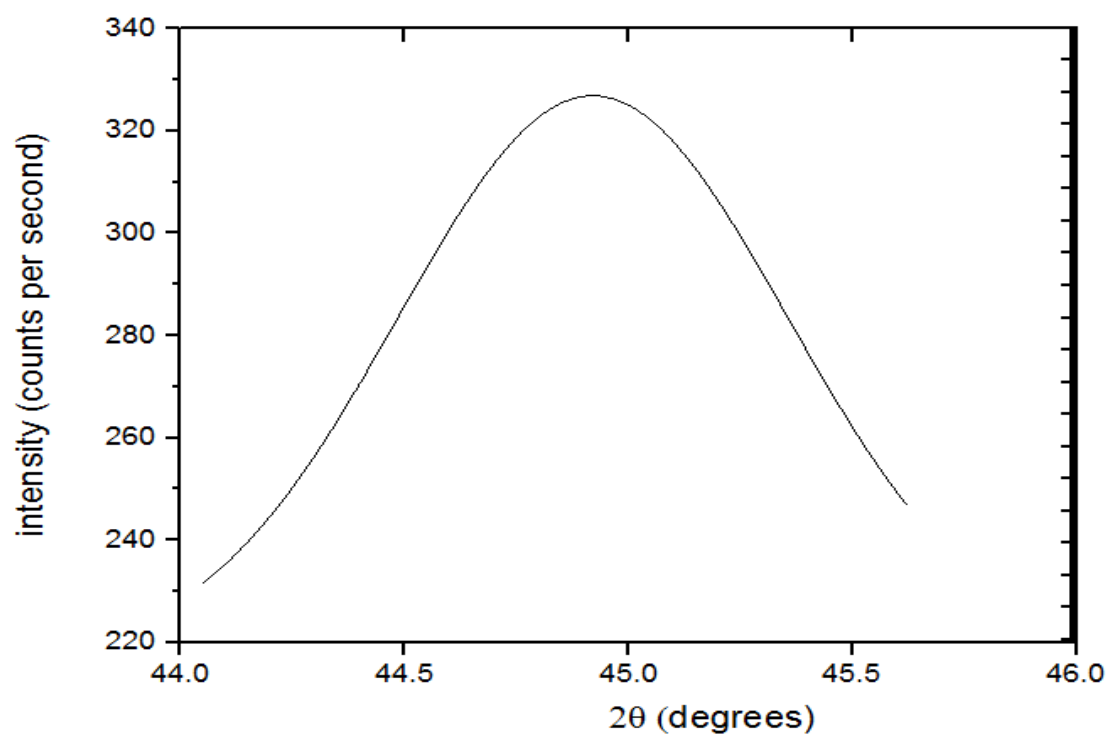


**Figure (3.9):** The fitted curve of the profile line (220)

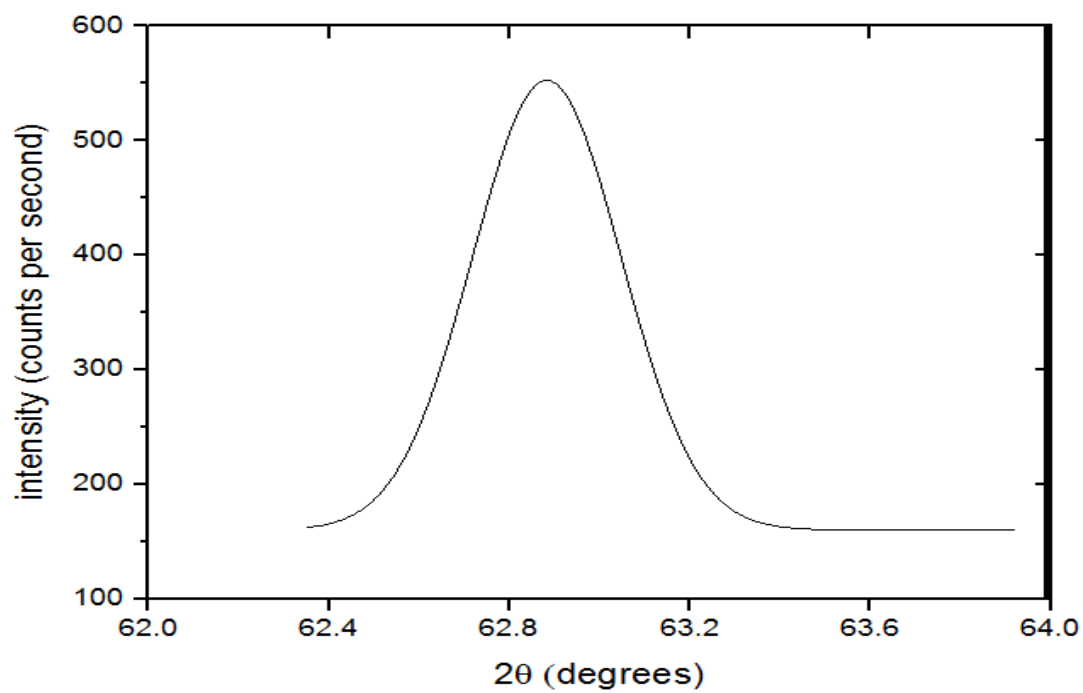


**Figure (3.10):** The fitted curve of the profile line (221)

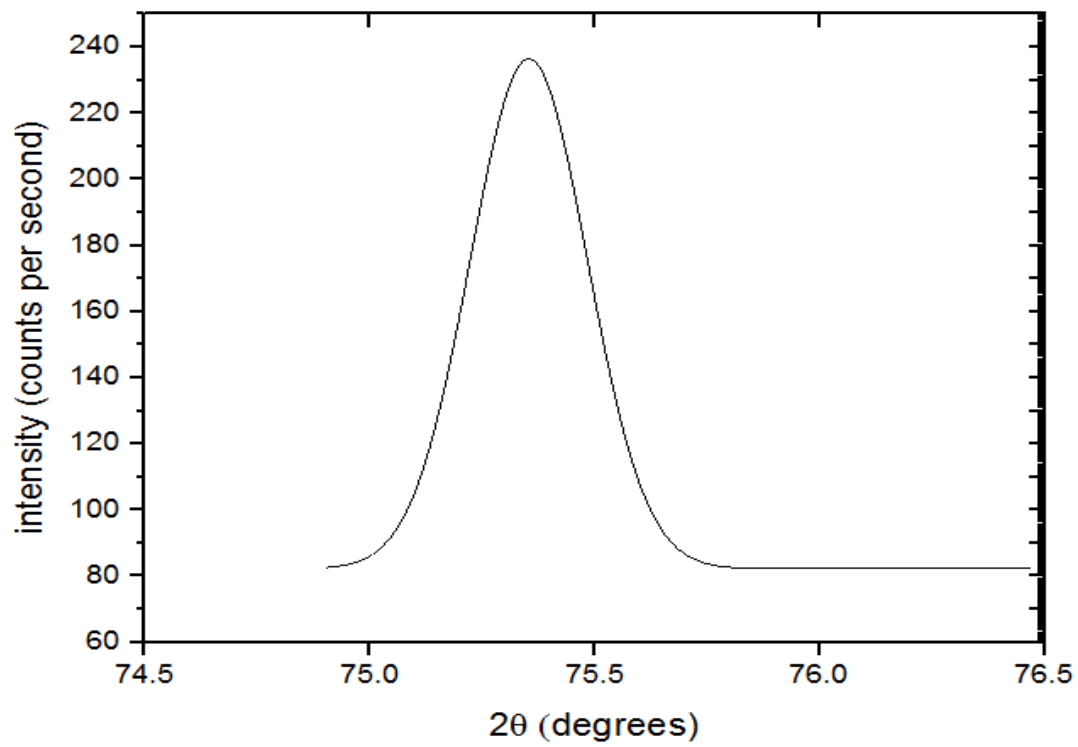


**Figure (3.11):** The fitted curve of the profile line (222)

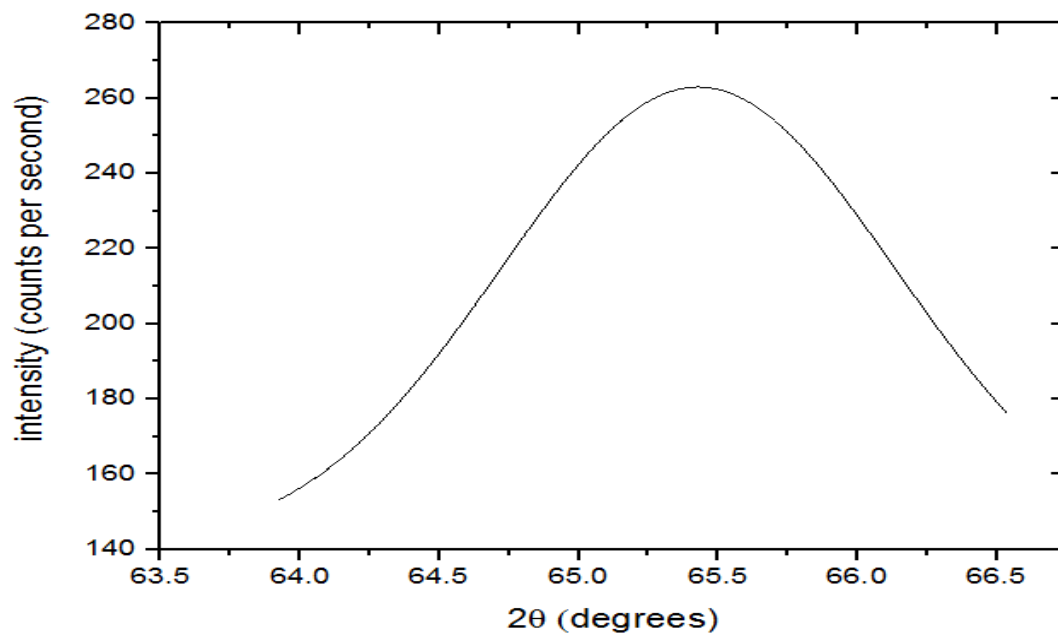


**Figure (3.12):** The fitted curve of the profile line (311)

To calculate the integral Breadth take 20 steps to the right and 20 steps to the left as shown in figures (3.13),(3.14),(3.15),(3.16),(3.17),and(3.18).

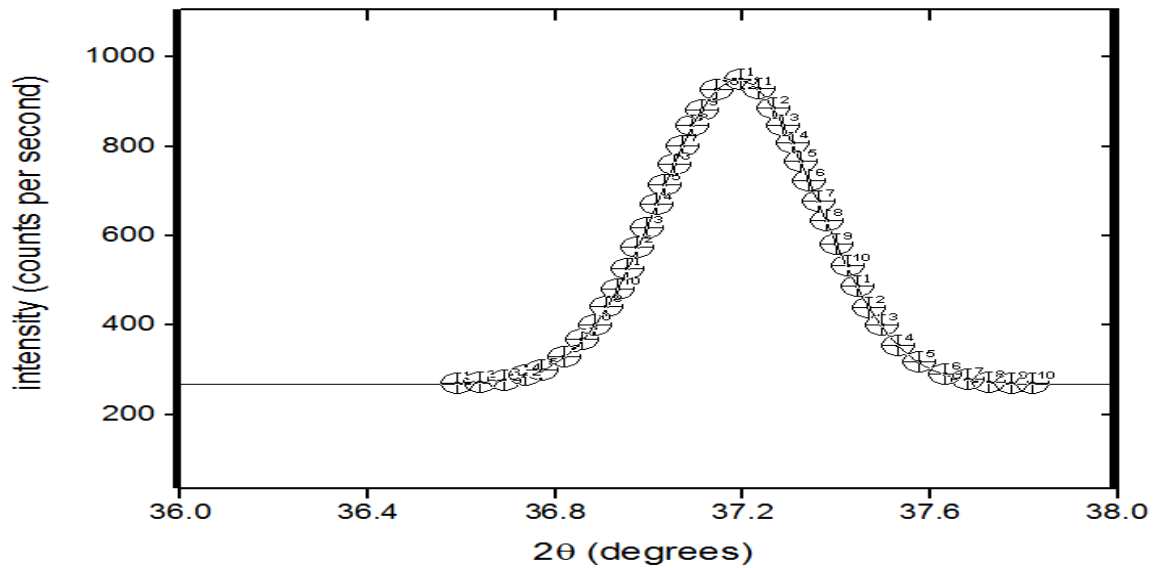


**Figure (3.13):** Fitted profile line (111) with 20 steps to the right and 20 steps to the left.

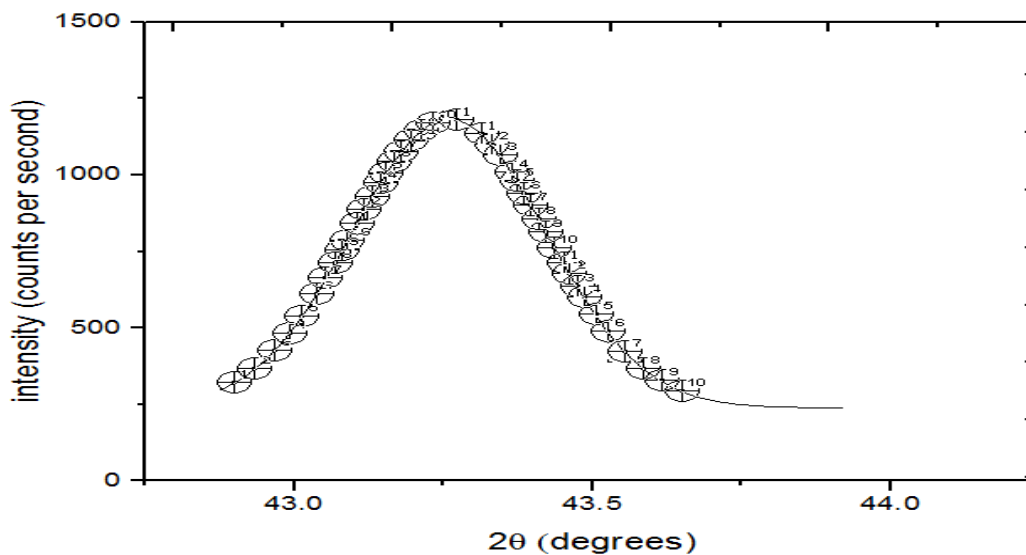


**Figure (3.14):** Fitted profile line (200) with 20 steps to the right and 20 steps to the left.

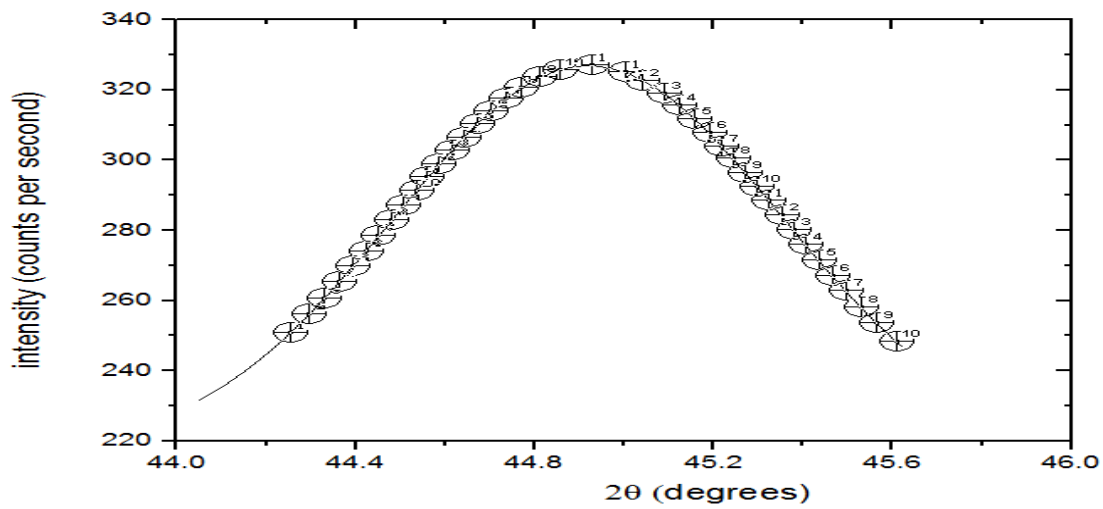


**Figure (3.15):** Fitted profile line (220) with 20 steps to the right and 20 steps to the left.

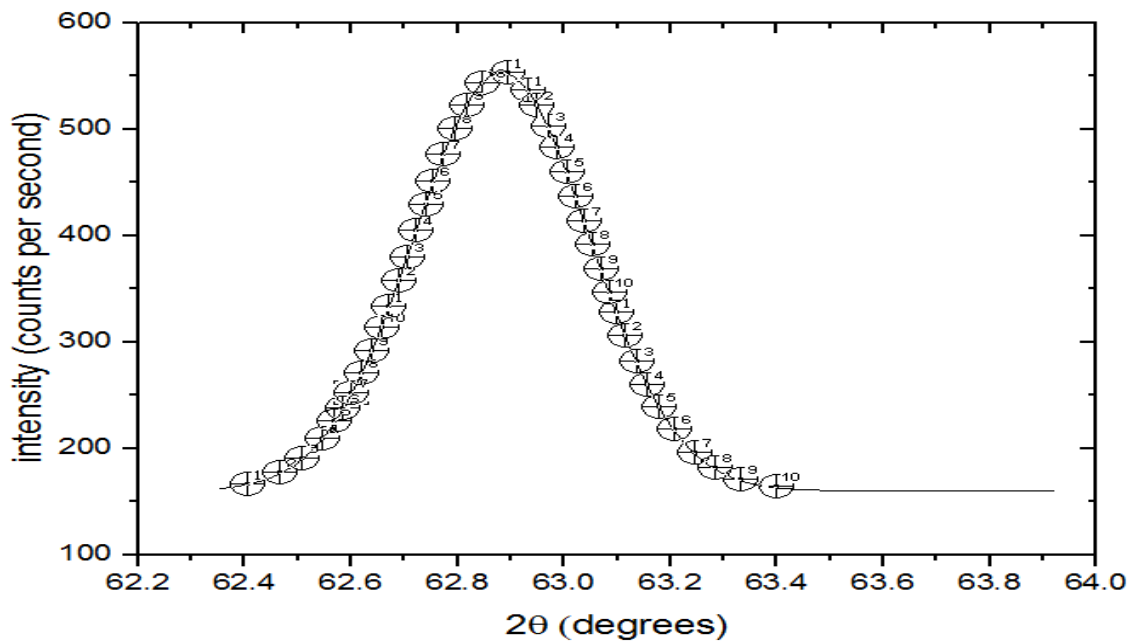


**Figure (3.16):** Fitted profile line (221) with 20 steps to the right and 20 steps to the left.

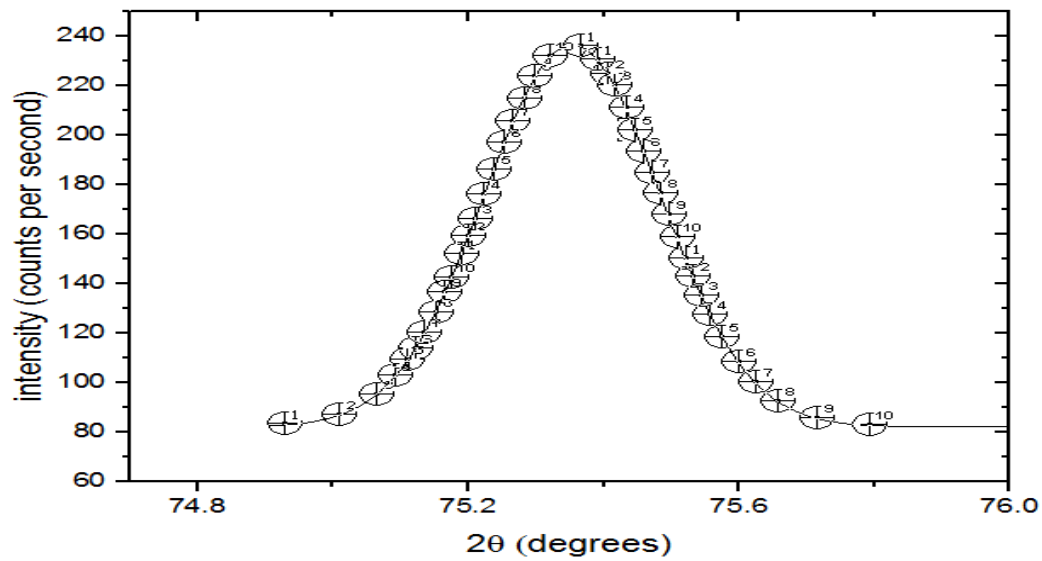


**Figure (3.17):** Fitted profile line (222) with 20 steps to the right and 20 steps to the left.

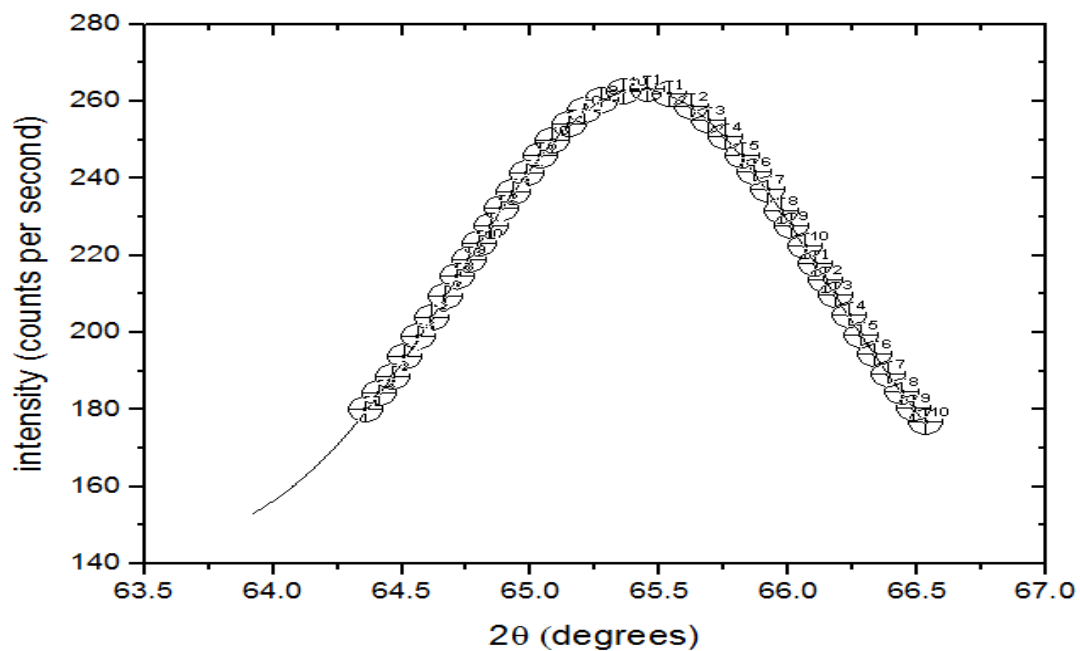


**Figure (3.18):** Fitted profile line (311) with 20 steps to the right and 20 steps to the left.

Used the 40 points to calculate the total area under the curve by calculate the sum of spaces between each two points on the peak and lie on the same horizontal line,

$(x_1, y_1)$  and  $(x_2, y_2)$  represented the point data of the left and right steps respectively. Areas under the curves was calculate after subtracting intensity to get rid of background values for each peak. The results is listed in the tables (3.1), (3.2), (3.3), (3.4), (3.5) and (3.6).

**Table (3.1):** The area under the curve for line (111)

X1	Y1	X2	Y2	Area=(y1+y2)/2*(x2-x1)
36.569211	1.787323	37.795825	0	0.728559677
36.6173141	3.581833	37.7525518	2.023812	2.468930075
36.668216	7.170853	37.7046058	7.842273	7.242991971
36.7150947	10.759873	37.6566599	15.937522	14.17713558
36.767396	30.050857	37.6103392	31.875045	36.73195418
36.800456	47.771644	37.5479689	73.616175	81.19446434
36.8471598	88.372435	37.5065241	117.381117	156.0241827
36.8761966	123.81401	37.4744247	167.217497	243.2445977
36.9064578	166.209311	37.4409032	226.919962	367.7918016
36.9353197	219.147359	37.4120544	288.64624	532.5746154
36.9613829	273.879917	37.3929572	330.640346	700.366383
36.9752016	305.732472	37.3754854	374.405289	849.5694317
36.9972416	358.67052	37.3529346	428.289293	1106.234608
37.0122848	393.887781	37.3387133	463.958987	1313.988772
37.0343248	446.825829	37.3161625	515.819179	1707.800284
37.0495429	482.267403	37.3019412	547.694224	2040.349771
37.0673848	524.662704	37.2793904	593.482979	2637.066386
37.0826028	556.515259	37.2682165	611.444313	3146.210576
37.1046428	600.480756	37.2426183	649.390795	4529.324231
37.1293066	641.305861	37.2251465	669.122966	6836.551515

**Table (3.2):** The area under the curve for line (200)

X1	Y1	X2	Y2	Area=(y1+y2)/2*(x2-x1)
42.8858683	3.79107	43.6370602	0	2.523369861
42.9212826	43.807919	43.6019864	37.910699	60.02509315
42.9536322	98.989048	43.5709989	87.615838	151.1296981
42.9798524	150.379107	43.5403519	148.694187	266.7917581
42.9999432	201.769166	43.5233258	188.711036	373.0351391
43.0261635	272.114574	43.4940409	272.114574	581.5937551
43.0414869	319.713564	43.4739501	329.401853	750.4863038
43.0554484	367.733783	43.4633939	367.733783	901.4287031
43.0690692	409.435552	43.4507946	409.435552	1072.591847
43.0782633	441.870261	43.4402384	445.661331	1225.956691
43.0939274	497.05139	43.4249149	497.05139	1501.722542
43.1061862	540.859309	43.4109535	548.441449	1787.102419
43.1184449	584.667228	43.3986947	592.249368	2099.76349
43.1324064	632.266217	43.3864359	634.372367	2493.093487
43.1429625	664.700927	43.3738365	672.283066	2895.484102
43.1555619	704.717776	43.3615778	712.299916	3439.097885
43.1678207	740.943556	43.3523837	738.837406	4008.877624
43.1845062	784.751476	43.3339955	788.542546	5262.229544
43.2015323	820.977256	43.318672	818.871106	6999.541411
43.2199205	851.305816	43.3016459	847.514746	10393.4674

**Table (3.3):** The area under the curve for line (220)

X1	Y1	X2	Y2	Area=(y1+y2)/2*(x2-x1)
44.2437684	0.336984	45.6011578	0	0.12412945
44.2869012	5.526537	45.5562997	5.324347	4.274025848
44.3201135	9.941028	45.5209308	9.907329	8.264519923
44.3528944	14.658804	45.4877185	14.625105	12.90240003
44.3843814	18.904802	45.4566629	19.039595	17.69330022
44.4137117	23.352991	45.4256073	23.622578	23.21166778
44.4426107	27.598989	45.3980023	27.902274	29.04634236
44.471941	32.181971	45.3691033	32.148273	35.85206601
44.4991146	36.259477	45.3436549	36.259477	42.93398077
44.5267196	40.673968	45.3143246	40.673968	51.64259749
44.5538933	44.650379	45.2910329	44.2123	60.2753393
44.5793417	48.323504	45.2638593	48.155012	70.47190313
44.6065153	52.434709	45.2362543	52.266217	83.13041276
44.633689	56.074136	45.2112372	55.636057	96.71071003
44.6630193	60.050547	45.1836322	59.443976	114.7633136
44.6945062	63.723673	45.15042	63.386689	139.4017488
44.7272872	67.3631	45.1154824	67.194608	173.3119163
44.7643814	70.73294	45.0805448	70.395956	223.1898063
44.8053575	73.90059	45.0356867	73.90059	320.8476824
44.8484904	76.192081	44.9947106	76.057287	520.6167411

**Table (3.4):** The area under the curve for line (221)

X1	Y1	X2	Y2	Area=(y1+y2)/2*(x2-x1)
62.3884904	1.26369	63.397798	0	0.626018272
62.4493076	9.68829	63.3175709	9.12665	10.83481244
62.4963224	22.184779	63.2688309	22.746419	29.08136156
62.5347106	39.174389	63.232168	38.612749	55.7647951
62.5627469	57.427689	63.2024064	57.427689	89.77852905
62.5925085	79.472058	63.1748014	79.472058	136.4812417
62.6132123	100.533558	63.151941	100.533558	186.61259
62.6343473	122.718337	63.1312372	122.718337	246.9728948
62.6516005	143.639427	63.1135528	143.639427	310.9399542
62.6671283	163.577646	63.098025	164.139286	380.2731977
62.6848127	189.132266	63.0803405	189.693906	478.8869101
62.6986152	207.245156	63.066538	207.245156	563.284352
62.7162997	231.676495	63.0510102	232.238135	693.0087792
62.7301022	252.176355	63.0350511	252.176355	826.9462687
62.7439047	272.535804	63.0212486	272.535804	982.6637759
62.7581385	291.771974	63.0074461	291.771974	1170.32924
62.771941	310.586914	62.9932123	310.586914	1403.647531
62.7909194	333.333333	62.9742338	333.333333	1818.369604
62.8120545	355.939343	62.9530988	355.939343	2523.599628
62.8418161	377.000842	62.9254938	377.562482	4508.747994

**Table (3.5):** The area under the curve for line (222)

X1	Y1	X2	Y2	Area=(y1+y2)/2*(x2-x1)
74.9225653	0	75.7865153	0	0
75.0045176	3.6281944	75.7084449	3.1479922	4.813129566
75.0571396	10.884583	75.6497843	10.884583	18.36611886
75.0981158	21.7158101	75.6092395	21.9825891	42.74738111
75.1214075	30.8930081	75.5855165	30.6262291	66.27671215
75.1373666	38.1493961	75.5699886	37.6691941	87.62683151
75.1507378	45.6192081	75.5544608	46.0994101	113.5910243
75.1684222	54.5296261	75.5406583	54.3162031	146.2053643
75.1817934	63.4400451	75.5251305	64.1870261	185.8626277
75.191714	70.9632131	75.5156413	70.4296551	218.2478417
75.2033598	78.3796691	75.5035641	77.8994661	260.2879692
75.2150057	87.3434431	75.4919183	86.8632411	314.551747
75.2266515	95.2934571	75.4802724	95.7736591	376.6785707
75.2387287	103.0300481	75.4707832	102.5498451	442.9560582
75.2464926	108.5790511	75.462588	108.0988491	501.3477848
75.2542565	115.0884581	75.4530988	114.6082561	577.5851371
75.2676277	123.2518951	75.4392963	123.7320981	719.3627524
75.2797049	130.0280821	75.429807	129.5478801	864.6646589
75.2913507	136.8042681	75.4160045	136.3240661	1095.547565
75.3068785	144.0073011	75.4004767	143.5270991	1536.003899

**Table (3.6):** The area under the curve for line (311)

X1	Y1	X2	Y2	Area=(y1+y2)/2*(x2-x1)
64.3381385	0	66.5183314	0.157259	0.036065387
64.3890465	4.403258	66.46521	4.560517	2.158735331
64.4370034	8.531311	66.4165153	8.963774	4.419040118
64.4908627	13.524291	66.3663451	13.524291	7.211099928
64.5410329	18.635215	66.3102724	18.949733	10.62178071
64.591941	23.628194	66.2615778	23.903398	14.23411127
64.642849	28.896377	66.2114075	29.053637	18.47237894
64.6937571	34.164561	66.1627128	34.32182	23.31124792
64.7365494	38.567818	66.1228717	38.449874	27.77770076
64.7741771	42.695872	66.0830306	42.577928	32.57576192
64.8191827	47.256389	66.0402384	46.823926	38.52417011
64.8649262	51.816905	65.9893303	52.249368	46.27618887
64.9077185	56.220163	65.9494892	56.102219	53.90935932
64.96084	61.213142	65.89563	61.370402	65.5674237
65.0139614	66.206122	65.8454597	65.773659	79.36262828
65.0626561	70.058972	65.7945516	69.901713	95.61521078
65.1268445	74.580174	65.7325766	74.46223	123.0266681
65.1880817	78.433024	65.6661748	78.590284	164.2183374
65.2522701	81.578208	65.5990352	81.853412	235.6517712
65.3378547	84.29093	65.5363224	83.937096	423.81714

Now plot a new peaks for the new intensity values (after subtracting intensity to get rid of background values for each peak) to calculate FWHM. The figures

(3.19), (3.20), (3.21), (3.22), (3.23), and (3.24) used to calculate the FWHM by the same way as shown in the figure (2.3).

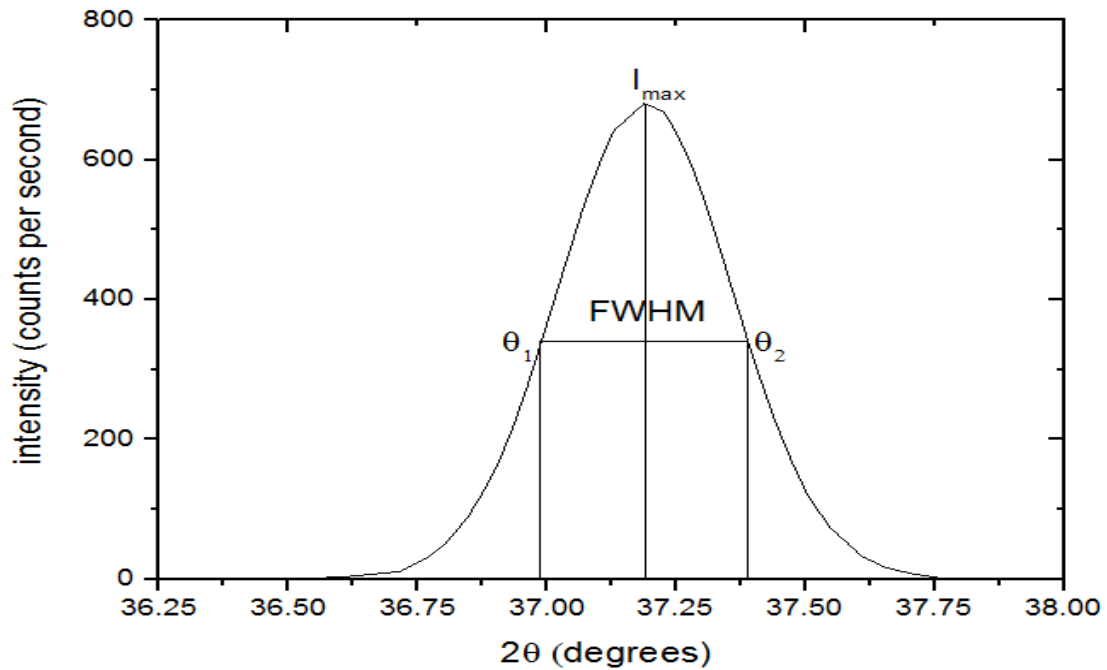


**Figure (3.19):** Calculated (FWHM) for line (111)

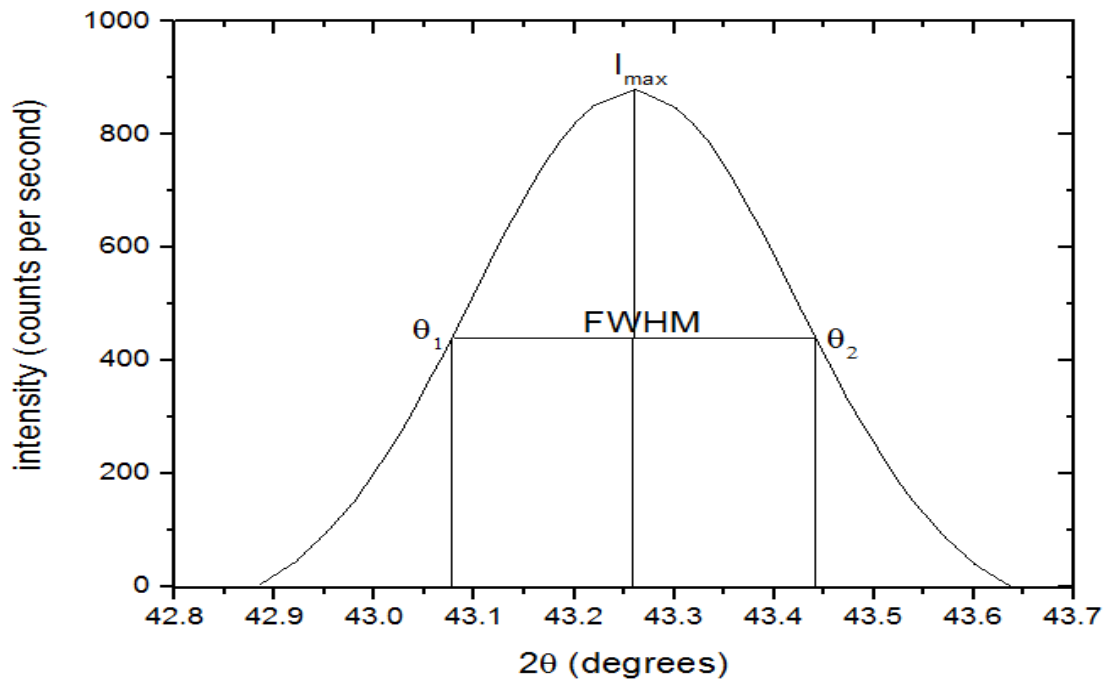


**Figure (3.20):** Calculated (FWHM) for line (200)

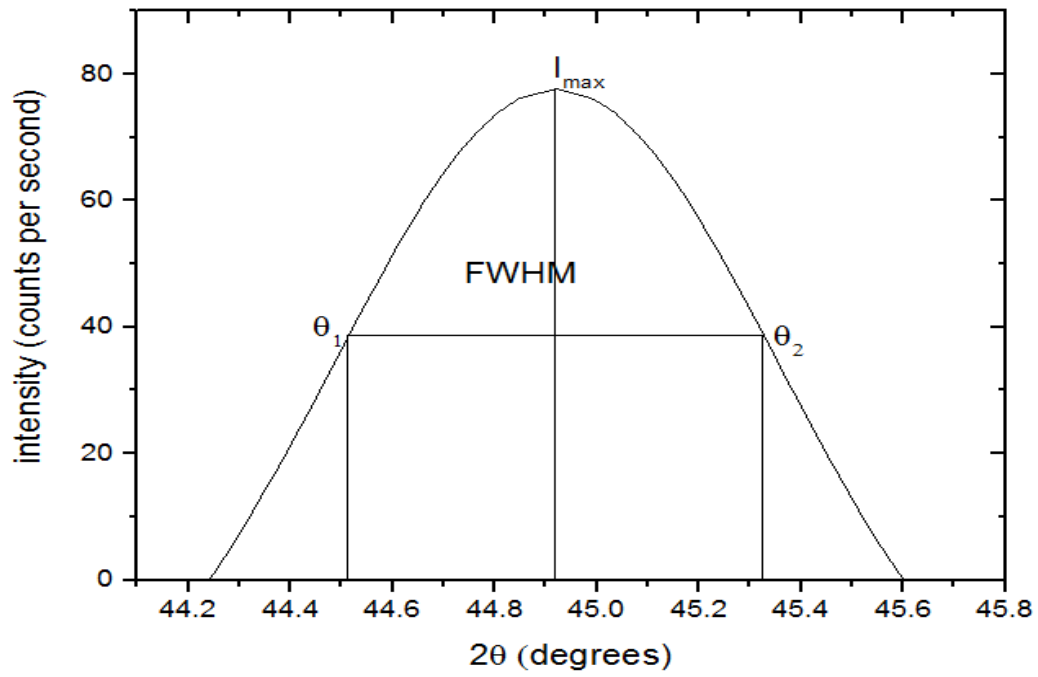


**Figure (3.21):** Calculated (FWHM) for line (220)

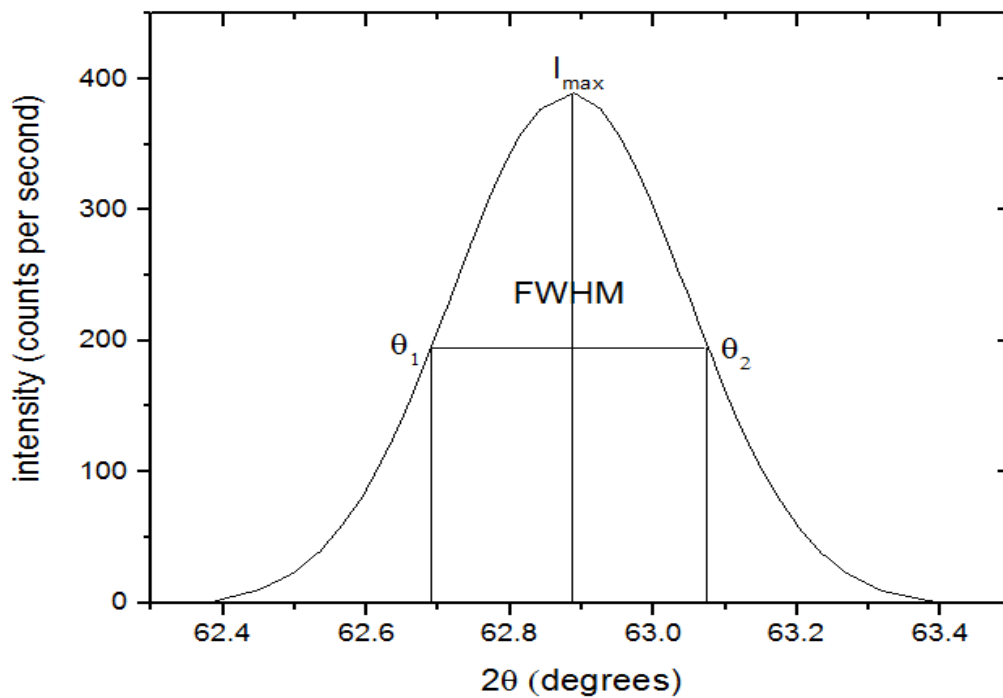


**Figure (3.22):** Calculated (FWHM) for line (221)

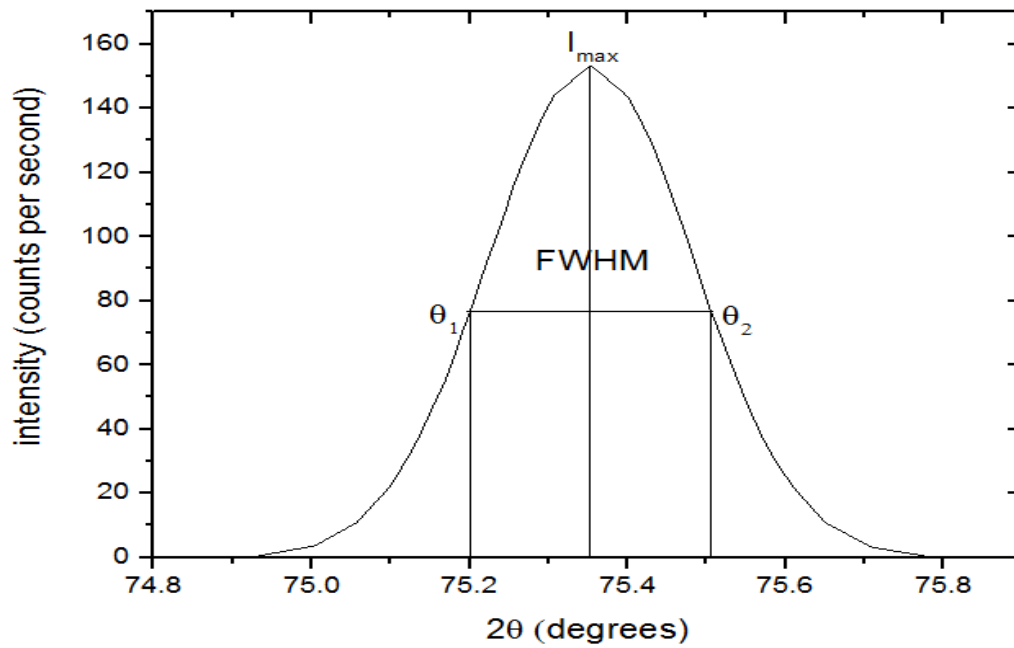


**Figure (3.23):** Calculated (FWHM) for line (222)

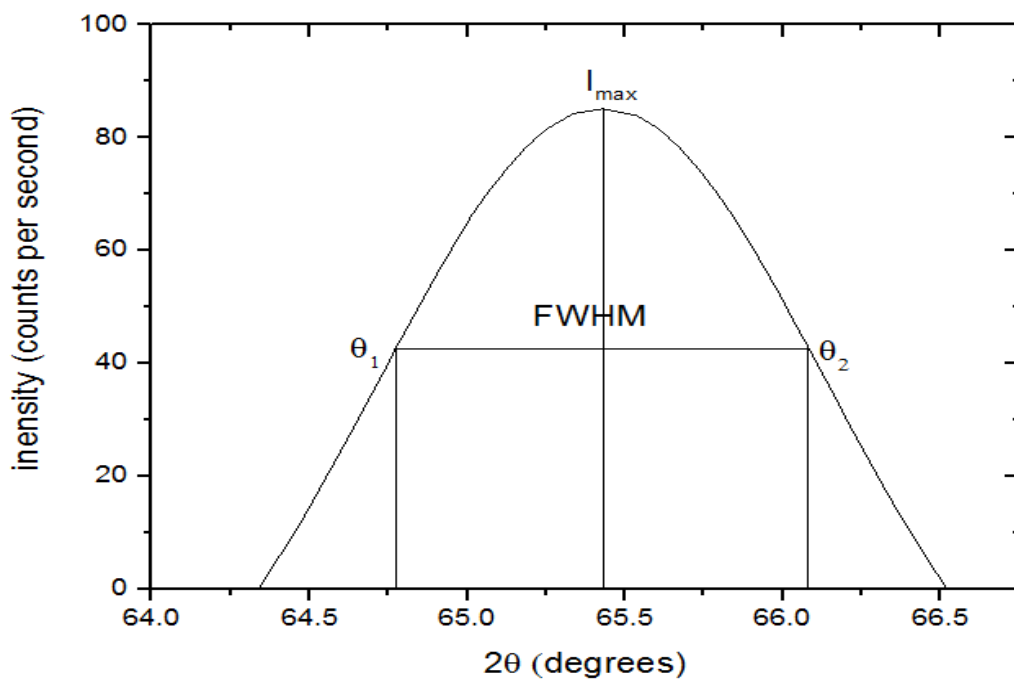


**Figure (3.24):** Calculated (FWHM) for line (311)

By calculate  $(2\theta_1)$ ,  $(2\theta_2)$  from the previews figures for all new peaks, the FWHM represented by  $(2\theta_2 - 2\theta_1)$ . The results of  $(\beta)$  and (FWHM) for all peak listed in the table (3.7).

**Table (3.7):** The FWHM and integral breadth ( $\beta$ ) of the lines (111), (200), (220), (221), (222), and (311) for NiO powder

<i>hkl</i>	$2\theta_1$	$2\theta_2$	$2\theta/2$	$I_0/2$ intensity	FWHM	Area Under The Curve	$\beta = \text{Area}/I_0$
111	36.99211	37.38700	18.49606	340.5088	0.39489	26309.64119	38.63284
200	43.07664	43.44256	21.62980	439.97472	0.36592	46265.94227	52.57795
220	44.51371	45.32686	22.46014	38.85425	0.81314	2028.66460	26.10608
221	62.68765	63.07503	31.44067	194.74867	0.38738	16416.84948	42.14881
222	75.20030	75.50620	37.67662	76.72564	0.30590	7572.72317	49.34937
311	64.77037	66.08076	32.71278	42.55827	1.310386	1466.78682	17.23269

Table (3.7) shows the differences in the values of FWHM for all lines profiles. While the line (311) has largest width, the line (222) has smallest width. The line (200) has the highest intensity and the maximum area under the curve while, the line (220) has the lowest intensity and the minimum area under the curve, that is mean the crystal orientation (311) constitutes the largest percentage of the NiO powder while the crystal orientation constitutes the lowest percentage of the powder. . Therefore, the line (200) has the biggest integral breadth and the line (311) has the smallest integral breadth, because the integral breadth depends on the number of the crystals that have the same crystal orientation and the diffraction angel.

### 3.3 Calculation of the crystallite size and the lattice strain

Three different methods including (Williamson-Hall, size-strain plot, and Halder-Wagner) were used to determine the crystallite size and lattice strain. The results of this method have been compared with the Scherrer and modified Scherrer methods.

#### 3.3.1 The Scherrer method

In this method, the equation (2.2) has been used to determine the crystallite size for the six line (111), (200), (220), (221), (222), and (311). The integral breadth value ( $\beta$ ) must be in the radian to calculate the crystallite size. The Gaussian function ( $\beta_f^2 = \beta_h^2 - \beta_g^2$ ) has used to correct the values of ( $\beta$ ), where ( $\beta_f$ ) is the correct value, ( $\beta_h$ ) is the calculate value from the area under the curve and ( $\beta_g$ ) is the standard value for the silicon sample . Table (3.8) shows the values of  $\beta$  for all the profile lines.

**Table (3-8):** The values of  $\beta$  for the profile lines (111), (200), (220), (221), (222), and (311)

<i>hkl</i>	$\beta_h$	$\beta_g$	$\beta_h^2$	$\beta_g^2$	$\beta_f^2$	$\beta_f$	$\beta_f * \pi \backslash 180$
111	38.63284	11.11800	1492.49633	123.60992	1368.88641	36.99846	0.64562
200	52.57795	11.11800	2764.44083	123.60992	2640.83091	51.38902	0.89674
220	26.10608	11.11800	681.52741	123.60992	557.91749	23.62028	0.41217
221	42.14881	11.11800	1776.52218	123.60992	1652.91226	40.65602	0.70945
222	49.34937	11.11800	2435.36032	123.60992	2311.7504	48.08067	0.83901
311	17.23269	11.11800	296.96560	123.60992	173.35568	13.16646	0.22975

Now, by the equation (2.2) we can calculate the (D) values for all the line profiles, when ( $k = 0.89$ ) and ( $\lambda = 0.15406$  nm).

$$D_{111} = \frac{0.89 * 0.15406}{0.64562 * 0.94835} = \frac{0.13711}{0.61227} = 0.22394 \text{ nm}$$

$$D_{200} = \frac{0.89 \cdot 0.15406}{0.89674 \cdot 0.92958} = \frac{0.13711}{0.83359} = 0.16448 \text{ nm}$$

$$D_{220} = \frac{0.89 \cdot 0.15406}{0.41217 \cdot 0.92415} = \frac{0.13711}{0.38091} = 0.35995 \text{ nm}$$

$$D_{221} = \frac{0.89 \cdot 0.15406}{0.70945 \cdot 0.85318} = \frac{0.13711}{0.60529} = 0.22652 \text{ nm}$$

$$D_{222} = \frac{0.89 \cdot 0.15406}{0.83901 \cdot 0.79147} = \frac{0.13711}{0.66405} = 0.20648 \text{ nm}$$

$$D_{311} = \frac{0.89 \cdot 0.15406}{0.22975 \cdot 0.84139} = \frac{0.13711}{0.19331} = 0.70928 \text{ nm}$$

The line (311) has the biggest value of the crystallite size while the line (200) has the smallest value of the crystallite size.

The lattice strain was determined from equation (2.3), then the results of crystallite size and lattice strain are listed in table (3.9).

$$\varepsilon_{111} = \frac{0.64562}{1.33808} = 0.48250$$

$$\varepsilon_{200} = \frac{0.89674}{1.58612} = 0.56537$$

$$\varepsilon_{220} = \frac{0.41217}{1.65360} = 0.24926$$

$$\varepsilon_{221} = \frac{0.70945}{2.44551} = 0.29010$$

$$\varepsilon_{222} = \frac{0.83901}{3.08895} = 0.27162$$

$$\varepsilon_{311} = \frac{0.22975}{2.56921} = 0.08942$$

**Table (3.9):** The values of crystallite size and lattice strain determined by the Scherrer method

<i>hkl</i>	D nm	$\varepsilon$
111	0.22394	0.48250
200	0.16448	0.56537
220	0.35995	0.24926
221	0.22652	0.29010
222	0.20648	0.27162
311	0.70928	0.08942

The line (311) showed the lowest lattice strain while the line (200) has the highest lattice strain, that because lattice strain is reversely proportional with the crystalline size.

### 3.3.2 The modified Scherrer method

In this method, equation (2.4) was used to determine the crystallite size .Table (3.10) presents the values of  $\ln\beta_{hkl}$  and  $\ln\frac{1}{\cos\theta}$  for all the profile line. These values were used to draw a straight line. The Y-axis intercept and the slope of the straight line were extract from the equation (2.4). The figure (3.25) was used to calculate the slope and the intercept of the plot, while the crystallite size extracted from equation (2.4).

**Table (3.10):** The values of  $\ln\beta_{hkl}$  and  $\ln\frac{1}{\cos\theta}$  for all the profile line

$hkl$	$\cos\theta$	$1/\cos\theta$	$\ln(1/\cos\theta)$	$\ln\beta$
111	0.948346	1.054467	0.053035	-0.4373506
200	0.929585	1.075749	0.073017	-0.108802
220	0.9241455	1.08208	0.078885	-0.88612
221	0.853181	1.172084	0.158783	-0.34308
222	0.791473	1.263467	0.2338595	-0.1753467
311	0.84139	1.188509	0.1726996	-1.4705546

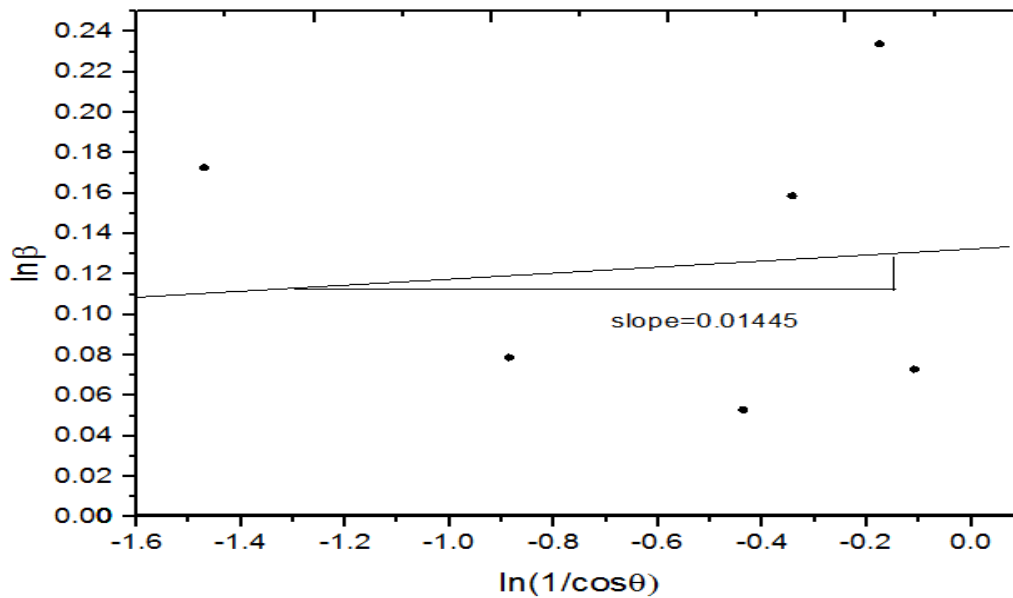


**Figure (3.25):** Plot of modified Scherrer method

From figure (3.25) the value of crystallite size was 0.1350 nm, this value nearly from that was calculated by the Scherrer method.

### 3.3.3 The Williamson- Hall method

In this method, equation (2.5) was used to determine the crystallite size and the lattice strain.  $\beta \cos\theta$  and  $4\sin\theta$  are calculated and listed in the table (3.11) to used in drawing the figure (3.26).

**Table (3-11):** The values of the  $\beta\cos\theta$  and  $4\sin\theta$  for all profile lines

$hkl$	$\beta\cos\theta$	$\sin\theta$	$4\sin\theta$
111	0.612389688	0.31723944	1.26895776
200	0.833752223	0.3686081	1.4744324
220	0.380980831	0.38204061	1.52816244
221	0.605401027	0.52161537	2.08646148
222	0.664177232	0.61120412	2.44481648
311	0.193349739	0.54042801	2.16171204

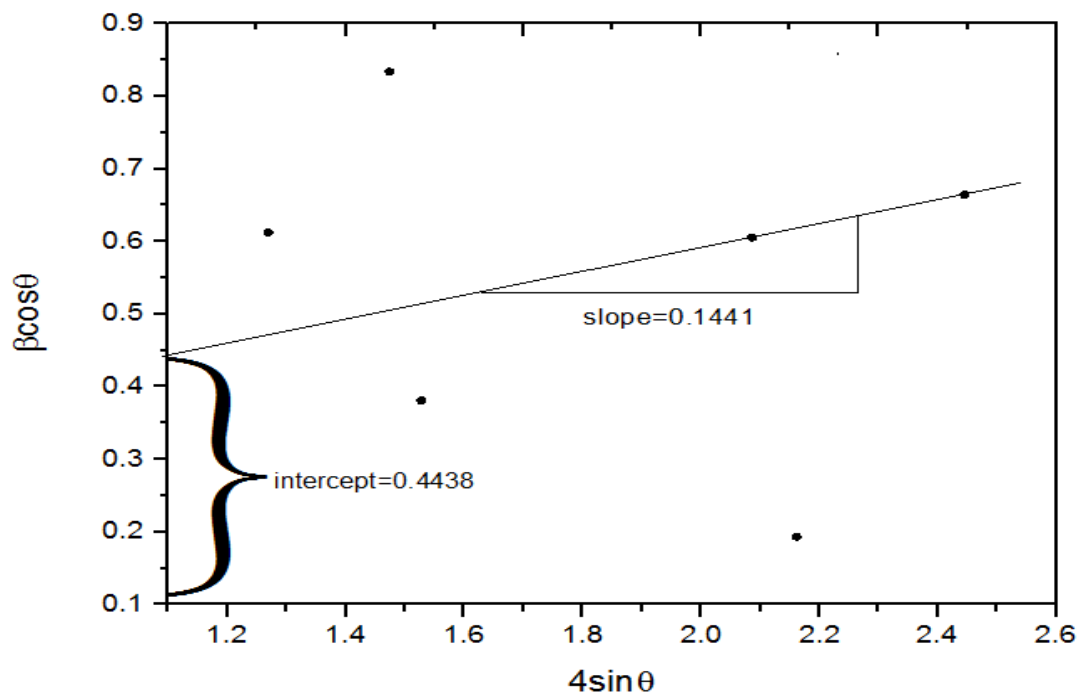


**Figure (3.26):** Plot of Williamson-Hall method

Figure (3.26) was used to calculate the slope and the intercept of the plot, while the crystallite size extracted from the y-intercept by equation (2.5).

$$D = 0.3087 \text{ nm}$$

and the lattice strain extracted from the slope by equation (2.5).

$$\varepsilon = 0.1441$$

### 3.3.4 The size-strain plot method

In this method, equation (2.6) was used to determine the crystallite size, and the lattice strain.  $(d_{hkl}^2 \beta_{hkl} \cos \theta)$  and  $(d_{hkl} \beta_{hkl} \cos \theta)^2$  are calculated for all the lines profile as shown in table (3.12). The results used to plot the relation between  $(d_{hkl}^2 \beta_{hkl} \cos \theta)$  and  $(d_{hkl} \beta_{hkl} \cos \theta)^2$  then calculated the crystallite size and lattice strain.

**Table (3.12):** The results of  $(d_{hkl}^2 \beta_{hkl} \cos \theta)$  and  $(d_{hkl} \beta_{hkl} \cos \theta)^2$  for all the profile lines

$hkl$	$d = \lambda/2\sin\theta$	$d^2$	$d\beta\cos\theta$	$d^2\beta\cos\theta$	$(d\beta\cos\theta)^2$
111	2.42813395	5.895834479	1.567955358	3.610548236	2.458484003
200	2.08975388	4.367071279	1.874316973	3.641055388	3.513064115
220	2.01627838	4.065378506	0.831214795	1.54883128	0.690918035
221	1.47675826	2.180814958	1.047879603	1.320267616	1.098051662
222	1.26029934	1.588354426	1.057600356	1.054948846	1.118518513
311	1.42535176	2.03162764	0.327542984	0.392814674	0.107284406

Figure (3.27) was used to calculate the slope and the intercept of the plot, while the crystallite size extracted from the slope and the lattice strain extracted from y-intercept by equation (2.6)

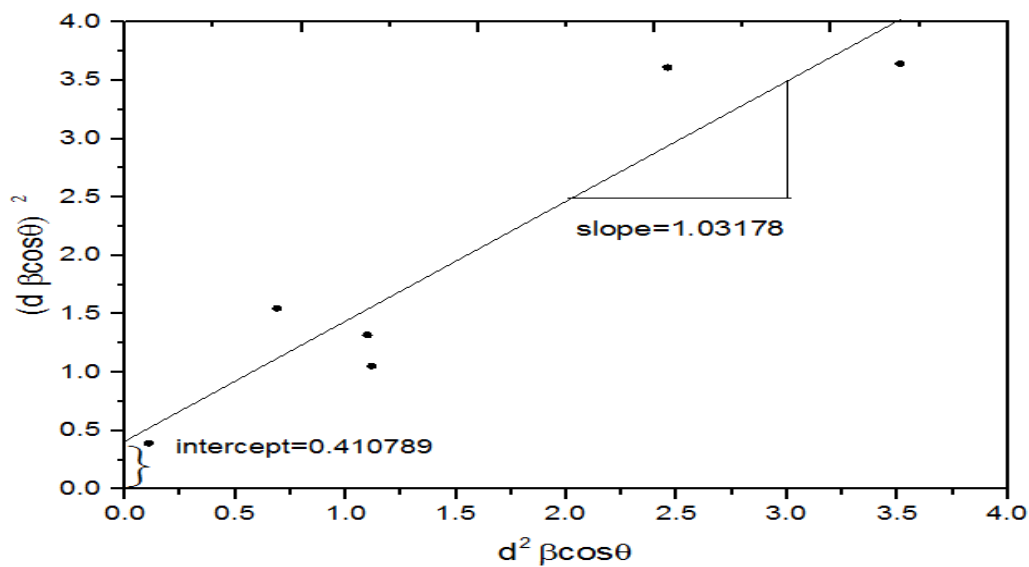


**Figure (3.27):** Plot of Size-Strain plot method

From figure (3.27) the crystallite size is (0.8626 nm) and the lattice strain is (0.8216).

### 3.3.5 The Halder -Wagner method

In this method, equation (3.7) was used to determine the crystallite size, and the lattice strain. Calculated  $(\beta^*/d^*)^2$  and  $(\beta^*/d^{*2})$  for all the profile lines is shown in table (3.13). Then, from the plot between  $(\beta^*/d^*)^2$  and  $(\beta^*/d^{*2})$  we find the crystallite size and lattice strain.

**Table (3.13):** The results of  $(\beta^*/d^*)^2$  and  $(\beta^*/d^{*2})$  for all profile lines.

<i>hkl</i>	$\beta^* = \beta \cos\theta/\lambda$	$d^* = 2\sin\theta/\lambda$	$d^{*2}$	$\beta^*/d^*$	$(\beta^*/d^*)^2$	$\beta^*/d^{*2}$
111	3.97501	4.11839	16.96112	0.96519	0.93158	0.23436
200	5.41187	4.78525	22.89865	1.13095	1.27904	0.23634
220	2.47294	4.95963	24.59797	0.49861	0.24861	0.10053
221	3.92964	6.77159	45.85439	0.58031	0.33676	0.08570
222	4.31116	7.93462	62.95826	0.54334	0.29521	0.06848
311	1.25503	7.01581	49.22162	0.17889	0.03200	0.02550

Figure (3.28) used to calculate the slope and the intercept of the plot, while the crystallite size extracted from the slope and the lattice strain extracted from y-intercept by equation (3.7).

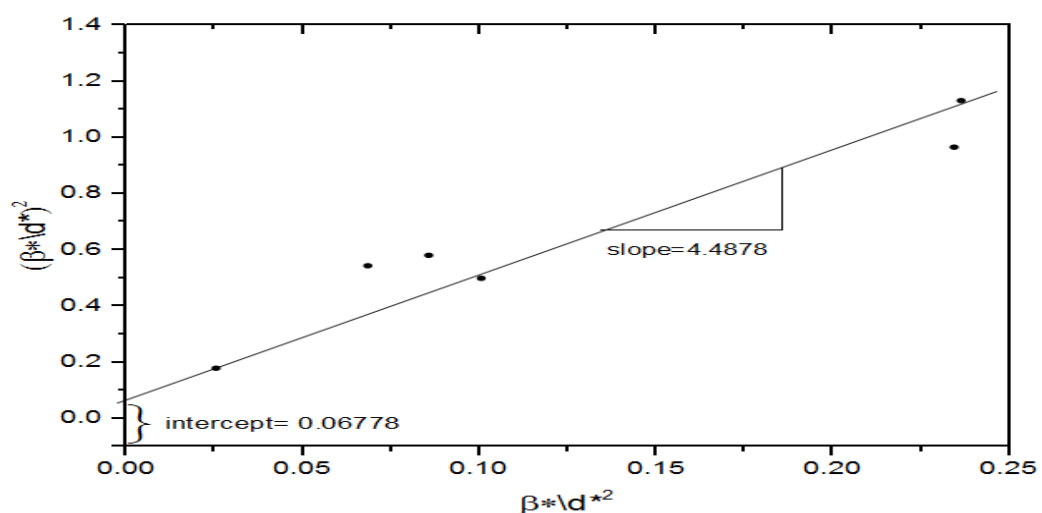


**Figure (3.28):** Plot of Halder-Wagner method

From figure (3.28) the crystallite size is (0.2228 nm) and the lattice strain is (0.5207). All the values of the crystallite size and lattice strain that was obtained from Scherrer, Williamson-Hall, Size-Strain Plot and Halder-Wagner methods are listed in table (3.3).

**Table (3.14):** The values of crystallite size and lattice strain for all applied methods.

Scherrer method		Williamson-Hall method		Size-Strain plot method		Halder-Wagner method	
D nm	E	D nm	$\epsilon$	D nm	$\epsilon$	D nm	$\epsilon$
0.31511	0.32471	0.3087	0.1441	0.8626	0.8216	0.2228	0.5207

The highest value of the crystallite size obtained by Halder-Wagner method, while the smallest value obtained by Scherrer method. This is because Halder-Wagner uses approximate average values of the crystallite size.

### 3.4 Determination of the lattice parameters

#### 3.4.1 Specific Surface Area (SSA)

The SSA was calculated using equation (2.8) by considering the crystallite size values from Halder-Wagner method, where,  $\rho = 6.67 \text{ g/cm}^3$  and  $D = 3.60880 \text{ nm}$ .

$$s = \frac{6 * 10^3}{(0.2228 * 10^{-9} * 6.67)} = 4.03748 * 10^9 \text{ m}^2/\text{g}$$

#### 3.4.2 Dislocation Density

The dislocation density ( $\delta$ ) was calculated using equation (2.9) by considering the crystallite size values from Halder-Wagner method.

$$\delta = 1/0.4720 * 10^{-18} = 2.1186 * 10^{18}$$

### 3.4.3 Morphology Index (MI)

MI is calculated from FWHM for all the profile lines of NiO. Equation (2.10) was used to obtain MI. The results of MI for the lines (111), (200), (220), (221), (222), and (311), are listed in table (3.15).

**Table (3.15):** The results of MI for all profile lines.

<i>hkl</i>	<i>FWHM</i>	$FWHM_h - FWHM_p$	<i>M.I</i>
111	0.3948922	0.9154937	1.431343438
200	0.3659251	0.9444608	1.387443396
220	0.8131441	0.4972418	2.63530922
221	0.387378	0.9230079	1.419690882
222	0.3059024	1.0044835	1.304537008
311	1.3103859	0	

The (220) reflection exhibits the highest (MI), while (222) reflection exhibits the lowest value of (MI). This is because (MI) depends on the difference between the highest value of the FWHM for the standard (311) reflection and other values of FWHM for other reflection.

### 3.4.4 Texture Coefficient

Texture coefficient was calculated using equation (2.11) for all the profile lines in the x-ray diffraction pattern of NiO powder. The results of Texture Coefficient for all the profile lines is listed in table (3.16).

**Table (3.16):** The results of ( $T_c$ ) for (111), (200), (220), (221), (222), and (311) profile lines.

$hkl$	$I(hkl)$	$I(hkl)/I_0(hkl)$	$T_c$
111	681.017525	0.773928003	1.802634619
200	879.949456	1	2.329201957
220	77.708509	0.088310196	0.205692282
221	389.497332	0.442636028	1.030988703
222	153.4512781	0.174386469	0.406181304
311	85.11654	0.096728897	0.225301135
	Total	2.575989592	0.429331599

### 3.5 Modified Halder-Wagner method

The strain was calculated from equation (2.12):

where,  $Y = 7 * 10^{10} \text{N/m}^2$  and  $\epsilon = 0.5207$

$$\sigma = 36449 * 10^6 \text{N/m}^2$$

The energy density ( $u$ ) was calculated from equation (2.14):

$$u = 9489 * 10^6 \text{ N/m}^2$$

Also, equation (2.15) was used to calculate the energy density ( $u$ ):

$$\left(\frac{\beta^*_{hkl}}{d^*_{hkl}}\right)^2 = \left(\frac{1}{D}\right) \left(\frac{\beta^*_{hkl}}{d^*_{hkl}^2}\right) + \frac{u}{2Y}$$

From equation (2.15) ( $u$ ) was extracted using the y- intercept value for Halder - Wagner plot :

$$u = 2 * 7 * 10^{10} * 0.06778$$

$$u = 9489 * 10^6 \text{ N/m}^2$$

### 3.6 The crystallite size at different calcination temperatures

Figure (2.4) was used to determine the crystallite size from the integral breadth at different calcination temperatures (200, 300, and 400) °C. Similarly, the integral breadth was calculated from figure (2.1). The analysis steps to the profile lines (111), and (200) lines are seen in figures ( 3.29) - (3.34) ).

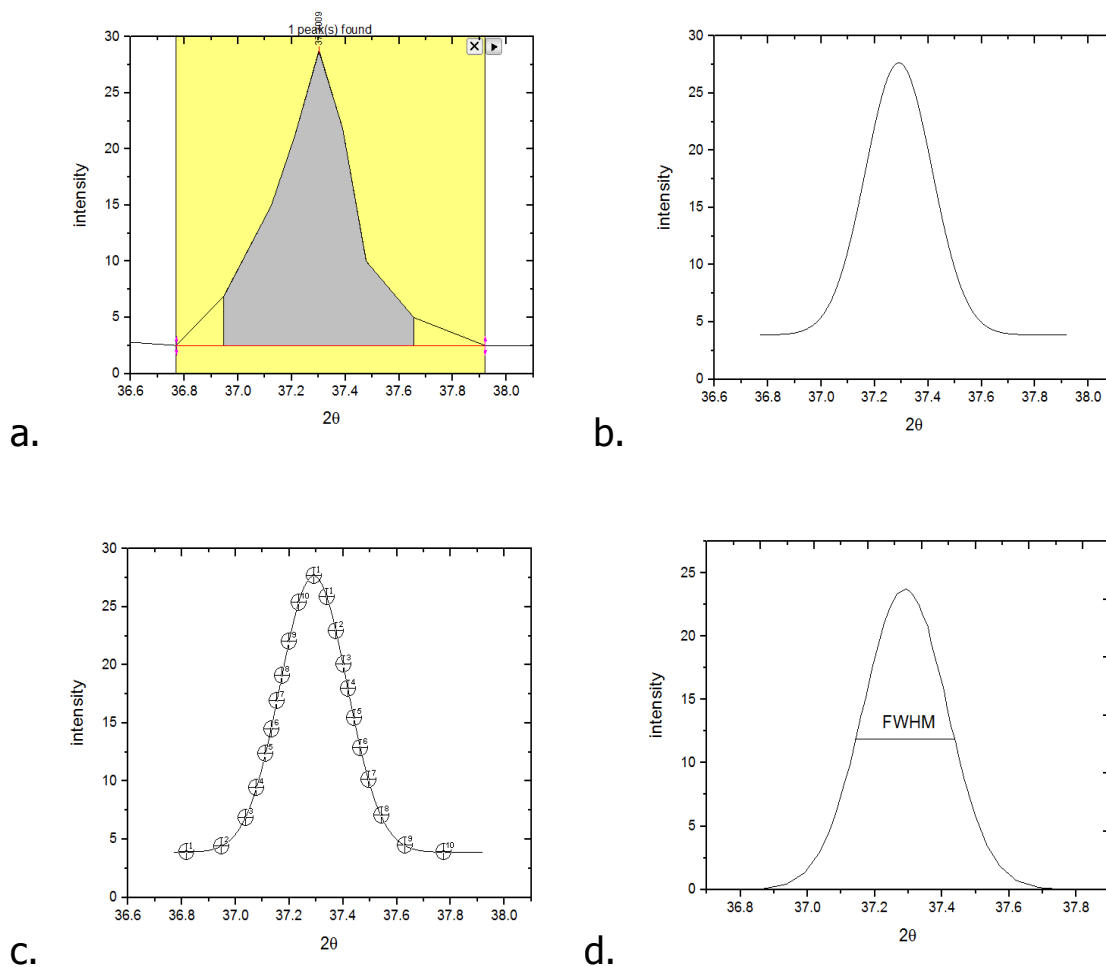


**Figure (3.29):** Analysis steps of (111) line at (200°C)

a. (111) profile line with the fitted curve. b. fitted curve for (111) line

c. fitted profile steps of (111) line with the 10 steps on the right and 10 steps on the left.

d. Determined (FWHM) for the line (111)

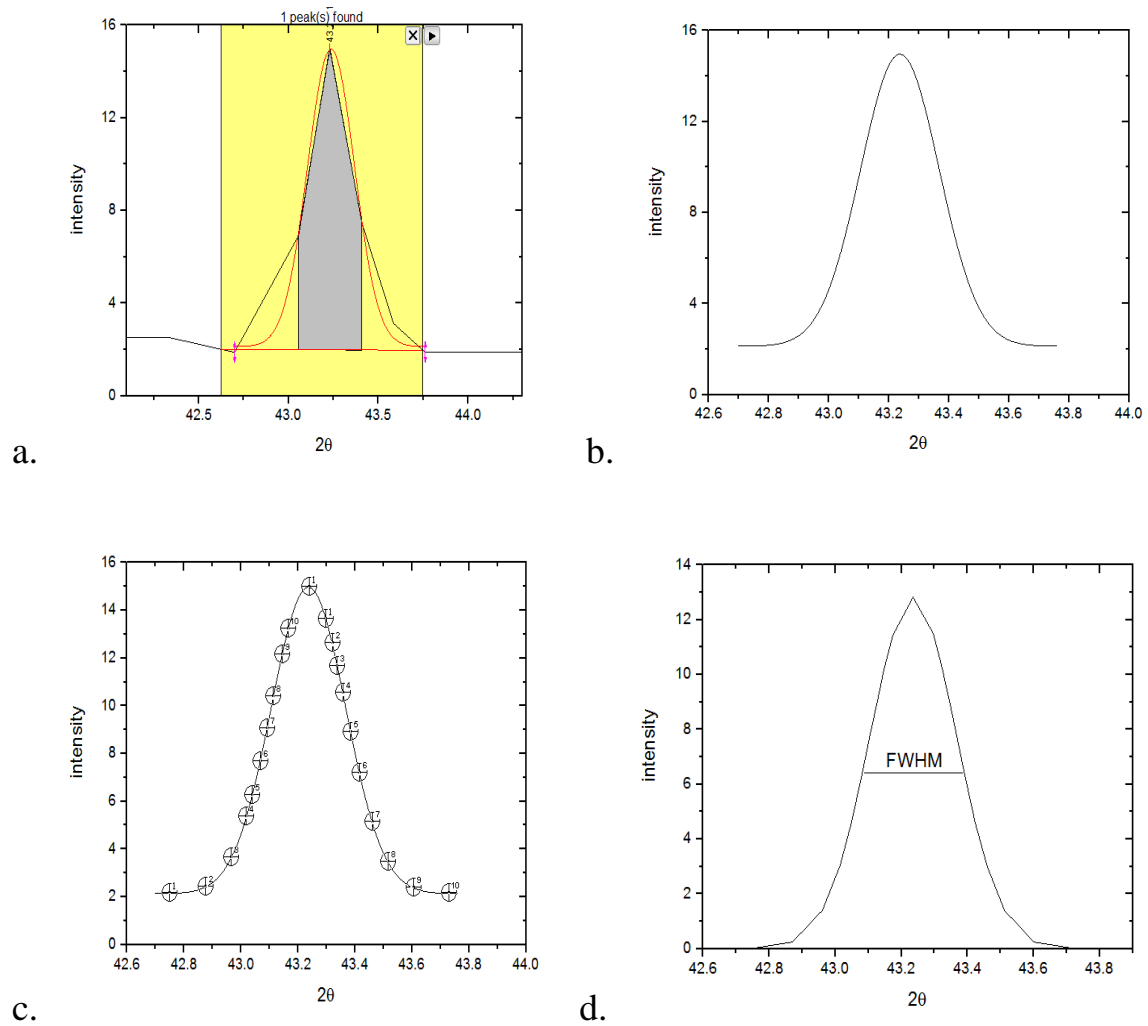


**Figure (3.30):** Analysis steps of (200) line at (200°C)

a. (200) profile line with the fitted curve. b. fitted curve for (200) line

c. fitted profile steps of (200)line with the 10 steps on the right and 10 steps on the left.

d. Determined (FWHM) for the line (200)

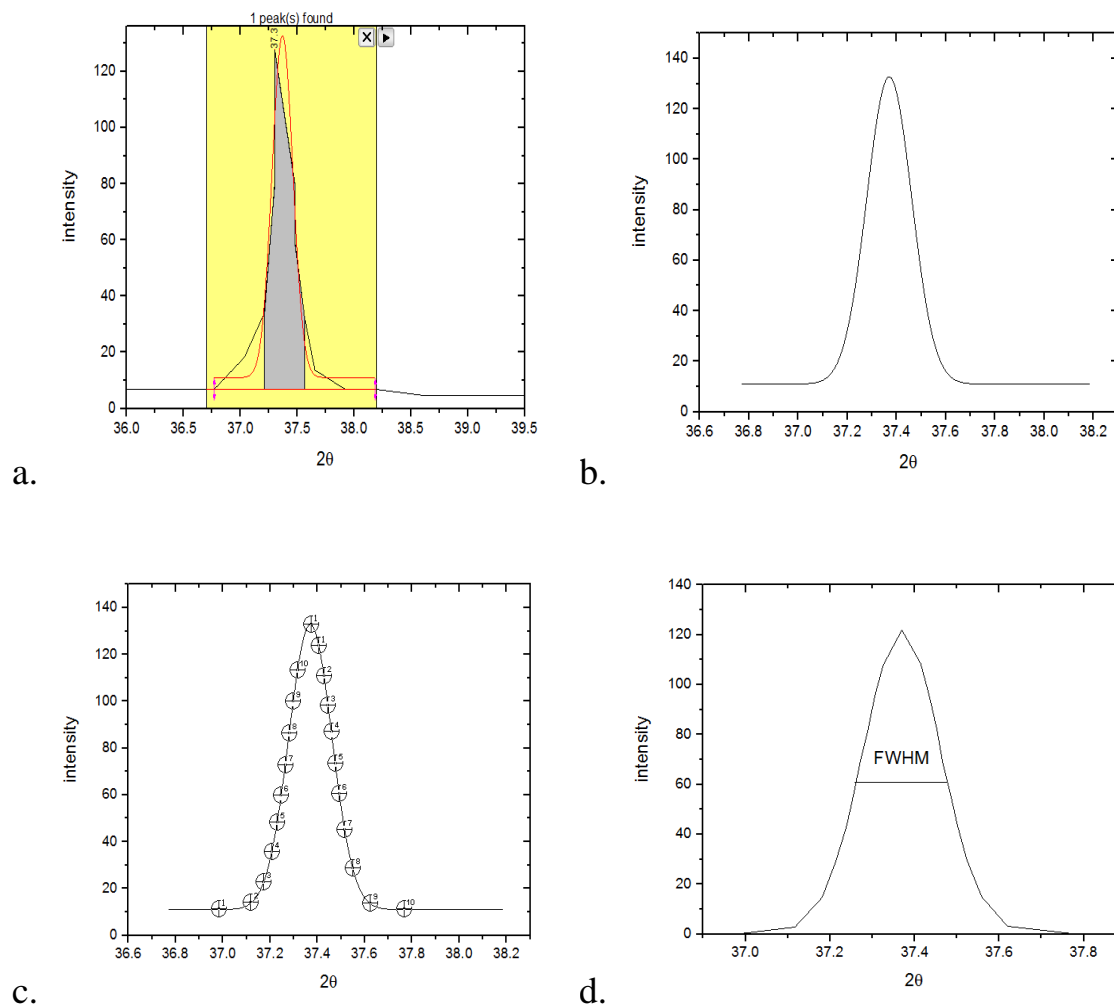


**Figure (3.31):** Analysis steps of (111) line at (300°C)

a. (111) profile line with the fitted curve. b. fitted curve for (111) line

c. fitted profile steps of (111) line with the 10 steps on the right and 10 steps on the left.

d. Determined (FWHM) for the line (111)

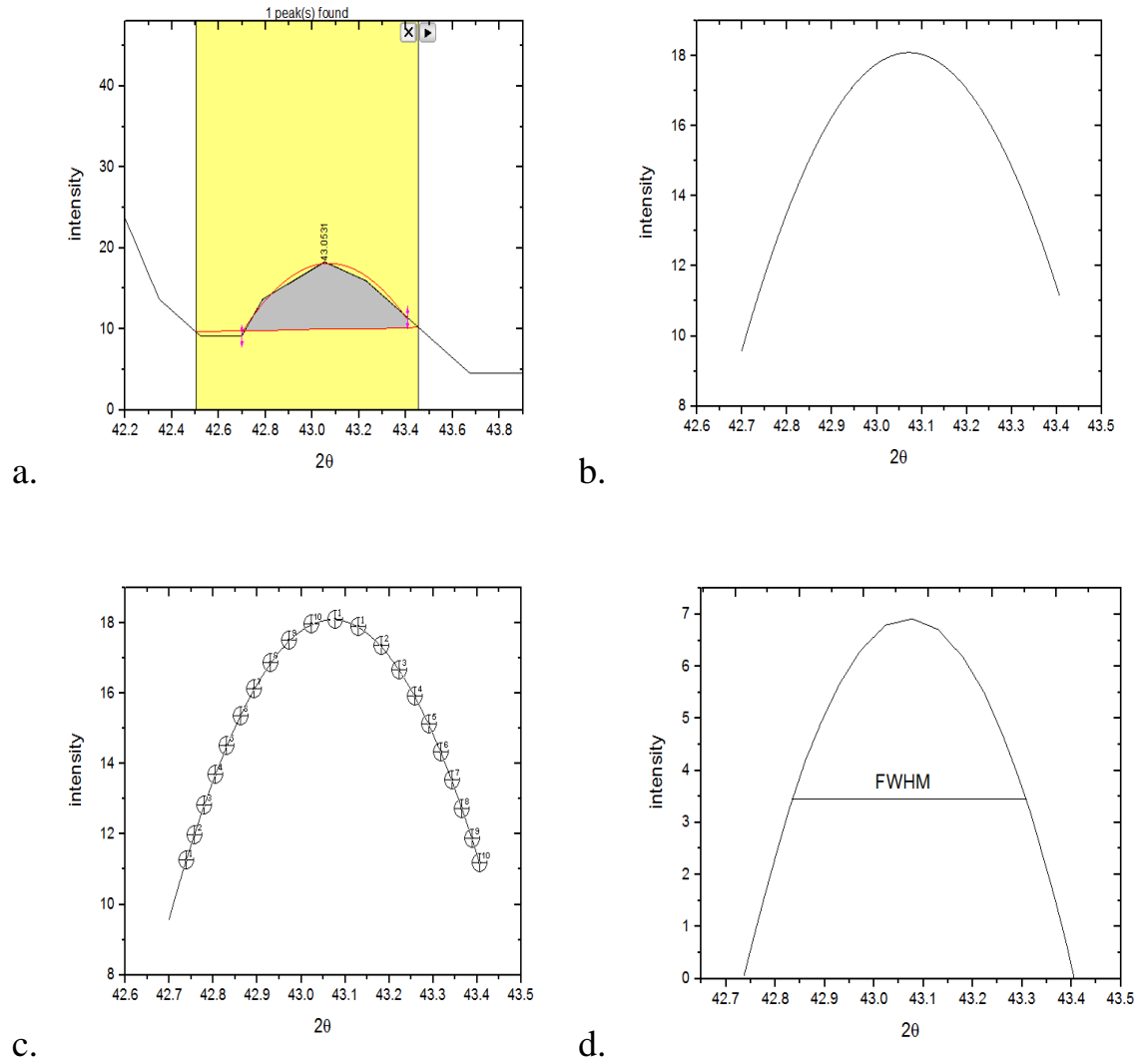


**Figure (3.32):** Analysis steps of (200) line at (300°C)

a. (200) profile line with the fitted curve. b. fitted curve for (200) line

c. fitted profile steps of (200)line with the 10 steps on the right and 10 steps on the left.

d. Determined (FWHM) for the line (200)

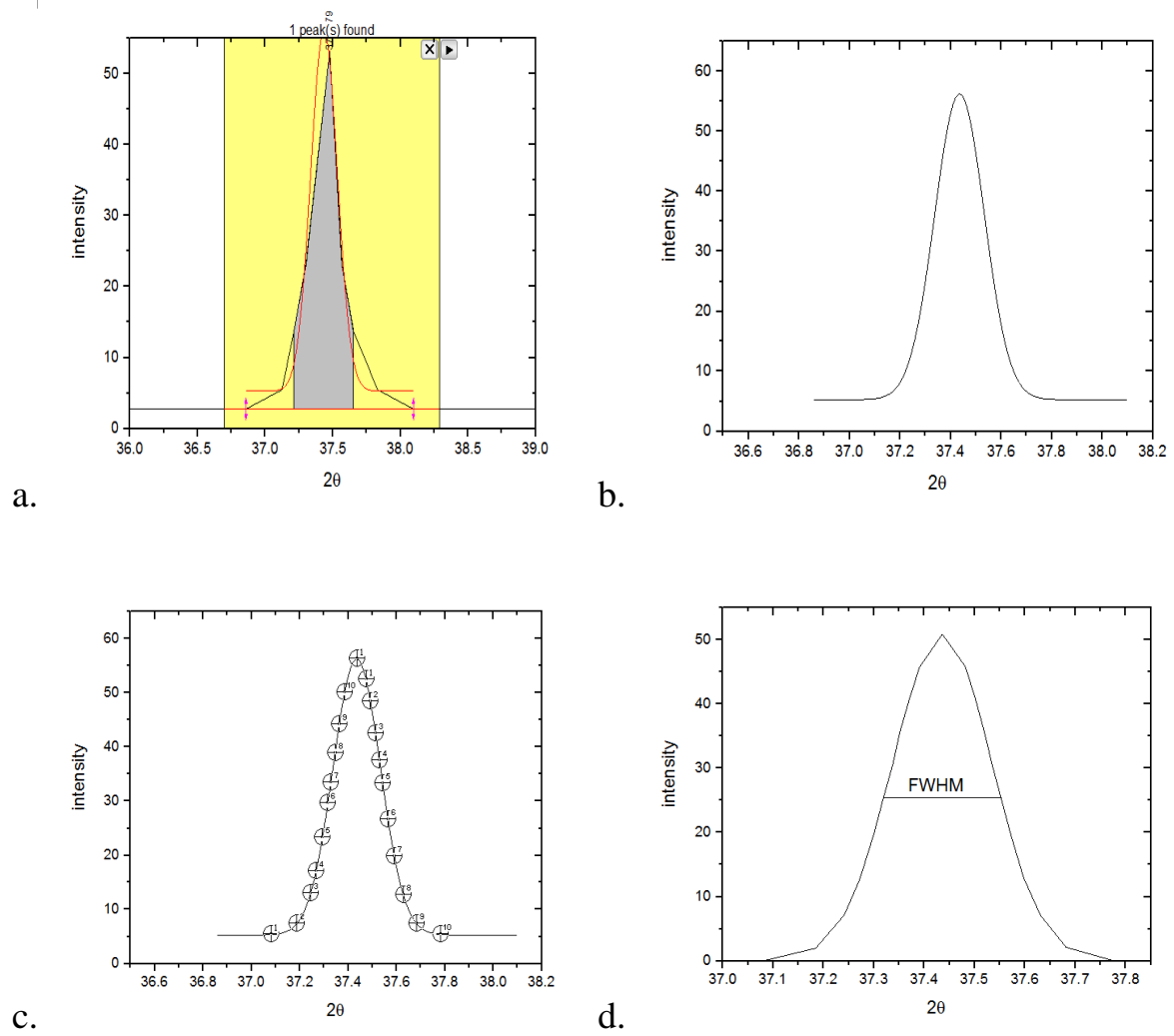


**Figure (3.33):** Analysis steps of (111) line at (400°C)

a. (111) profile line with the fitted curve. b. fitted curve for (111) line

c. fitted profile steps of (111) line with the 10 steps on the right and 10 steps on the left.

d. Determined (FWHM) for the line (111)

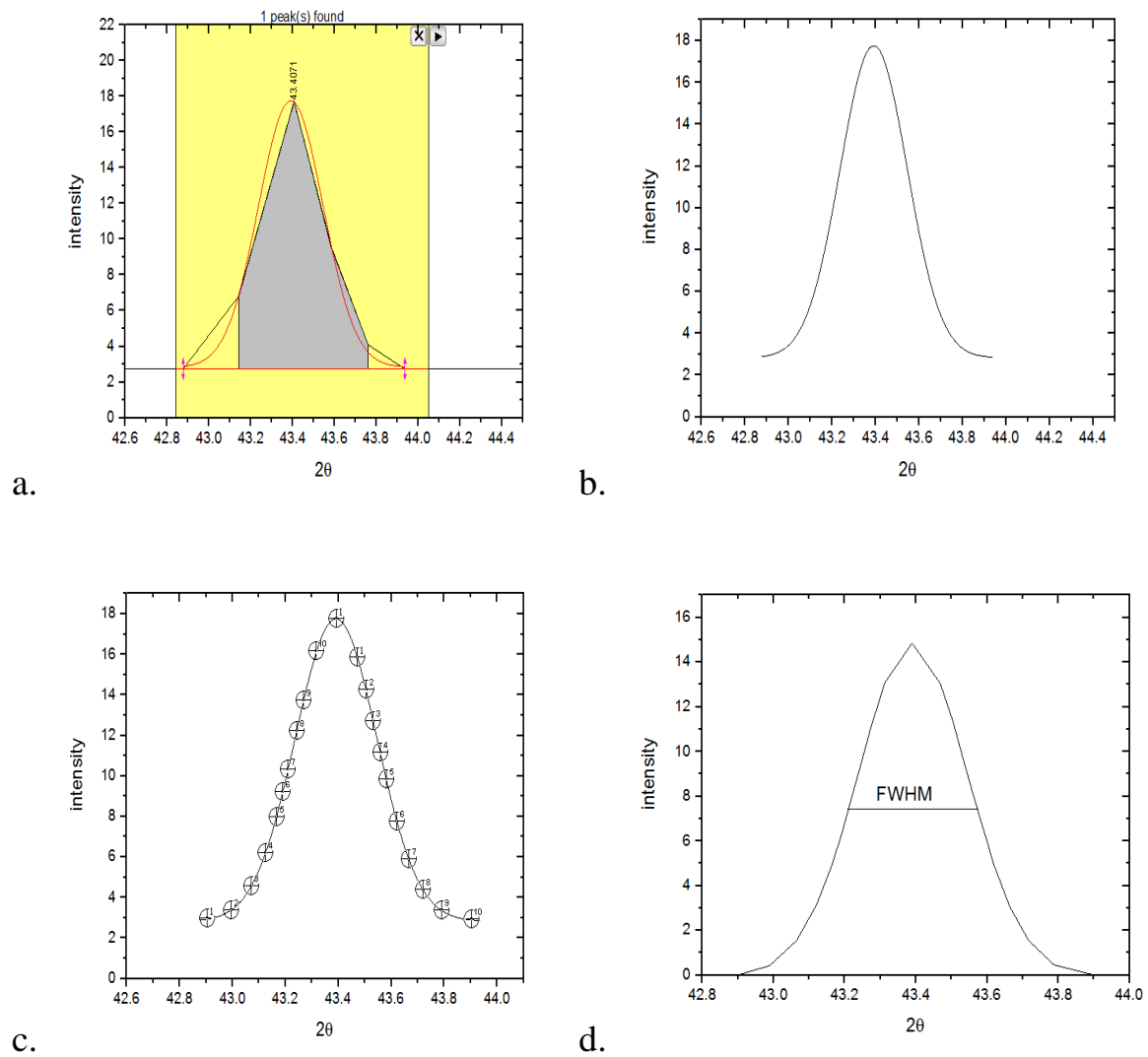


**Figure (3.34):** Analysis steps of (200) line at (400°C)

a. (200) profile line with the fitted curve. b. fitted curve for (200) line

c. fitted profile steps of (200) line with the 10 steps on the right and 10 steps on the left.

d. Determined (FWHM) for the line (200)

The results of the area under the curve of the profile lines (111), and (200) at the (200, 300, and 400) °C listed in table (3.17), (3.18), (3.19), (3.20), (3.21), and (3.22) respectively.

**Table (3.17):** The area under the curve for the line (111) at 200°C

X1	Y1	X2	Y2	Area=(y1+y2)/2*(x2-x1)
36.8135074	0	37.7594779	0	0
36.937798	0.42134832	37.6212259	0.6994382	0.819974221
37.0338252	2.86516854	37.5337117	3.49719101	6.363804134
37.084563	6.08426971	37.4856981	6.98595501	16.29154956
37.1101022	8.46067411	37.4516459	10.27247191	27.42423008
37.1383655	11.32584271	37.4261067	13.00280901	42.27523156
37.1581158	13.70224721	37.4063564	15.72471911	59.27105864
37.1833144	16.42415731	37.3780931	18.45505621	89.53549213
37.2115778	19.43258431	37.3583428	20.75561801	136.9134409
37.24563	22.29775281	37.3331442	22.43258431	255.5604526

**Table (3.18):** The area under the curve for the line (200) at 200°C

X1	Y1	X2	Y2	Area=(y1+y2)/2*(x2-x1)
42.7457889	0	43.7246992	0	0
42.8706243	0.24438203	43.5998638	0.24438203	0.335119025
42.9612259	1.39887641	43.5119183	1.39887641	2.540213756
43.0149376	3.04213484	43.4605675	2.97050562	6.746226476
43.0468104	4.50842697	43.4236776	4.58005618	12.05793865
43.0786833	6.22331461	43.3920999	6.32443821	20.01769022
43.1031782	7.68960675	43.367605	7.75702248	29.20776039
43.1253121	8.91151689	43.347832	8.91151689	40.04817947
43.147151	10.17134829	43.3233371	10.23876409	57.92202784
43.1740068	11.42696629	43.2964813	11.49859549	93.59320422

**Table (3.19):** The area under the curve for the line (111) at 300°

X1	Y1	X2	Y2	Area=(y1+y2)/2*(x2-x1)
36.9797503	0	37.7635641	0.3370787	0.215024729
37.1171396	2.7808989	37.6196141	3.1179776	5.869826728
37.1812032	14.6629214	37.5586379	15	39.29543495
37.213235	28.9887641	37.5235187	29.7050562	94.58089532
37.238706	42.9775281	37.5011351	43.6516854	165.0526056
37.2549149	55.1966293	37.4853121	55.9129214	241.1260873
37.2707378	68.4691012	37.4660159	69.1853933	352.4575836
37.2900341	82.1207866	37.4532804	81.7415731	501.8869025
37.305857	95.3932582	37.4339841	96.0674162	747.1513614
37.3251532	107.6123592	37.4146879	108.3286522	1205.906824

**Table (3.20):** The area under the curve for the line (200) at 300°C

X1	Y1	X2	Y2	Area=(y1+y2)/2*(x2-x1)
42.7364813	0.0525281	43.4058116	0	0.039239296
42.7552781	0.7693821	43.3888536	0.716854	1.172895811
42.7789784	1.6129214	43.3651532	1.5882023	2.730519719
42.8043133	2.4842697	43.3414529	2.3823034	4.530082217
42.8296481	3.3061798	43.3177526	3.1764045	6.640570103
42.8602951	4.1775281	43.2889444	3.9735955	9.507916612
42.8923723	4.9191012	43.2585017	4.7398877	13.19067644
42.9297616	5.6637641	43.2227469	5.5092697	19.06756721
42.9720545	6.3033708	43.180454	6.1766854	29.9426251
43.0229285	6.7915731	43.12958	6.7143259	63.31790458

**Table (3.21):** The area under the curve for the line (111) at 400°C

X1	Y1	X2	Y2	Area=(y1+y2)/2*(x2-x1)
37.0800227	0	37.777412	0	0
37.184563	1.97191011	37.6817253	2.11797753	4.113231876
37.2410897	7.12078653	37.630647	7.12078653	18.27917621
37.2720772	12.72612363	37.5969353	13.01825843	39.6240421
37.3003405	19.84691013	37.5713961	19.84691013	73.22080831
37.3200908	25.74438203	37.5516459	25.59831463	110.8649662
37.3371169	30.43679773	37.5346198	30.58286513	154.4778909
37.3510783	35.43960673	37.5206583	35.29353933	208.5539157
37.3708286	40.88061793	37.5009081	41.04494383	314.9057375
37.3905789	45.73735953	37.4811578	45.88342693	505.7512647

**Table (3.22):** The area under the curve for the line (200) at 400°C

X1	Y1	X2	Y2	Area=(y1+y2)/2*(x2-x1)
42.8992736	0	43.9007264	0	0
42.988899	0.41966292	43.7875823	0.46011236	0.550766042
43.0651759	1.55224719	43.7163905	1.55224719	2.383618534
43.1207946	3.14494382	43.6636322	3.05898877	5.714354155
43.1627469	4.86404495	43.6188195	4.95	10.75930121
43.1916686	6.33033708	43.5924404	6.3758427	15.85213802
43.2155051	7.71573031	43.5635187	7.92808991	22.47587482
43.2444268	9.35393261	43.5317367	9.72808991	33.20808388
43.2733485	11.07303371	43.5053575	11.28033711	48.17349935
43.313076	13.08539331	43.4684904	13.04494381	84.0666538

Calculated FWHM and integral breadth values for all lines at three different temperatures are listed in table (3.23).

**Table (3.23):** The FWHM and integral breadth ( $\beta$ ) of the lines (111), and (200) at three different temperatures

temperature	<i>hkl</i>	$2\theta_1$	$2\theta_2$	$2\theta/2$	$I_0$	FWHM	Area	$\beta = \text{Area}/I_0$
200	111	37.14186	37.43771	18.64489	23.76404	0.29585	634.45523	26.69812
	200	43.08104	43.39033	21.61784	12.82584	0.30928	262.46836	20.46403
300	111	37.26254	37.47730	18.68496	121.93820	0.21476	3353.54255	27.50198
	200	42.83505	43.30704	21.53552	6.91826	0.47199	150.14000	21.70199
400	111	37.31935	37.55149	18.71771	50.88624	0.23213	1429.79103	28.09780
	200	43.21026	43.57176	21.69551	14.84494	0.36150	223.18429	15.03436

Calculate integral breadth in radian after used Gaussian function to correct the values of ( $\beta$ ) are seen in table (3.24).

**Table (3-24):** The values of  $\beta$  for profile lines (111), and (200) at three different temperatures

T	<i>hkl</i>	$\beta_h$	$\beta_g$	$\beta_h^2$	$\beta_g^2$	$\beta_f^2$	$\beta_f$	$\beta_f * \pi / 180$
200	111	26.69812	11.11800	712.78961	123.60992	589.17969	24.27302	0.42343
	200	20.46403	11.11800	418.77652	123.60992	295.1666	17.18041	0.29970
300	111	27.50198	11.11800	756.35890	123.60992	632.74898	25.15450	0.43881
	200	21.70199	11.11800	470.97637	123.60992	347.36645	18.63777	0.32513
400	111	28.09780	11.11800	789.48636	123.60992	665.87644	25.80458	0.45015
	200	15.03436	11.11800	226.03198	123.60992	102.42206	10.12038	0.17654

Equation (2.2) was used to determine the crystallite size for all profile line at three different temperatures using the integral breadth values in table (3.24).

At 200 °C

$$D_{111} = \frac{0.89 * 0.15406}{\beta_{111} * \cos\theta} = \frac{0.89 * 0.15406}{0.42343 * 0.94752} = \frac{0.13711}{0.40121} = 0.34174 \text{ nm}$$

$$D_{200} = \frac{0.89 * 0.15406}{\beta_{200} * \cos\theta} = \frac{0.89 * 0.15406}{0.29970 * 0.92966} = \frac{0.13711}{0.27862} = 0.49210 \text{ nm}$$

At 300 °C

$$D_{111} = \frac{0.89 \cdot 0.15406}{\beta_{111} \cdot \cos\theta} = \frac{0.89 \cdot 0.15406}{0.43881 \cdot 0.94729} = \frac{0.13711}{0.41568} = 0.32985 \text{ nm}$$

$$D_{200} = \frac{0.89 \cdot 0.15406}{\beta_{200} \cdot \cos\theta} = \frac{0.89 \cdot 0.15406}{0.32513 \cdot 0.93019} = \frac{0.13711}{0.30243} = 0.45336 \text{ nm}$$

At 400 °C

$$D_{111} = \frac{0.89 \cdot 0.15406}{\beta_{111} \cdot \cos\theta} = \frac{0.89 \cdot 0.15406}{0.45015 \cdot 0.94711} = \frac{0.13711}{0.42634} = 0.32160 \text{ nm}$$

$$D_{200} = \frac{0.89 \cdot 0.15406}{\beta_{200} \cdot \cos\theta} = \frac{0.89 \cdot 0.15406}{0.17654 \cdot 0.92916} = \frac{0.13711}{0.16403} = 0.83588 \text{ nm}$$

The results of the crystallite size at three different temperature are listed in table (3.25), and figure (3.35) shows the relation between the crystallite size and the temperatures.

**Table (3.25):** The results of crystallite size for two lines profile of the NiO at three different temperatures

<i>hkl</i>	D at 200 °C	D at 300 °C	D at 400 °C
111	0.34174 nm	0.32985 nm	0.32160 nm
200	0.49210 nm	0.45336 nm	0.83588 nm

From the results in the table (3.25), the crystallite size was decreased along with increasing the calcination temperatures at diffraction line (111), that is mean the relation is inversely between the crystallite size with the calcination temperatures. At the diffraction line (200), the crystallite size was decreased at (200-300)° C then increased at (400)° C, with compare the two line, the line (200) have a different behavior due the line (111), this different behavior by the interference of two intensity in the line (one for the line (200) and other is noise). The figure (3.35) show the relation between the crystallite size with the calcination temperatures.

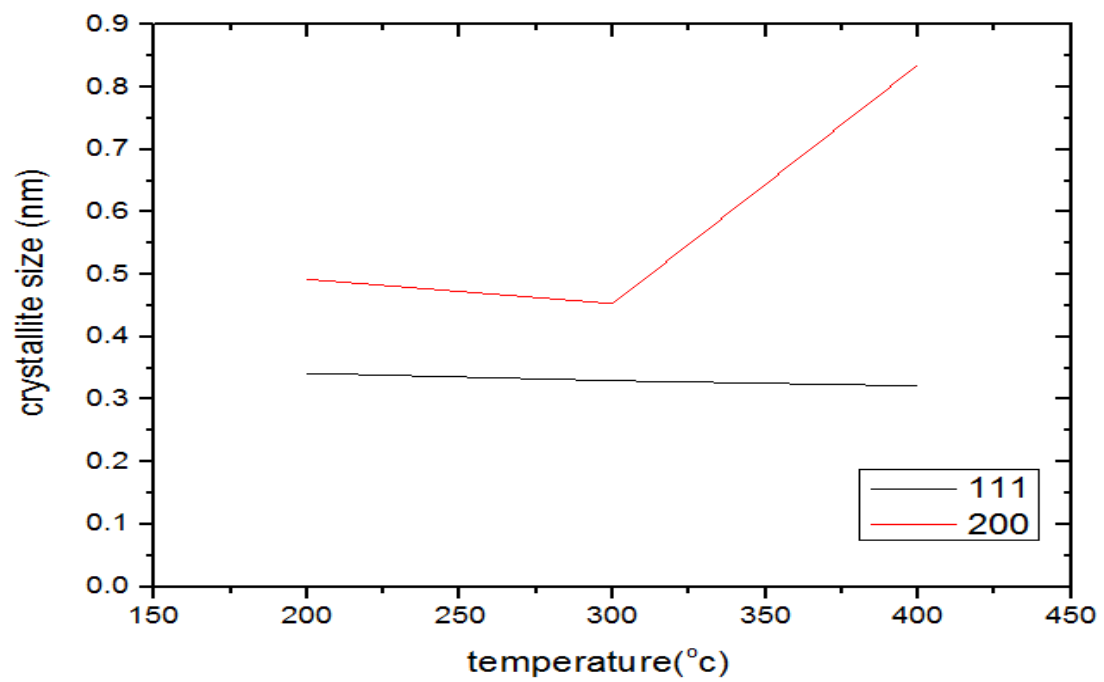


**Figure (3.35):** Relation between crystallite size and temperature

*Chapter Four*

*Conclusions and Suggestions*

*for Future Work*

## 4.1 Conclusions

From the results that have been obtained through this study, we conclude:

1- The Debye - Scherrer method is a simple way to calculate the crystallite size and the strain and it is not expected to be valid for very small crystallite sizes (<10 nm) however, it is used in this study to compare its results with other methods.

2-The result of the modified Scherrer method was nearly from that was calculated by the Scherrer method.

3- In Williamson-Hall approach, the larger the slope the larger the lattice strain will be, while the larger the intercept the smaller the crystallite size will be. Intercept with origin D is infinity or broadening only due to lattice strain broadening, while zero slope means horizontal line free of lattice strain or broadening is related to crystallite size broadening.

4- The size-strain plot method (SSP ) gives information about the lattice strain ( $\epsilon$ ) and the crystallite size (D) of NiO that obtained from  $\beta_{hkl}$  and planar spacing  $d_{hkl}$ . The SSP method is more precise, particularly at high diffraction angles.

5- The Halder-Wagner method is more accurate, with most of data points touching the fitting line compared with other methods. Therefore, one method is more accurate data points of (x,y) are more touching the fitting line.

6-The Specific Surface Area (SSA) was calculated by using the crystallite size of the Halder –Wagner method ( $s = 4.03748 * 10^9 m^2/g$ ), this value mean these crystal of NiO powder have a small crystallite size with large surface.

7- The dislocation density ( $\delta$ ) depends on the crystallite size of Halder-Wagner ( $\delta = 2.1186 * 10^{18}$ ), this value show that is the powder have big number of dislocation.

8- Morphology Index (MI) is calculated from FWHM and the highest value was (2.63530922) for the line (220) and the lowest value was (1.304537008) for the line (222), therefore the best angle diffraction at the line (220).

9- Texture coefficient calculated for all line profiles was (0.429331599).

10- By Modifying Halder-Wagner method the strain and the energy density (u) were, ( $\sigma = 36449 \times 10^6 \text{ N/m}^2$ ), ( $u = 9489 \times 10^6 \text{ N/m}^2$ ). Also, the y- intercept was used to calculate the energy density (u) which gives the same value.

11- The relation between the crystallite size with the calcination temperatures was inversely, as shown at the line (111) and (200) in the different calcination temperatures .While, the line (200) has a different behavior compare to (111) at  $(400)^\circ \text{C}$ , this is due to interference of the two intensity in the line (200) (one for line (200) and other is noise).

## 4.2 Future works

At the end of this study, these are some suggestions as a future work :-

- 1 - A comparative study between Halder-Wagner method and other methods with the same order of accuracy in calculating the crystallite size and lattice strain.
- 2 - Calculating the mechanical properties of NiO by using a suitable technique .
- 3- Calculating new lattice parameters such as Burgers vector and determine some types of defects that may exist in the lattice.
- 4 - Calculating the crystallite size and lattice strain of NiO using of Halder-Wagner method by separating variables without using the diagram.

# *References*

## References

- [1] Madani, Hisham ALtayeab. "Determination of Energy Gap in Nickel Oxide (NiO) Using Optical Properties." PhD diss., University of Gezira, 2016.
- [2] Greenwood, Norman Neill, and Alan Earnshaw. Chemistry of the Elements. Elsevier, 2012.
- [3] Lascelles, Keith, Lindsay G. Morgan, David Nicholls, and Detmar Beyersmann. "Nickel compounds." Ullmann's Encyclopedia of Industrial Chemistry (2000).
- [4] Handbook of Inorganic Chemicals", Pradniak, Pradyot; McGraw-Hill Publications,2002.
- [5] Monshi, Ahmad, Mohammad Reza Foroughi, and Mohammad Reza Monshi. "Modified Scherrer equation to estimate more accurately nano-crystallite size using XRD." World journal of nano science and engineering ,vol.2, no. 3, pp.154-160, 2012.
- [6] Prabhu, Yendrapati Taraka, Kalagadda Venkateswara Rao, Vemula Sesha Sai Kumar, and Bandla Siva Kumari. "X-ray analysis by Williamson-Hall and size-strain plot methods of ZnO nanoparticles with fuel variation." World Journal of Nano Science and Engineering, vol.4, no. 01, pp.21, 2014.
- [7] Gonçalves, N. S., J. A. Carvalho, Z. M. Lima, and J. M. Sasaki. "Size–strain study of NiO nanoparticles by X-ray powder diffraction line broadening." Materials Letters, no.72 , pp. 36-38, 2012.
- [8] Shukla, Pratik, Subhasisa Nath, Guanjun Wang, Xiaojun Shen, and Jonathan Lawrence. "Surface property modifications of silicon carbide ceramic following laser shock peening." Journal of the European Ceramic Society, vol. 37, no. 9, pp. 3027-3038, 2017.
- [9] Kibasomba, Pierre M., Simon Dhlamini, Malik Maaza, Chuan-Pu Liu, Mohamed M. Rashad, Diaa A. Rayan, and Bonex W. Mwakikunga. "Strain

- and grain size of TiO<sub>2</sub> nanoparticles from TEM, Raman spectroscopy and XRD: The revisiting of the Williamson-Hall plot method." *Results in Physics*, no 9, pp. 628-635, 2018.
- [10] Abdullah, Mikrajuddin, and Khairurrijal Khairurrijal. "Derivation of Scherrer relation using an approach in basic physics course." *Jurnal Nanosains & Nanoteknologi*, vol. 1, no. 1, pp. 28-32, 2009.
- [11] Biju, V., Neena Sugathan, V. Vrinda, and S. L. Salini. "Estimation of lattice strain in nanocrystalline silver from X-ray diffraction line broadening." *Journal of Materials Science*, vol. 43, no. 4, pp. 1175-1179, 2008.
- [12] Jeyaprakash, B. G., K. Kesavan, R. Ashok Kumar, S. Mohan, and A. Amalarani. "Temperature dependent grain-size and microstrain of CdO thin films prepared by spray pyrolysis method." *Bulletin of Materials Science*, vol. 34, no. 4, pp. 601, 2011.
- [13] Khorrami, Gh H., A. Khorsand Zak, and Ahmad Kompany. "Optical and structural properties of X-doped (X= Mn, Mg, and Zn) PZT nanoparticles by Kramers–Kronig and size strain plot methods." *Ceramics International*, vol. 38, no. 7, pp. 5683-5690, 2012.
- [14] Izumi, Fujio, and Takuji Ikeda. "Implementation of the Williamson-Hall and Halder-Wagner methods into RIETAN-FP.", pp. 33-38, 2015.
- [15] Gaber, A., M. A. Abdel-Rahim, A. Y. Abdel-Latief, and Mahmoud N. Abdel-Salam. "Influence of calcination temperature on the structure and porosity of nanocrystalline SnO<sub>2</sub> synthesized by a conventional precipitation method." *Int J Electrochem Sci*, vol. 9, no. 1, pp. 81-95, 2014.
- [16] Sarma, Hiten, and K. C. Sarma. "X-ray peak broadening analysis of ZnO nanoparticles derived by precipitation method." *Int. J. Sci. Res. Publ*, vol. 4, no. 3, pp. 1-7, 2014.
- [17] Parra, Mohammad Ramzan, and Fozia Z. Haque. "Aqueous chemical route synthesis and the effect of calcination temperature on the structural and

- optical properties of ZnO nanoparticles." *Journal of Materials Research and Technology*, vol. 3, no. 4, pp. 363-369, 2014.
- [18] Motevalizadeh, L., Z. Heidary, and M. Ebrahimizadeh Abrishami. "Facile template-free hydrothermal synthesis and microstrain measurement of ZnO nanorods." *Bulletin of materials science*, vol. 37, no. 3, pp. 397-405, 2014.
- [19] Bindu, P., and Sabu Thomas. "Estimation of lattice strain in ZnO nanoparticles: X-ray peak profile analysis." *Journal of Theoretical and Applied Physics*, vol. 8, no. 4, pp. 123-134, 2014.
- [20] Thandavan, Tamil Many K., Siti Meriam Abdul Gani, Chiow San Wong, and Roslan Md Nor. "Evaluation of Williamson–Hall strain and stress distribution in ZnO nanowires prepared using aliphatic alcohol." *Journal of Nondestructive Evaluation*, vol. 34, no. 2, pp. 14, 2015.
- [21] Patle, L. B., P. K. Labhane, V. R. Huse, and A. L. Chaudhari. "Structural analysis of Cu doped TiO<sub>2</sub> nanoparticles using Williamson–Hall method." *International Journal of Scientific Research in Science, Engineering and Technology*, vol. 1, no. 5, pp. 66-70, 2015.
- [22] Chenari, Hossein Mahmoudi, Hadi Fallah Moafi, and Omid Rezaee. "A study on the microstructural parameters of Zn (1-x) LaxZrxO nanopowders by X-ray line broadening analysis." *Materials Research*, vol. 19, no. 3, pp. 548-554, 2016.
- [23] Muniz, Francisco Tiago Leitao, Marcus Aurélio Ribeiro Miranda, Cássio Morilla dos Santos, and José Marcos Sasaki. "The Scherrer equation and the dynamical theory of X-ray diffraction." *Acta Crystallographica Section A: Foundations and Advances*, vol. 72, no. 3, pp.385-390, 2016.
- [24] Solanki, Rekha Garg, Poolla Rajaram, and P. K. Bajpai. "Growth, characterization and estimation of lattice strain and size in CdS nanoparticles: X-ray peak profile analysis." *Indian Journal of Physics*, vol. 92, no. 5, pp. 595-603, 2018.
- [25] Sakae, Toshiro, Tetsuro Kono, Hiroyuki Okada, Hiroshi Nakada, Hidehito Ogawa, Tsuneyuki Tsukioka, and Takashi Kaneda. "X-ray micro-

- diffraction analysis revealed the crystallite size variation in the neighboring regions of a small bone mass." *Journal of Hard Tissue Biology*, vol. 26, no. 1, pp. 103-107, 2017.
- [26] Tatarchuk, Tetiana, Mohamed Bououdina, Wojciech Macyk, Olexander Shyichuk, Natalia Paliychuk, Ivan Yaremiy, Basma Al-Najar, and Michał Pacia. "Structural, optical, and magnetic properties of Zn-doped CoFe<sub>2</sub>O<sub>4</sub> nanoparticles." *Nanoscale research letters*, vol. 12, no. 1, pp. 141, 2017.
- [27] Rajesh Kumar, B., and B. Hymavathi. "X-ray peak profile analysis of solid-state sintered alumina doped zinc oxide ceramics by Williamson–Hall and size-strain plot methods." *Journal of Asian Ceramic Societies*, vol. 5, no. 2, pp. 94-103, 2017.
- [28] Shashidhargouda, H. R., and Shridhar N. Mathad. "Synthesis and structural analysis of Ni<sub>0.45</sub>Cu<sub>0.55</sub>Mn<sub>2</sub>O<sub>4</sub> by Williamson–Hall and size–strain plot methods." *Ovidius University Annals of Chemistry*, vol. 29, no. 2, pp. 122-125, 2018.
- [29] Lima, Francisco Marcone, Felipe Mota Martins, Maia Júnior, Paulo Herbert França, Ana Fabíola Leite Almeida, and Francisco Nivaldo Aguiar Freire. "Nanostructured titanium dioxide average size from alternative analysis of Scherrer's Equation." *Matéria (Rio de Janeiro)*, vol. 23, no. 1, 2018.
- [30] Gupta, Rashi, R. P. Chauhan, S. K. Chakarvarti, and Rajesh Kumar. "Effect of SHI on properties of template synthesized Cu nanowires." *Ionics*, vol. 25, no. 1, pp. 341-352, 2019.
- [31] Geravand, Mosayeb, and Farid Jamali-Sheini. "Al-doped Ag<sub>2</sub>S nanostructures: Ultrasonic synthesis and physical properties." *Ceramics International*, vol. 45, no. 5, pp. 6175-6182, 2019.
- [32] Kumar, B. Rajesh, and B. Hymavathi. "X-ray peak profile analysis of Sb<sub>2</sub>O<sub>3</sub>-doped ZnO nanocomposite semiconductor." *Advances in Natural Sciences: Nanoscience and Nanotechnology*, vol. 9, no. 3, pp. 035018, 2018.

- [33] Irfan, H., Mohamed Racik K, and S. Anand. "Microstructural evaluation of CoAl<sub>2</sub>O<sub>4</sub> nanoparticles by Williamson–Hall and size–strain plot methods." *Journal of Asian Ceramic Societies*, vol. 6, no. 1, pp. 54-62, 2018.
- [34] Kafashan, Hosein. "X-ray Diffraction Line Profile Analysis of Undoped and Se-Doped SnS Thin Films Using Scherrer's, Williamson–Hall and Size–Strain Plot Methods." *Journal of Electronic Materials*, vol. 48, no. 2, pp. 1294-1309, 2019.
- [35] Al-Tabbakh, Ahmed A., Nilgun Karatepe, Aseel B. Al-Zubaidi, Aida Benchaabane, and Natheer B. Mahmood. "Crystallite size and lattice strain of lithiated spinel material for rechargeable battery by X-ray diffraction peak-broadening analysis." *International Journal of Energy Research*, vol. 43, no. 5, pp. 1903-1911, 2019.
- [36] Korchef, Atef, Yannick Champion, and Nabil Njah. "X-ray diffraction analysis of aluminium containing Al<sub>8</sub>Fe<sub>2</sub>Si processed by equal channel angular pressing." *Journal of alloys and compounds*, vol. 427, no. 1-2, pp. 176-182, 2007.
- [37] Azhagu Raj, Ramakrishnan, Mohamad AlSalhi, and Sandhanasamy Devanesan. "Microwave-assisted synthesis of nickel oxide nanoparticles using coriandrum sativum leaf extract and their structural-magnetic catalytic properties." *Materials*, vol. 10, no. 5, pp. 460, 2017.
- [38] Kafashan, Hosein. "X-ray Diffraction Line Profile Analysis of Undoped and Se-Doped SnS Thin Films Using Scherrer's, Williamson–Hall and Size–Strain Plot Methods." *Journal of Electronic Materials*, vol. 48, no. 2, pp. 1294-1309, 2019.
- [39] Epp, J. "X-ray diffraction (XRD) techniques for materials characterization." In *Materials characterization using Nondestructive Evaluation (NDE) methods*, pp. 81-124. Woodhead Publishing, 2016.
- [40] P.Scherrer, "Bestimmung der Grösse und der inneren Struktur von Kolloidteilchen mittels Röntgenstrahlen, *Nachrichten von der Gesellschaft der Wissenschaften, Göttingen*", pp. 98–100, 1918.

- [41] Holzwarth, Uwe, and Neil Gibson. "The Scherrer equation versus the Debye-Scherrer equation." *Nature nanotechnology*, vol. 6, no. 9, pp. 534, 2011.
- [42] Monshi, Ahmad, Mohammad Reza Foroughi, and Mohammad Reza Monshi. "Modified Scherrer equation to estimate more accurately nanocrystallite size using XRD." *World journal of nano science and engineering*, vol. 2, no. 3, pp. 154-160, 2012.
- [43] Gonçalves, N. S., J. A. Carvalho, Z. M. Lima, and J. M. Sasaki. "Size-strain study of NiO nanoparticles by X-ray powder diffraction line broadening." *Materials Letters*, vol. 72, pp. 36-38, 2012.
- [44] Rajesh Kumar, B., and B. Hymavathi. "X-ray peak profile analysis of solid-state sintered alumina doped zinc oxide ceramics by Williamson-Hall and size-strain plot methods." *Journal of Asian Ceramic Societies*, vol. 5, no. 2, pp. 94-103, 2017.
- [45] Izumi, Fujio, and Takuji Ikeda. "Implementation of the Williamson-Hall and Halder-Wagner methods into RIETAN-FP.", 33-38, 2015.
- [46] Charlot, F., E. Gaffet, B. Zeghmati, F. Bernard, and J. C. Niepce. "Mechanically activated synthesis studied by X-ray diffraction in the Fe-Al system." *Materials Science and Engineering: A*, vol. 262, no. 1-2, pp. 279-288, 1999.
- [47] Amigó, José M., Francisco J. Serrano, Marek A. Kojdecki, Joaquín Bastida, Vicente Esteve, María Mercedes Reventós, and Francisco Martí. "X-ray diffraction microstructure analysis of mullite, quartz and corundum in porcelain insulators." *Journal of the European Ceramic Society*, vol. 25, no. 9, pp. 1479-1486, 2005.
- [48] Theivasanthi, Thirugnanasambandan, and Marimuthu Alagar. "Titanium dioxide (tio<sub>2</sub>) nanoparticles xrd analyses: An insight." *arXiv preprint arXiv*., pp. 1307-1091, 2013.

- [49] Theivasanthi, T., and M. Alagar. "Chemical capping synthesis of nickel oxide nanoparticles and their characterizations studies." arXiv preprint arXiv:, pp. 1212-4595, 2012.
- [50] Ravichandran, K., P. V. Rajkumar, B. Sakthivel, K. Swaminathan, and L. Chinnappa. "Role of precursor material and annealing ambience on the physical properties of SILAR deposited ZnO films." *Ceramics International*, vol. 40, no. 8, pp. 12375-12382, 2014.
- [51] Fasaki, I., A. Koutoulaki, M. Kompitsas, and C. Charitidis. "Structural, electrical and mechanical properties of NiO thin films grown by pulsed laser deposition." *Applied Surface Science*, vol. 257, no. 2, pp. 429-433, 2010.
- [52] Prabhu, Yendrapati Taraka, Kalagadda Venkateswara Rao, Vemula Sesa Sai Kumar, and Bandla Siva Kumari. "X-ray analysis by Williamson-Hall and size-strain plot methods of ZnO nanoparticles with fuel variation." *World Journal of Nano Science and Engineering*, vol. 4, no. 01, pp. 21, 2014.

## الخلاصة

في هذه الرسالة طريقة ويليامسون-هال و طريقة رسم الحجم-الانفعال و طريقة هالدر-واكنر استخدمت لتحليل نموذج خطوط حيود الأشعة السينية و حساب الحجم البلوري و انفعال الشبكة لجسيمات أكسيد النيكل النانوية . النتائج احرزت من هذه الطرق ثم قورنت مع هذه المحرزة من طرق شيرر الكلاسيكية و شيرر المطورة. الحجم البلوري كان (0.3087) نانومتر, (0.8626) نانومتر, و(0.2228) نانومتر, بينما انفعال الشبكة كان: (0.1441), (0.8216), و(0.5207) لويليامسون-هال , هالدر-واكنر , و رسم الحجم-الانفعال على التوالي. من جهة اخرى , الحجم البلوري و انفعال الشبكة حسب من شيرر الكلاسيكية حيث كانت (D=0.31511) نانومتر, ( $\epsilon = 0.32471$ ), وطريقة شيرر المطورة (D=0.1350) . من النتائج المحسوبة لجميع الطرق في هذه الرسالة لاحظنا ان طريقة هالدر-واكنر افضل طريقة تحليل لحساب الحجم البلوري و انفعال الشبكة باعطاء نتائج دقيقة ومقاربة لتلك التي وجدت بواسطة طريقتي شيرر و شيرر المطورة. مساحة السطح المحددة (SSA) حسبت باستخدام الحجم البلوري لطريقة هالدر-واكنر  $4.0375 * 10^9$  متر<sup>2</sup>/غرام . كثافة الانخلاع ( $\delta$ ) حسبت وفقاً للحجم البلوري لهالدر-واكنر ( $\delta = 2.1186 * 10^{18}$ ) . معامل التشكيل (MI) تم حسابه من العرض الكلي عند منتصف الشدة (FWHM) واعلى قيمه كانت (2.63530922) لخط الانعكاس (220) و اقل قيمة كانت (1.304537008) لخط الانعكاس (222). معامل البنية البلورية لجميع الخطوط الجانبية كان (0.429331599). بتطوير هالدر-واكنر تم حساب الاجهاد وكثافة الطاقة حيث (الاجهاد  $\sigma = 36449 * 10^6$  نيوتن/متر<sup>2</sup>), كثافة الطاقة  $u = 9489 * 10^6$  نيوتن/متر<sup>2</sup>. استخدم مخطط هالدر – واكنر لحساب كثافة الطاقة من القطع مع محور y و اعطى نفس القيمة التي اوجدت بواسطة طريقة هالدر – واكنر المطورة . الحجم البلوري لخطوط الانعكاس (111, 200) حسب عند درجات حرارة كل سنة مختلفة (200, 300, 400) °م. الحجم البلوري ل(111) يقل مع زيادة درجات الحرارة من (200-400) و كانت (0.34174 نانومتر), (0.32985 نانومتر), و(0.31260 نانومتر) على التوالي. الحجم البلوري للخط (200) كان (0.49210 نانومتر), (0.45336 نانومتر), و(0.83588 نانومتر) لل(200,300,400) درجة سيليزية على التوالي .



جمهورية العراق  
وزارة التعليم العالي والبحث العلمي  
جامعة بغداد  
كلية التربية للعلوم الصرفة - ابن الهيثم

# تصحيح الخطوط الجانبية لقمم حيود الاشعة السينية باستعمال ثلاث طرق تحليل

رسالة مقدمة

إلى مجلس كلية التربية للعلوم الصرفة - ابن الهيثم - جامعة بغداد كجزء من متطلبات  
نيل درجة ماجستير علوم في الفيزياء

من قبل

رشا منير جلاب

بإشراف

أ. د. خالد هلال حربي

2019 م

1441 هـ